Copy No. 1

102p

[redacted]

FINAL REPORT

MILLIMETER-WAVE CONVERTER STUDIES

CONTRACT NASw-430

for period

May 14, 1962 - January 15, 1963

Prepared for

Office of Lunar and Interplanetary Exploration Programs (SL)
NATIONAL AERONAUTICS AND SPACE ADMINISTRATION
400 Maryland Avenue, S.W.
Washington 25, D.C.

Prepared by: R. C. Wertman

R. C. Wertman, Senior Project Engineer

R. W. Wilmarth

R. W. Wilmarth, Senior Project Engineer

[redacted]

Approved by: A. W. McIlwan

A. W. McIlwan, Laboratory Director

ITT COMPONENTS DIVISION
a division of International Telephone and Telegraph Corporation
ELECTRON TUBE LABORATORY
500 Washington Avenue
Nutley 10, New Jersey

CONTENTS

CONTENTS
(continued)

FINAL REPORT

CONTRACT NASw-430

MILLIMETER-WAVE CONVERTER STUDIES

I. INTRODUCTION

This contract was directed toward the study of the feasibility of building a low noise, wide bandwidth, electronically tunable converter in the millimeter-wave range. The contract was divided into two basic study areas.

The first study area had as prime objectives the theoretical analysis of the backward wave converter operation and the theoretical analysis of r-f structures that would give good performance in the millimeter wave range.

The second study area was experimental in nature and included measurements to correlate the results of the theoretical study areas as well as the study of electron guns for use in a millimeter-wave converter and the weight and power requirements of a converter relative to possible use in a planetary spacecraft.

The information presented in Bimonthly Reports 1, 2, and 3 will not be repeated in detail in this report. The work accomplished since the last report (Bimonthly Report No. 3) will be reported on in Section II of this report, a summary of the over-all program will be presented in Section III and conclusions and recommendations for future work will be presented in Section IV.

II. WORK ACCOMPLISHED DURING THE PAST INTERVAL

A. Theoretical Analysis of the Operation of the Backward Wave Converter

1. Space Charge Analysis

For the sake of clarity the discussion of the space charge analysis done during the past interval will be deferred to Parts II B and III A of this report.

2. Ballistic Analysis

During the past interval two extensions of the ballistic theory were completed. In the first extension the approximate analysis presented as Appendix I of Bimonthly Report No. 2 has been modified to include the effect of the cosinusoidal variation of the envelope of the accelerating electric field. The analysis proceeds along the same lines as before, and it turns out that the cosinusoidal variation does not complicate the analysis to any significant extent. Likewise, the results do not differ greatly from those obtained previously for the constant amplitude case. The details of this analysis are presented in Appendix I of this report.

In the second extension the ballistic analysis has been further modified to include the effects of space-charge in addition to a cosinusoidal envelope variation of the electric field in the oscillator section of the device. This analysis, which is presented in Appendix II, combines the ballistic analysis presented in Appendix I with the pure space-charge analysis presented in Section III of this report.

B. Experimental Measurements on Low Frequency Converter and Correlation With Theory

1. Construction of Experimental Low Frequency Converters

During the course of this investigation and as described in earlier reports two experimental low frequency converters were constructed. The first designated the X-422 is a single helix device in which the input signal is injected into the collector end of the circuit. While numerous measurements were taken on this device they did not prove to be conclusive because of the difficulty in measuring the i.f. impedance. During the course of measurement a considerable effort was expended to determine the impedance of the i.f. load. Unfortunately this proved to be an elusive quantity to evaluate.

The second experimental converter designated the X-423 proved to be an extremely valuable device. This converter which is depicted schematically in Figure 1 was designad to operate in the 500 to 1000 mc frequency

range. The oscillator portion of this device was severed in three places so that four different circuit lengths could be investigated. Figure 2 shows the excellent agreement which was obtained between the calculated and measured parameters of this portion of the device. In studying the characteristics of the X-423, considerable data was obtained for each effective oscillator length. Figures 3, 4, 5 and 6 are typical of the data which was obtained. In the following sections of this report it is shown that excellent agreement with theory was obtained.

2. Correlation With Ballistic Theory

In Appendix I, the ballistic analysis of the BWC was extended to include the effect of the cosinusoidal electric field amplitude envelope in the BWO section. It was shown there that the conversion gain is given by:

$$CG(db) = 20 \log \left(\frac{KR_L a}{4\pi 2}\right) + 20 \log \left(\frac{\omega_{if} \omega \ell^2}{\eta V_o}\right) + 10 \log \left(\frac{K P}{2V_o^2}\right)$$

where all the quantities appearing in this expression have been defined in earlier reports.

Before the conversion gain may be evaluated numerically, values must be chosen for the various parameters appearing in the above expression. A calculation of K has been made for the no-space-charge case, and the results are presented in Figure 7 with $K\sqrt{K Z_L}/(2C)$ plotted as a function of gain. This calculation is straight-forward but somewhat tedious. The calculations were performed with a desk calculator.

On the basis of what appear to be reasonable assumptions, a value of 500 ohms has been chosen for R_L, the load impedance at the i.f. frequency. This value has been used in all of the subsequent calculations.

Representative comparisons between theoretical conversion gain and measured values are shown in Figures 8, 9, and 10. The Stanford nomograph was used to determine the circuit impedances, and in each case the

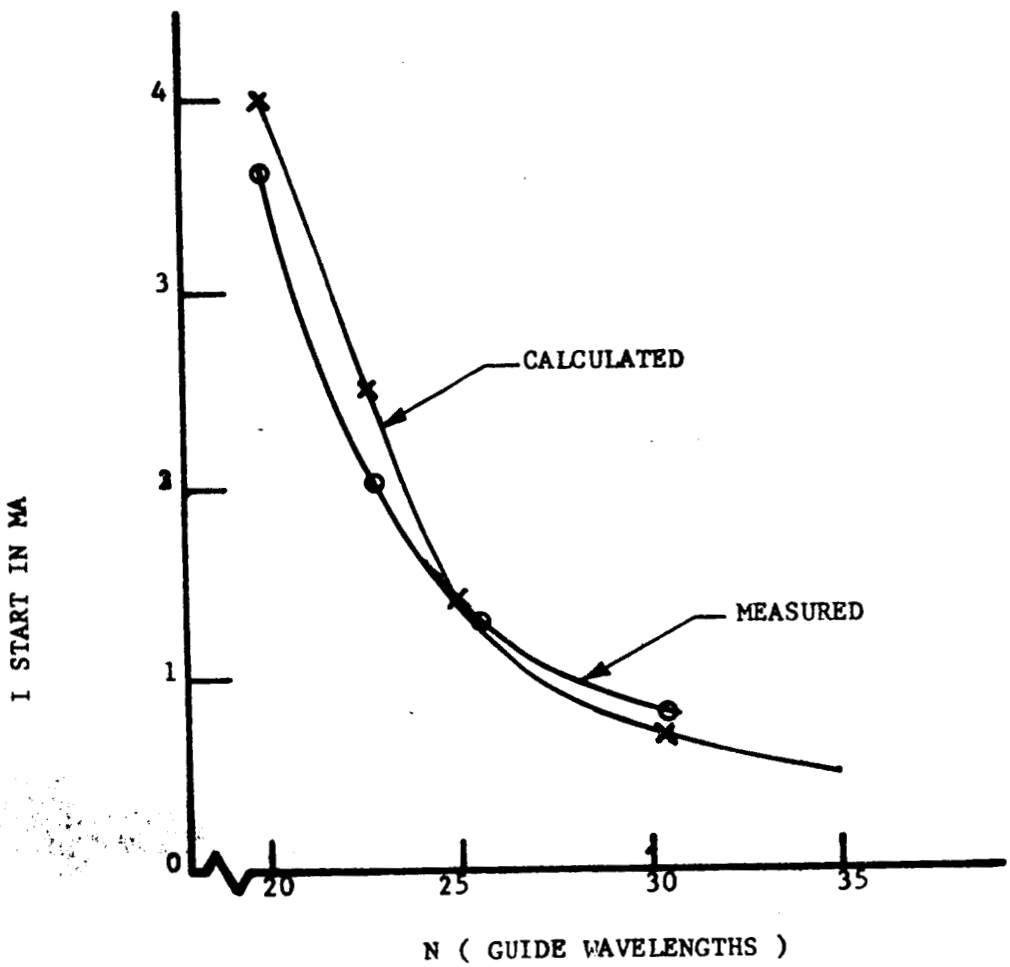

FIGURE 2 CALCULATED AND MEASURED STARTING CURRENTS FOR THE X-423 BWC

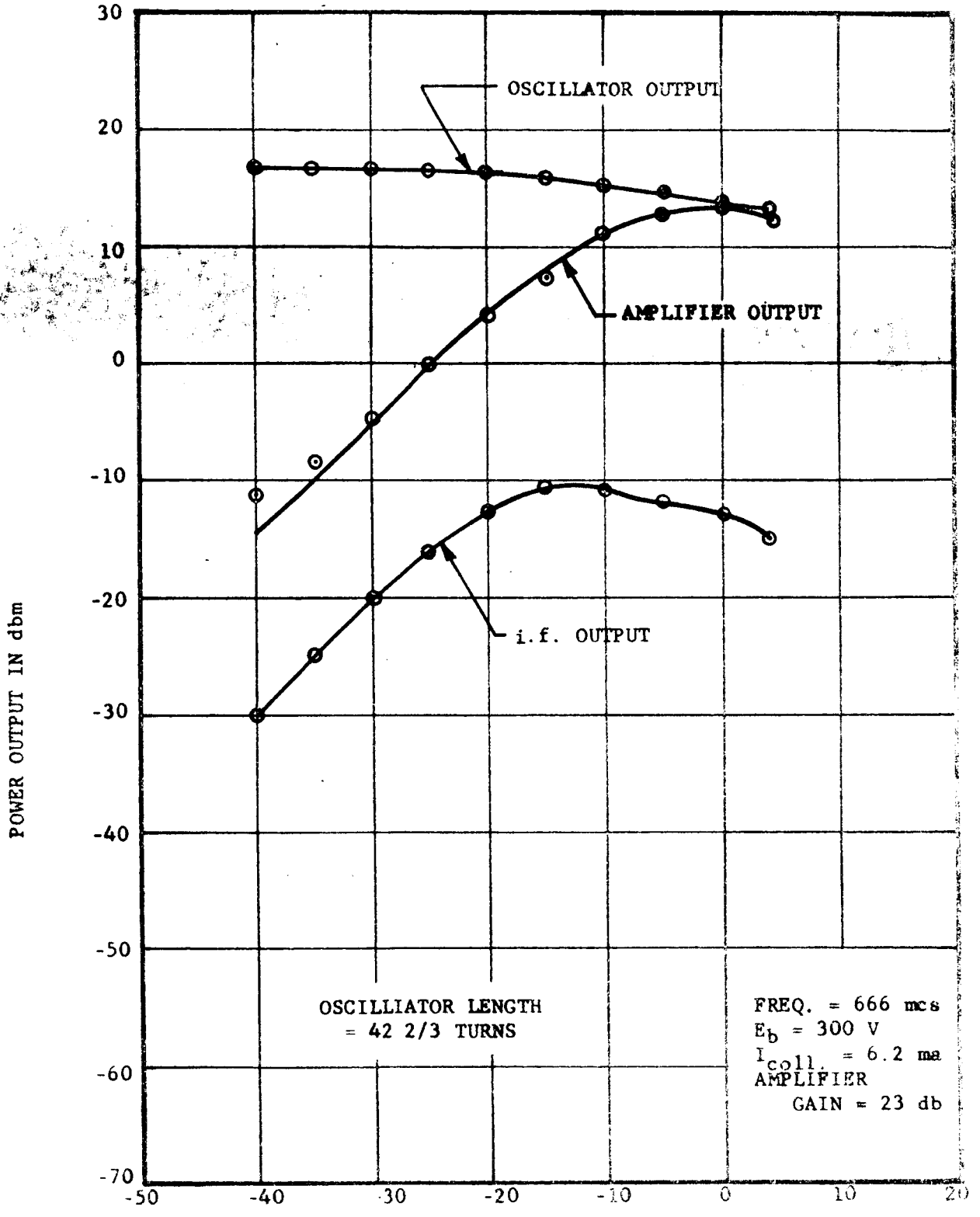

FIGURE 3 POWER OUTPUTS VERSUS AMPLIFIER POWER INPUT FOR 42 2/3 OSCILLATOR LENGTH.

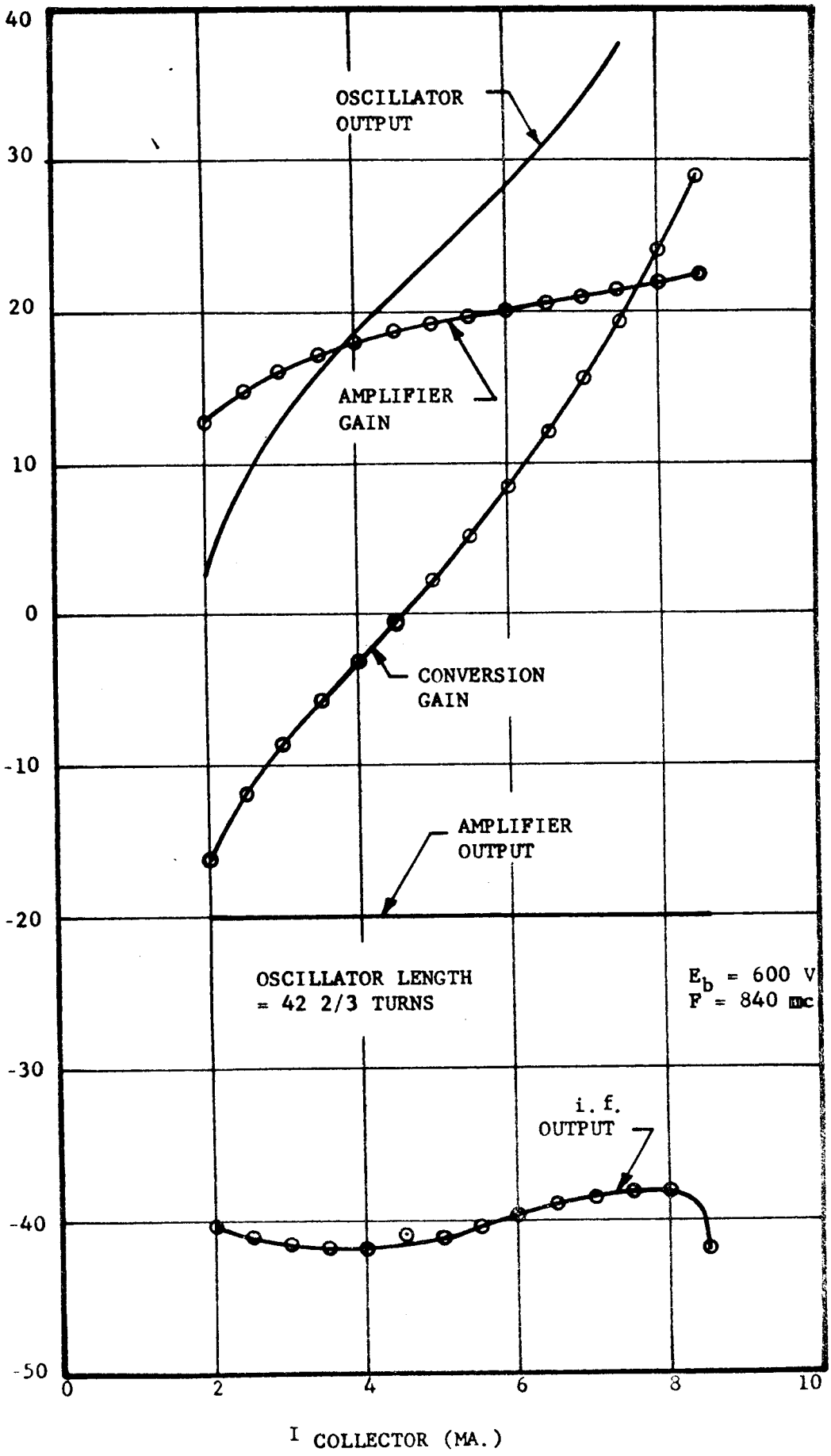

FIGURE 4 OSCILLATOR, AMPLIFIER, AND i.f. OUTPUT POWER, AND AMPLIFIER AND CONVERSION GAIN VERSUS COLLECTOR CURRENT.

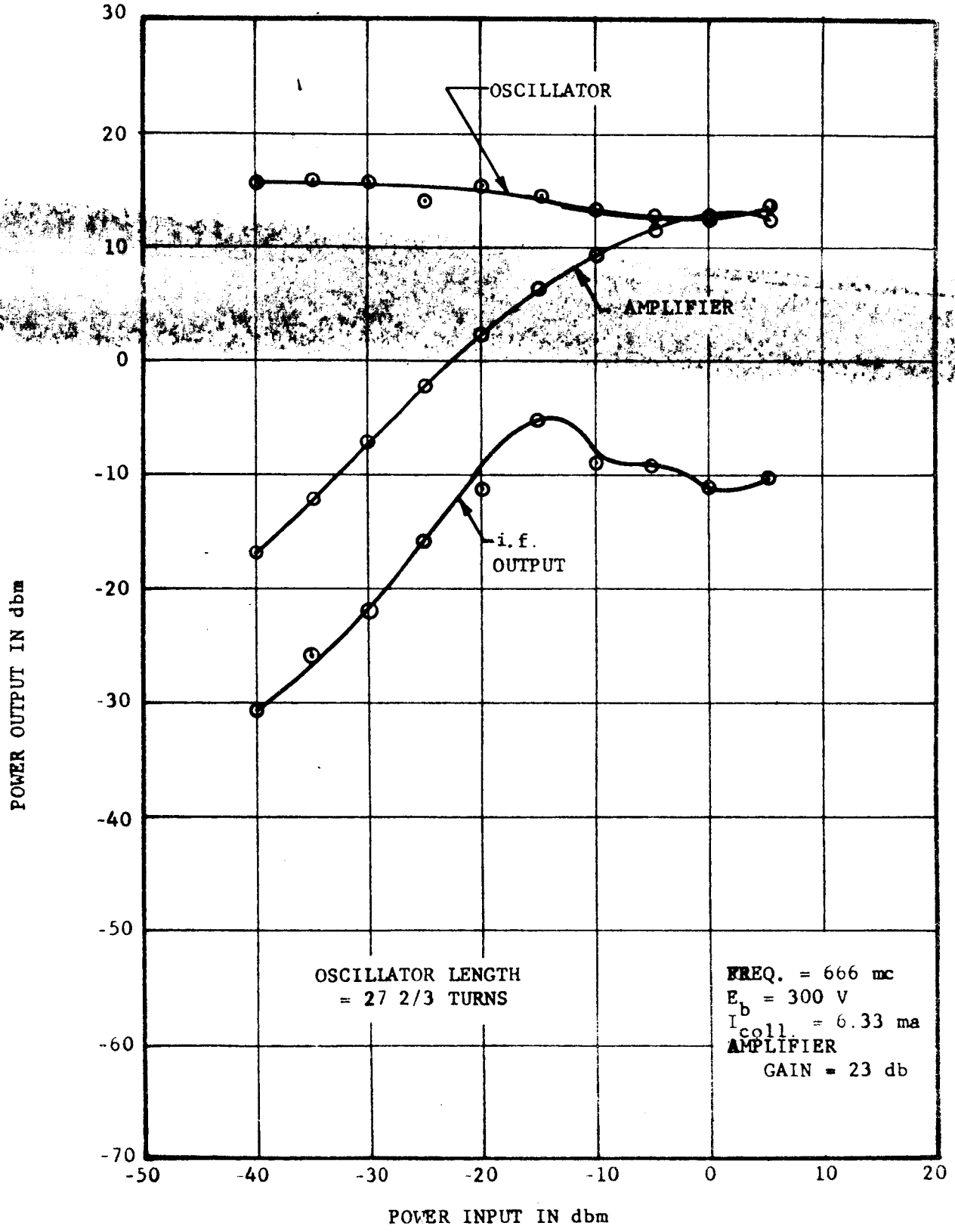

FIGURE 5 POWER OUTPUTS VERSUS AMPLIFIER POWER INPUT FOR 27 2/3 TURNS OSCILLATOR LENGTH

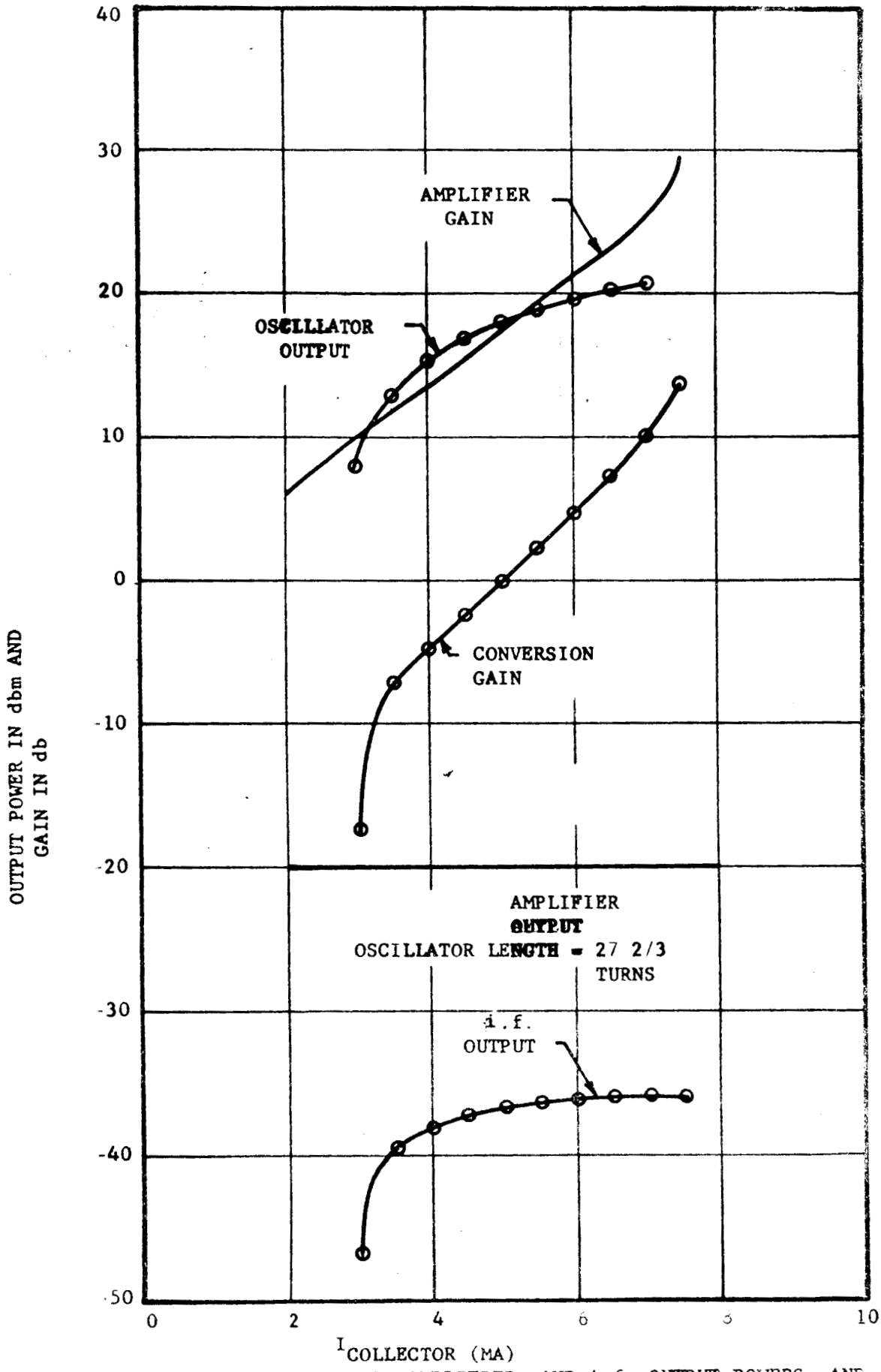

FIGURE 6 OSCILLATOR, AMPLIFIER, AND i.f. OUTPUT POWERS, AND AMPLIFIER AND CONVERSION GAIN VERSUS COLLECTOR CURRENT

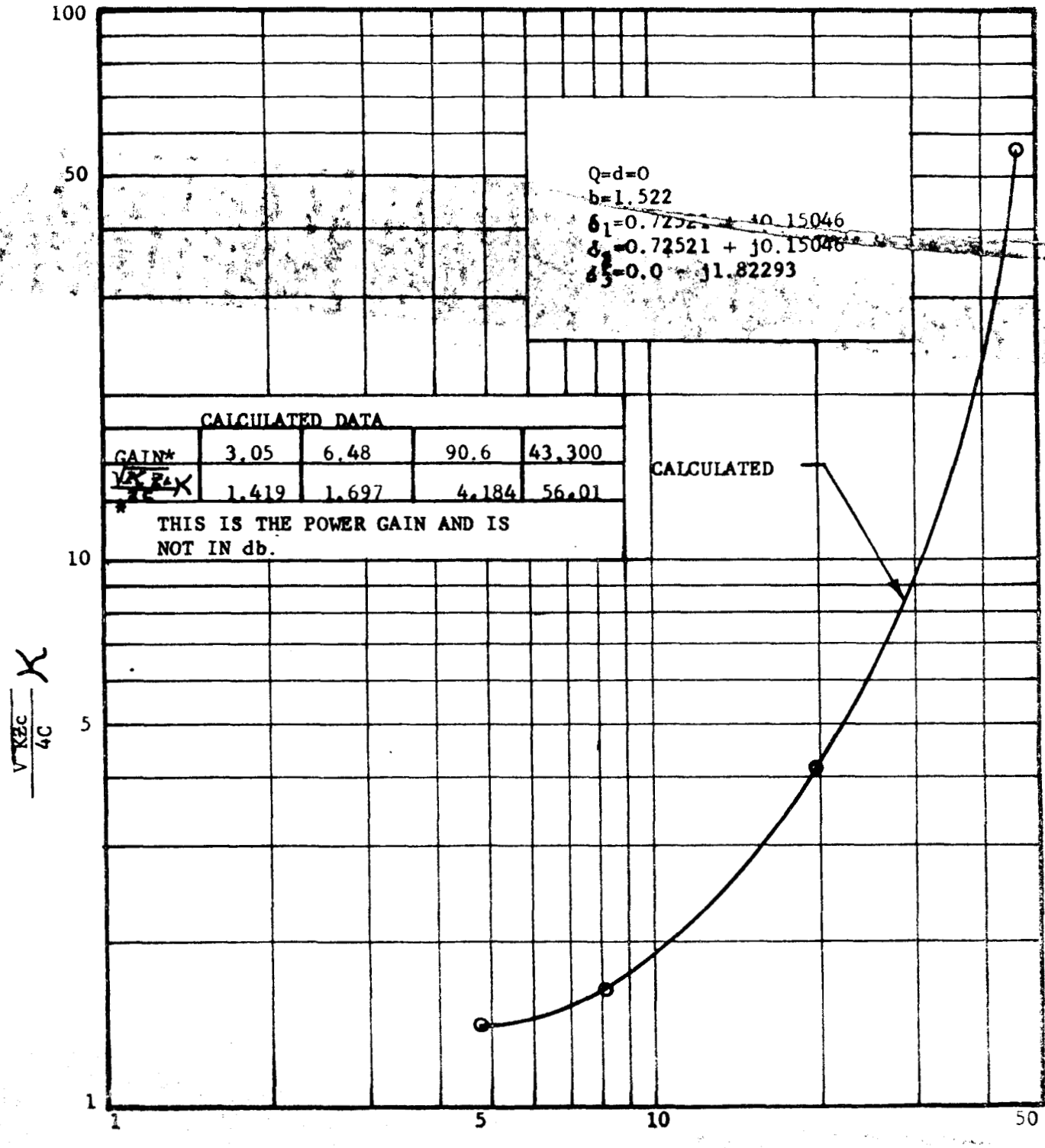

FIGURE 7 TRANSCONDUCTANCE PARAMETER X AS A FUNCTION OF BWA GAIN

CALCULATED DATA					
I_c (ma)	2.6	3.35	5.0	6.4	7.5
CG (db)	-9.6	-3.4	5.3	12.1	19.4

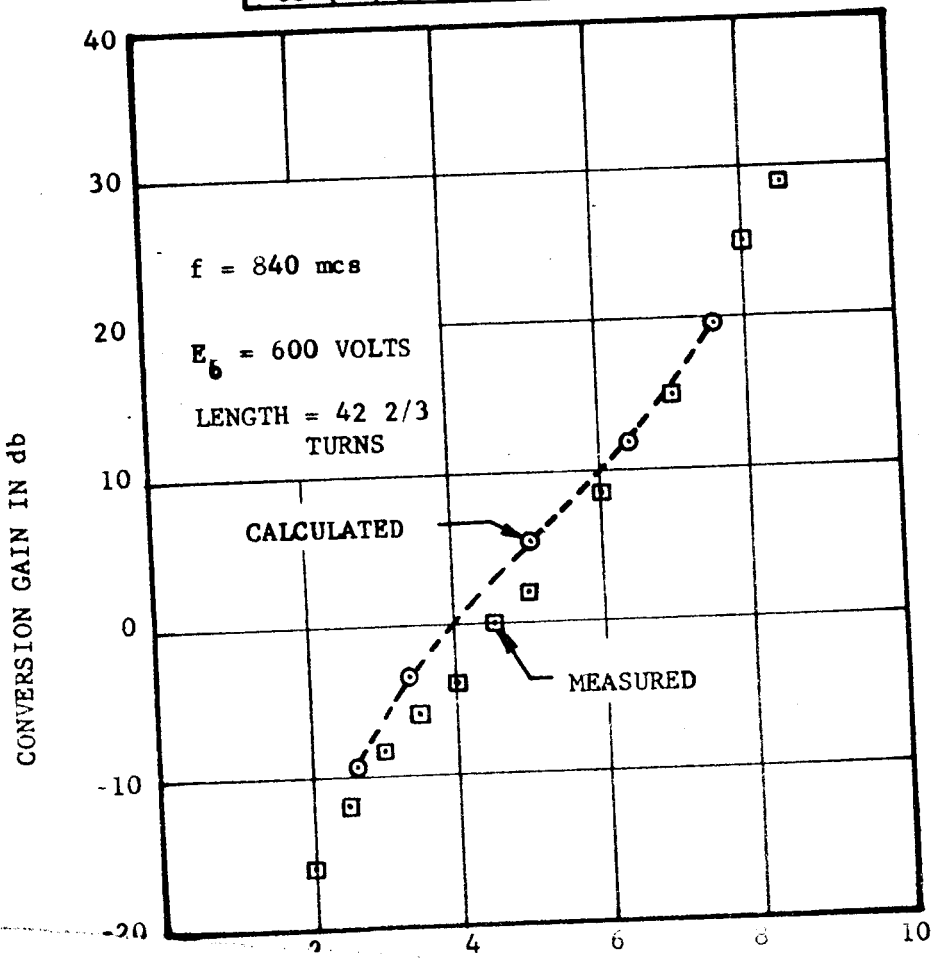

CALCULATED DATA					
I_c (ma)	2.76	4.15	5.25	6.55	7.5
CG (db)	-8.9	-1.5	3.1	12.6	23.4

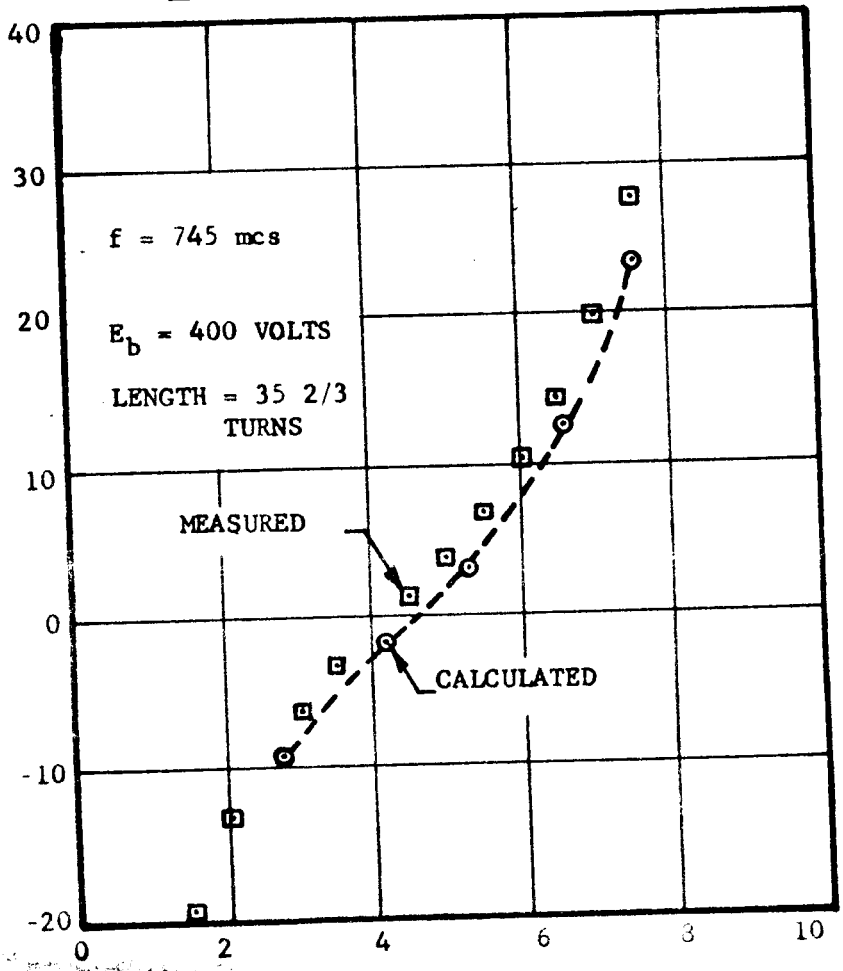

FIGURE 9 COMPARISON OF THEORY AND EXPERIMENT FOR X-423 AT 745 MC.

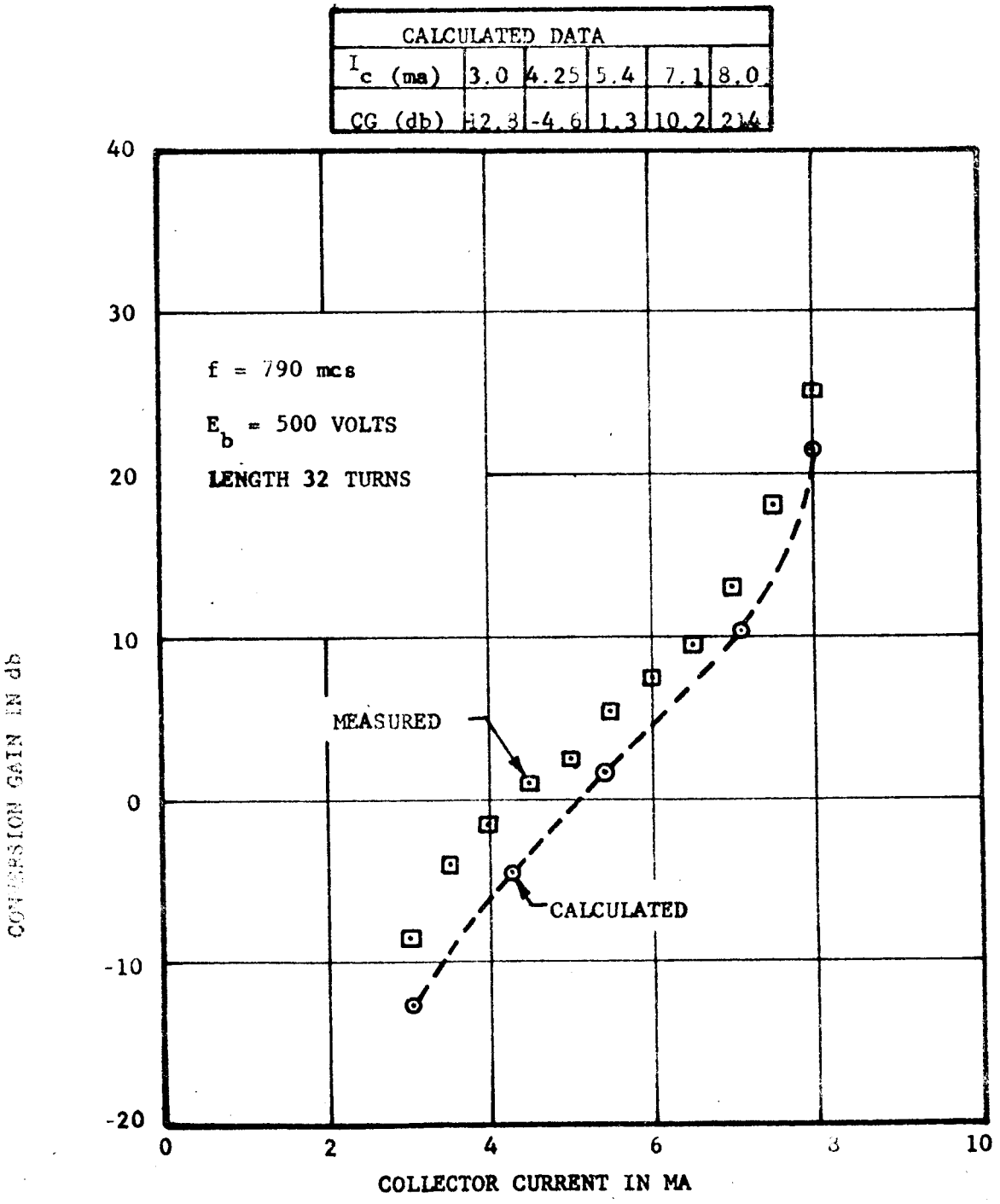

FIGURE 10 COMPARISON OF THEORY AND EXPERIMENT OF X-423 AT 790 MC.

gain parameter C was calculated, using the appropriate current. (100 per cent beam transmission was assumed.) The parameter X was then determined from Figure 7. All other parameters appearing in the [illegible] for the conversion gain are known; so it could then be evaluated. The conversion gain calculations were done with a slide rule.

3. Correlation With Non-Linear Space Charge Theory

Calculations were made using the theory developed in the non-linear space charge wave analysis to demonstrate the correlation with experimental results. The two circuit lossless case was assumed and the experimental results of the X-423 low frequency backward wave converter were chosen for correlation. Two experimental curves of conversion gain and the theoretically predicted conversion gains are shown in Figures 11 and 12. Figure 11 shows the correlation for the case where the oscillator helix length was made 35-2/3 turns and Figure 12 shows the correlation where the helix length was 32 turns. These figures provide evidence that the analysis used is reasonable and can be used to predict results with fair accuracy.

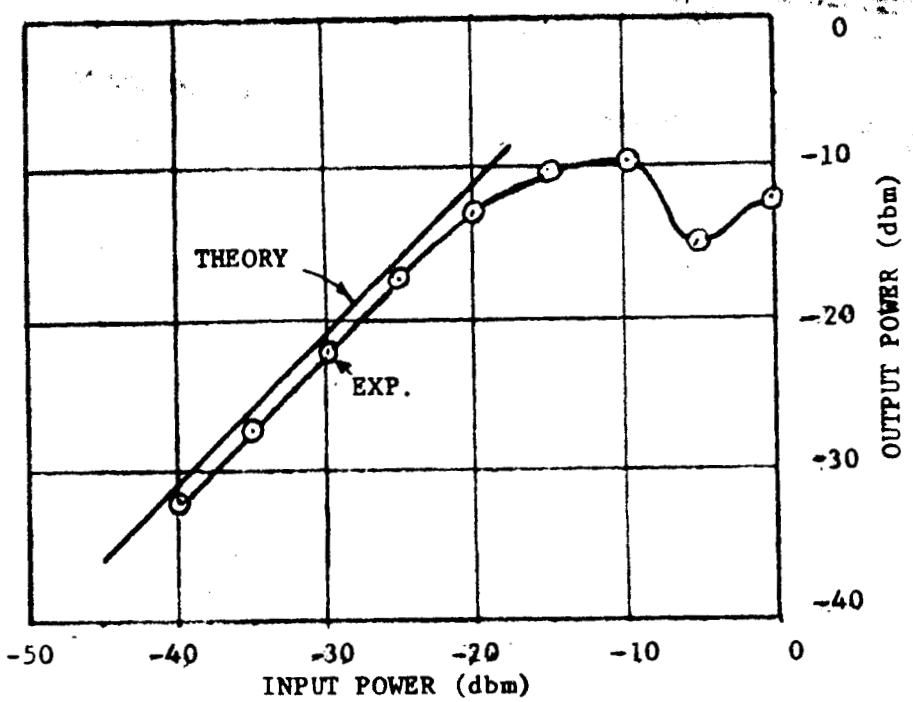

FIGURE 11.CONVERSION GAIN OF X-423 FOR 35 2/3TURNS OSCILLATOR LENGTH

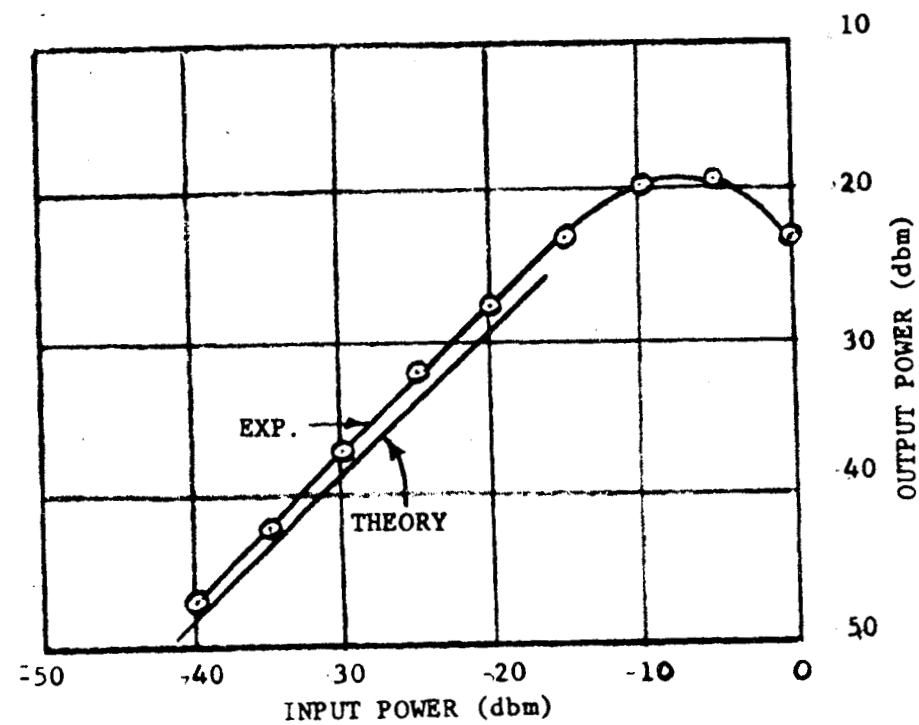

FIGURE 12.CONVERSION GAIN OF X-423 FOR 32 TURNS OSCILLATOR LENGTH

C. Measurements on Slow Wave Structures

1. Cold Test Measurements

During the past interval additional cold test measurements were conducted on the ridge loaded meander line. Efforts were concentrated on obtaining reliable impedance measurements as well as a simplification of the circuit. The impedance measurements can now be made reliably and are always repeatable. In fact the results obtained at this laboratory and our British affiliate, Standard Telecommunication Laboratories, are identical. Of particular interest is a simplification which has been made in the meander line. Figure 13 is a photograph of two circuits which have been used in the cold test measurements. It is seen that these circuits differ only in regard to the presence of the smaller slots. Measurements of these circuits yielded identical results for both the dispersion characteristics and impedance to within a fraction of one per cent. The values are well within experimental error. From the configurations shown in Figure 13, the importance of the simplification becomes apparent when one considers the fabrication of millimeter wave circuits. Figure 14 is a photograph of an actual 50 to 70 Gc circuit which has been enlarged approximately ten times. The circuit is constructed of .005" molybdenum sheet. The slots and spacings are approximately .005" wide. The pitch accuracy of this circuit is in the order of .0001". This circuit was fabricated using spark machining techniques.

2. Weak-Beam Phase Bridge Measurements

During the past interval work continued on the demountable exhaust station in an effort to obtain more definitive measurements of the dispersion and impedance characteristics of slow wave structures. Figure 15 is a photograph of the experimental setup. The circuit which is presently under study is a ridge loaded meander line similar to that shown in Figure 13, but scaled for operation in the 6000 mc region. While good dispersion data were obtained with little trouble the impedance measurements proved to be much more difficult. The bridge impedance readings which were obtained were of the correct magnitude to agree with the cold test measurements. Unfortunately however, they were difficult to repeat. The dispersion

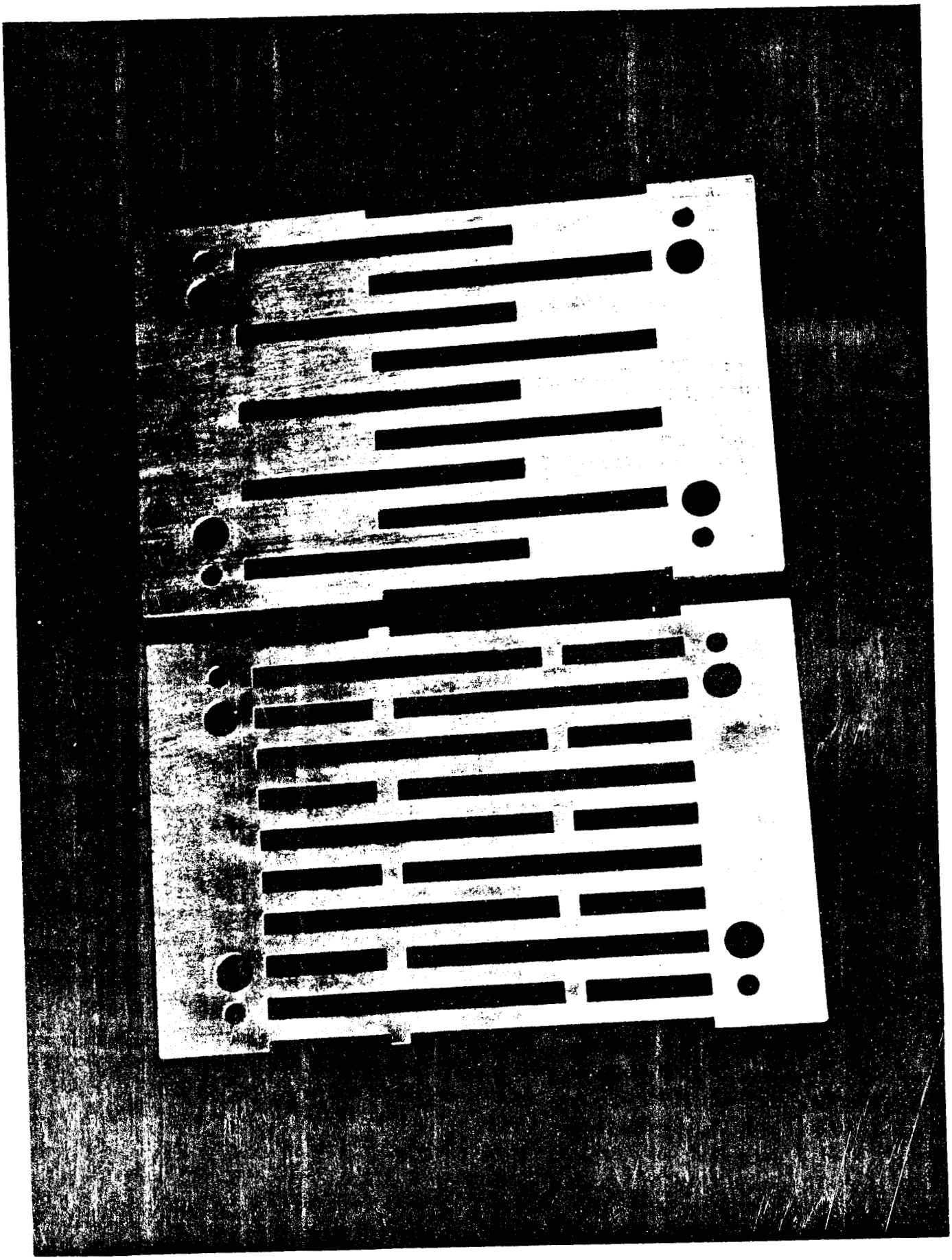

Figure 13 Original and Simplified Versions of the Meander Line

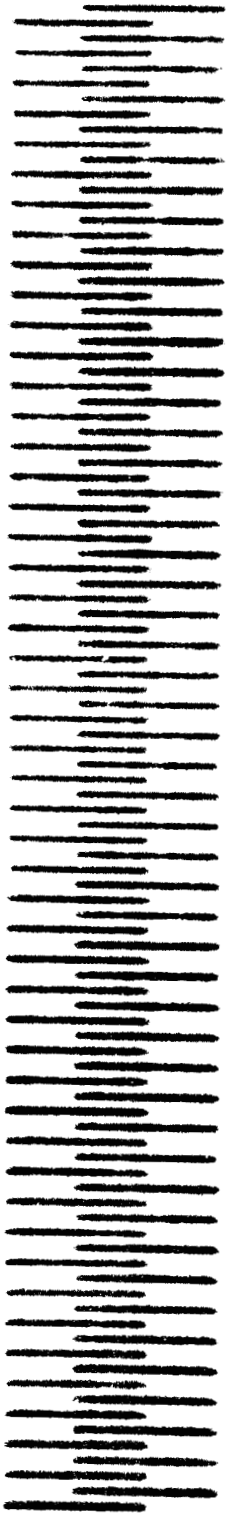

Figure 14 Spark Machined Simplified Meander Line for 50 to 70 Gcs Enlarged Approximately 10 Times

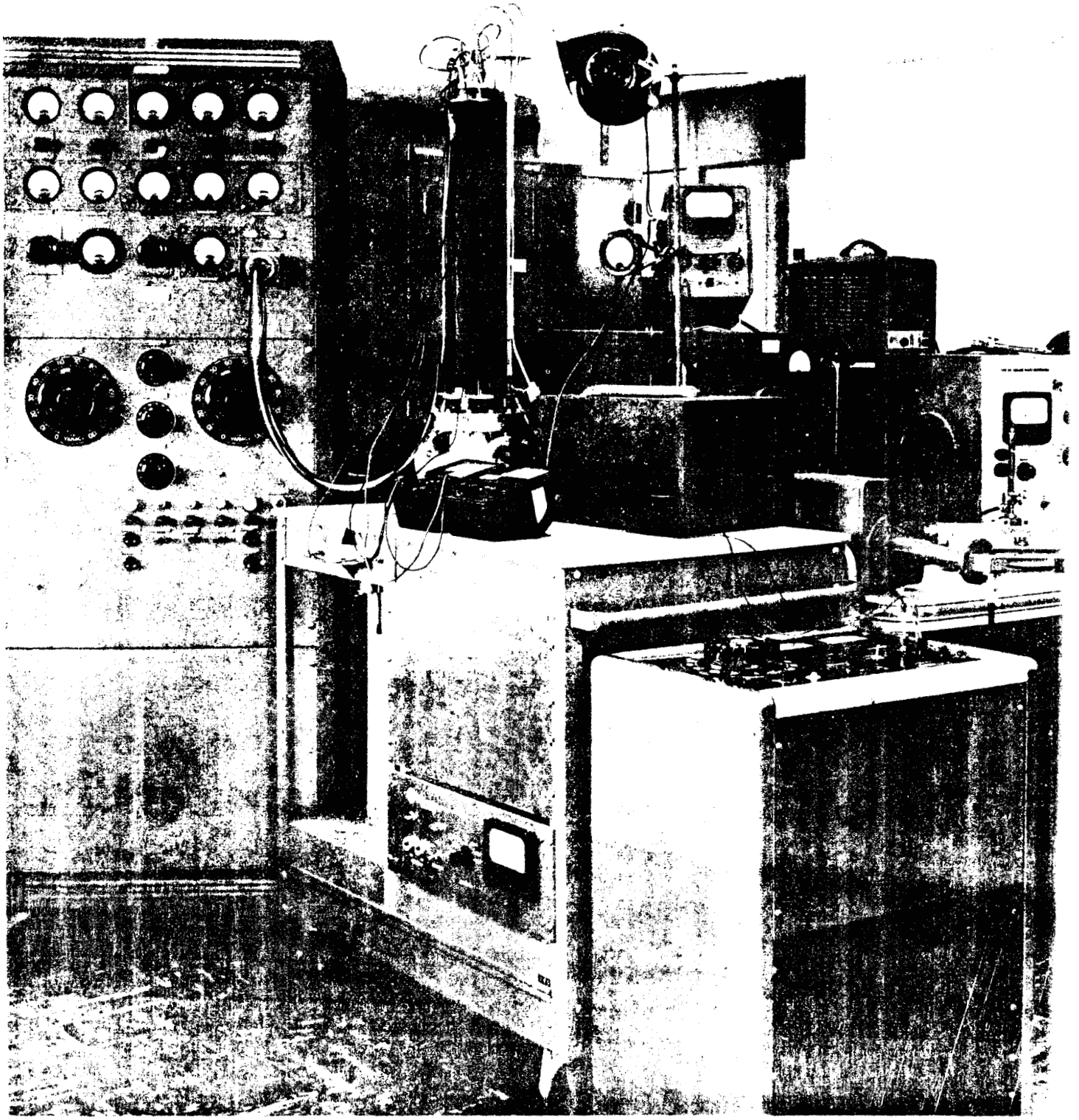

Figure 17 Beam Phase Bridge Setup

characteristics agreed within experimental error with the cold test measurements that were reported in Bimonthly Report No. 3. The difficulties encountered here have been attributed primarily to beam transmission and it is believed they can be eliminated with a modification of the equipment. It is the intension of this laboratory to continue on this work as we feel there are definate advantages to be obtained. While useful data can be obtained from cold test measurements there are always ambiguities to be resolved, especially when a circuit is to be operated in a higher space harmonic and passband.

3. Construction of an Experimental 50 to 70 Gc Backward Wave Oscillator Tube

Our British affiliate, Standard Telecommunication Laboratories, has been working on an experimental Backward Wave Oscillator for the 50 to 70 Gc frequency range. This tube is applicable to this program because the frequency range and type of slow wave circuit is similar to what would be required in a backward wave converter. The slow wave structure for the tube is fabricated using photo etching techniques. Figure 16 is a photographic enlargement of two actual meander line circuits while Figure 17 is a schematic representation of the circuit and its waveguide transitions. Figure 18 is a photgraph of the r-f portion of the tube while Figure 19 displays the insertion loss and VSWR measurements. At this writing initial operation had been obtained as an oscillator. Because both ends of the circuit are available the device will also be operated as an amplifier. It is intended that an attempt to operate the device as a single circuit converter will be made, although the i.f. detection circuit will not be optimum.

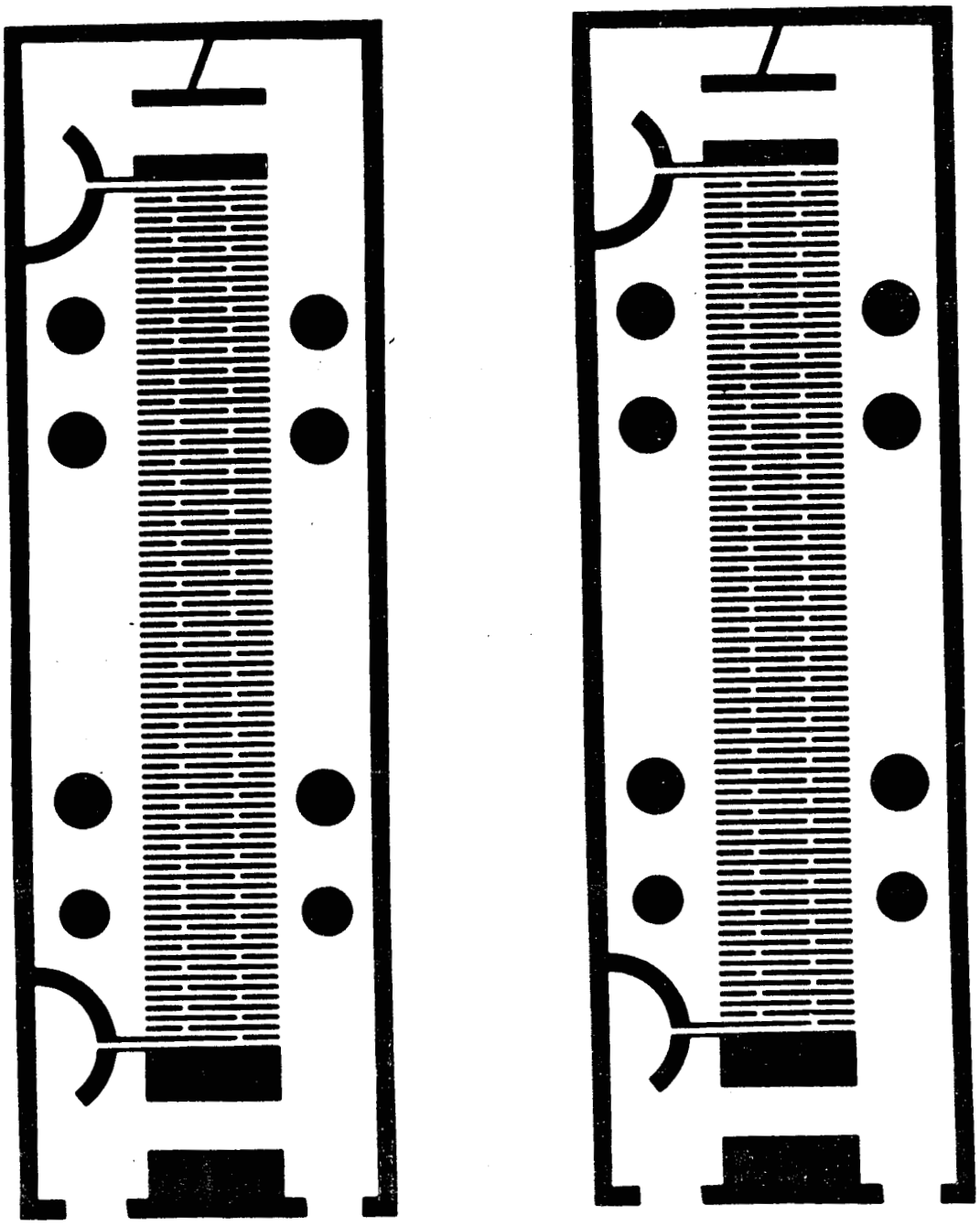

FIGURE 16 TWO PHOTOETCHED 50 TO 70 Gc. MEANDER LINES (ENLARGED APPROX. 6 TIMES)

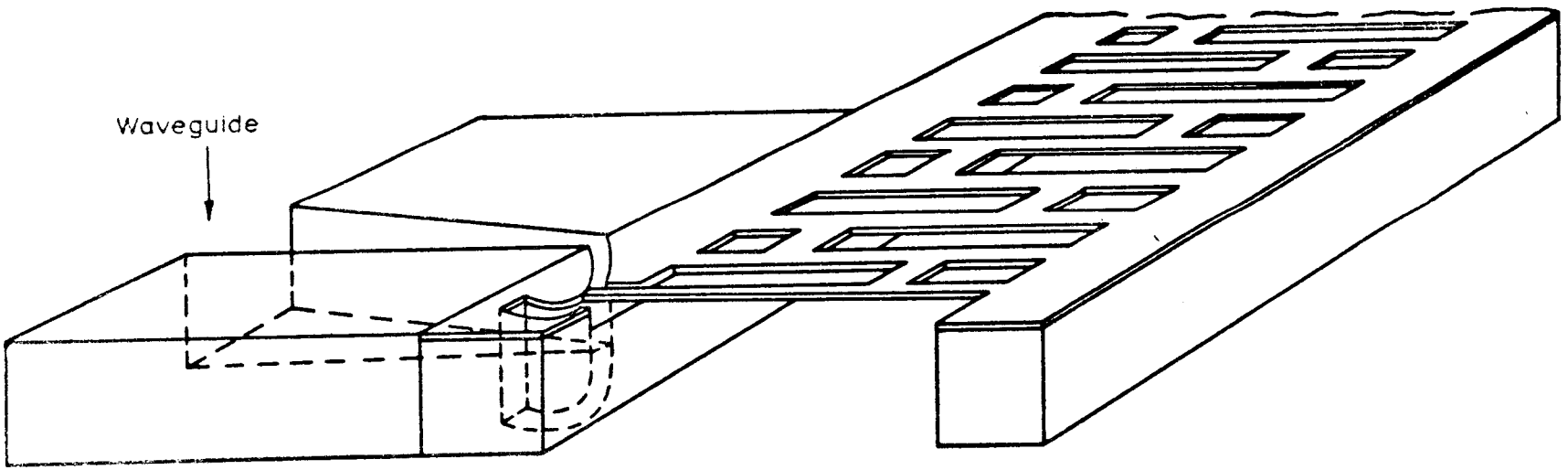

FIGURE 17 50 Gc Slow Wave Circuit Illustration of Waveguide Transitions

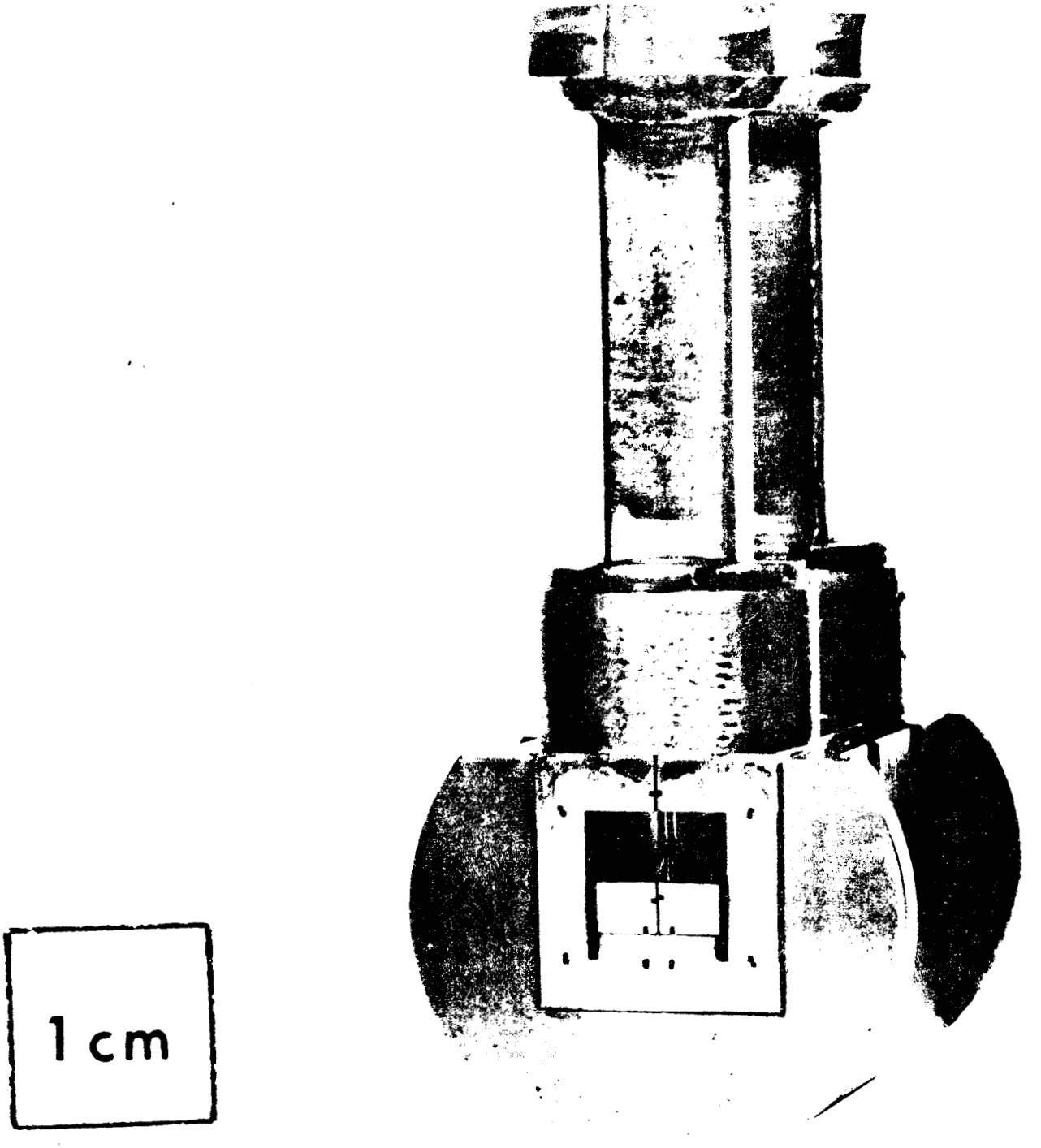

FIGURA 1

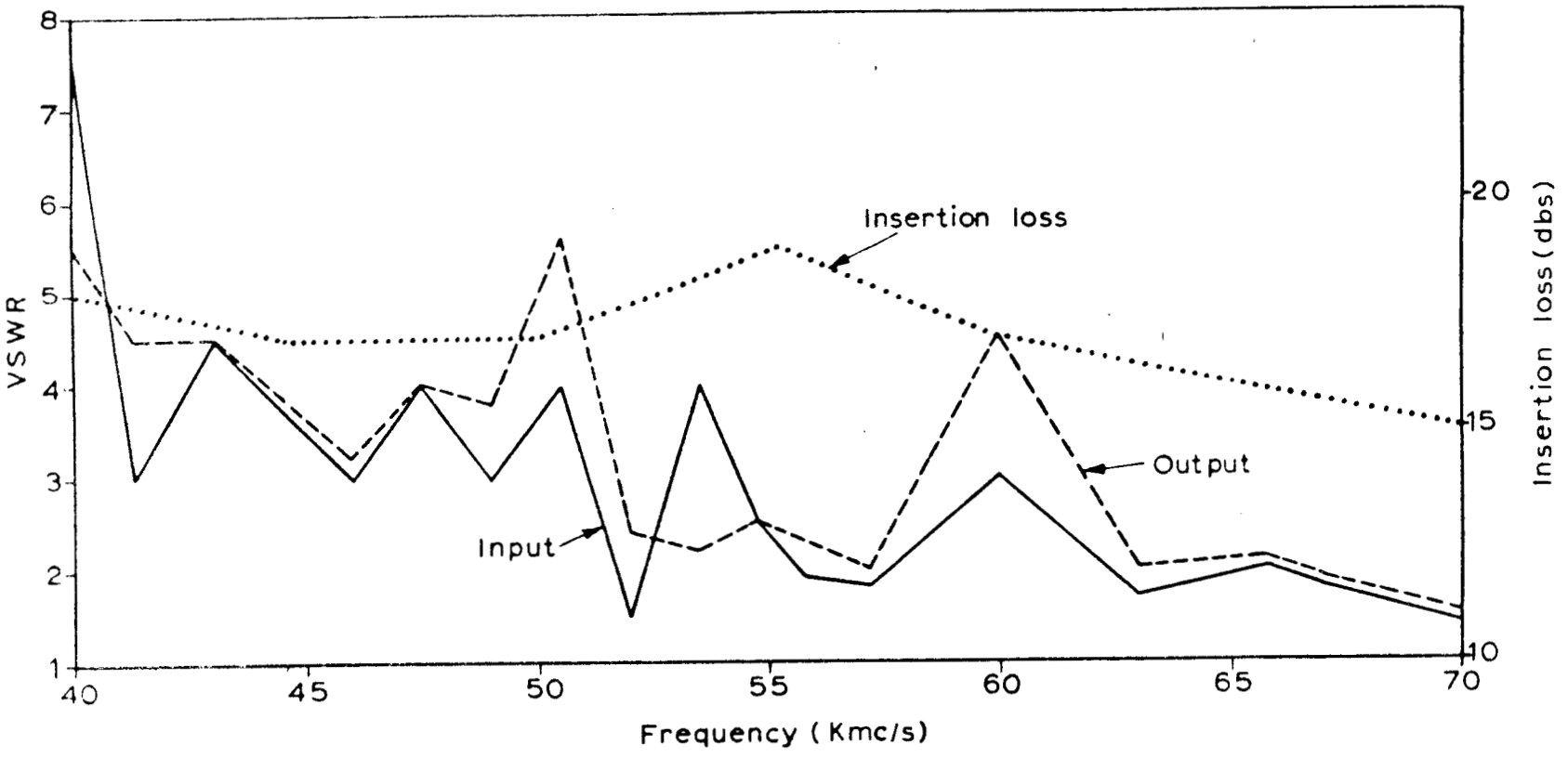

FIGURE 19 Input and Output VSWR and Insertion Loss of 50 Kmc/s Circuit

D. Electron Beam Studies

1. Thick Beam Optics for the Backward Wave Converter

The aim of this study is to examine the possibility of utilizing a "thick" beam in the BWC in order to provide a reservoir of new electrons to replace those which have been intercepted by the circuit. The consideration which led to this suggestion is that at millimeter wavelengths the problem of beam transmission becomes increasingly severe. There is a particular need to make the BWO section as efficient as possible, and since this is preceded by a relatively long structure, the idea of utilizing a thick beam becomes very attractive.

In Bimonthly Report No. 3 a characteristic equation for a BWO interacting with a thick beam tilted at an angle θ was derived. This dispersion curve has now been programmed and preliminary numerical results have been obtained. These results show the anticipated increase of starting current with θ for small values of θ . For larger values of θ the results indicate a decrease of starting current which is clearly non-physical, and appears to be due to certain assumptions relating to the smallness of θ. Further study to resolve this issue is called for. However, the results for sufficiently small θ appear to be sound, and suggest that the increase in starting current, for values of θ for which there is a considerable replenishment of current (say $\theta = 10^{-3}$), is not likely to be excessive. The interim conclusion for the theoretical study, therefore, supports the original hope that the use of the thick beam electron optics could lead to a substantial easing of the electron optical problems associated with the two circuit BWC.

In the case of the single circuit BWC, the use of the thick beam technique is considerably less attractive for two reasons:

(1) In the two circuit BWC, the beam would be tilted only onto the second circuit, namely, the oscillator circuit. Thus sufficient gain would by this point have accumulated to make the resulting interception noise insignificant. In the case of the single circuit BWC there is no prior gain, and hence the interception noise would probably prove prohibitive.

(2) The single circuit BWC is less than half the length of the two circuit BWC, and furthermore, the gun is located close to the input. The electron optical problems are therefore far less severe, and the use of thick beams would therefore not in any event be justifiable.

As will appear from other sections of the report, our thinking is tending in the direction of using a single circuit BWC in the final millimeter wavelength device. It is not therefore proposed to deploy very much further effort on this topic.

2. Cathode Considerations

The cathode and electron gun requirements for millimeter wave tubes will tend to be very much more severe than for comparable microwave tubes. This comes about primarily because smaller beam dimensions are required while the beam power levels remain relatively unchanged. The result, of course, is that the cathode and beam current densities are increased considerably. Under these conditions the trend has been to use cathodes of the Philips types, which permit loading densities of the order of several amperes per square centimeter, but at increased temperatures over that of the normal oxide cathode. A notable exception is a gun developed under the sponsorship of the Electronic Technology Laboratory under Contract No. AF33(616)-6441 which has an area convergence ratio greater than 1000. This gun would still permit the use of an oxide cathode in certain instances. The use of the higher temperature cathodes, while advantageous for high current densities, are not desirable where low noise operation is desired. In addition, to confine the excursion of electrons due to greater thermal velocities the magnetic focusing field must be further increased. In reviewing the cathode requirements our attention was called to a cathode presently under development at the Bell Telephone Laboratories[1]. We subsequently visited the Bell people to learn more about this cathode. The cathode comprises a relatively thick pellet of Ni powder mixed with ZrH on top of which is a thinner layer of Ni and $BaCO_3$. This is pressed and then heated to 600°C in N where the ZrH breaks down and the Zr alloys with the Ni. The pellet is then repressed, a 1000 Å layer of Ni is evaporated onto the top surface and the cathode is then activated at a high temperature, CO_2 being

1. Maurer, D. W., Becker, E. J., Koontz, " A New Nickel Matrix Cathode" Presented at the 1962 Electron Devices Meeting, Sheraton Park Hotel, Washington, D.C.

evolved and passing through the outer Ni layer. Ba diffuses through this layer and spreads evenly over it. If the cathode has subsequently to be exposed to air the Ni layer protects it from absorbing water vapor. Current densities of 1.5 amps/cm^2 at 900°C have been drawn for 3000 hrs in test diodes. Equal emission can be drawn at temperatures 100°C lower than the Philips impregnated cathode. It is believed that the cathode will have the advantages of long life and mechanical stability because the bariated layer is relatively thin and the cathode operates at a relatively low temperature. Uniform emissivity is expected because the outer surface is nickel of a uniform texture. It is the intention of this laboratory to explore the use of this cathode in any future program.

III. SUMMARY OF THE OVER-ALL PROGRAM

A. Theoretical Analysis of Operation of the Backward Wave Converter

1. Introduction

All problems of physics concerned with the motion of charged particles can be attacked by two distinct methods. In one case the particle nature is utilised, i.e. the trajectories of individual particles are followed while in the other case a continuous fluid is assumed where velocity and density variations can occur. This duality appeared also at the first analyses of velocity modulated tubes. Webster [1]* chose the ballistic analysis whilst Hahn [2] and Ramo [3] introduced the concept of space charge waves. The first approach is useful in the region of weak space charge and large signals and the second one finds application for small signals and strong space charge. Naturally both approaches can be further refined by including space charge corrections into Webster's theory or including nonlinear terms into space charge wave theory [4]. For the special case of a one-dimensional beam a more general theory can be devised [5] which contains both ballistic theory and space charge wave theory as limiting cases. In the general case, however, there is a no man's land between the two theories where neither of them applies. Thus the best one can do at the analysis of any electron device is to investigate its behavior at the two ends (i.e. ballistic and space charge) and hope that the discrepancy in the middle will not be excessive. This is the method chosen for the analysis of the BWC. Both type of calculations will be presented and it will be shown that under some simplifying assumptions the results given by the two different theories are very close to each other.

2. Space charge wave analysis

The physical model adopted in this Section is an electron beam excited simultaneously by signals at two different frequencies ω_a and ω_b. Due to the inherent nonlinearities there will be present in the electron beam a component $\omega_{if} = \omega_a - \omega_b$ which we wish to extract. The current and velocity at this difference frequency are given by a differential equation system devised by De Grasse [6] using a first order non-linear approach (perturbing the linear space charge wave solution and calculating the next nonlinear term). The differential equations are as follows :-

* **The references for this section as well as Appendicies III and IV will be given at the end of Appendix IV.**

$$\frac{dv_{if}}{dz} = -j \frac{\omega_{qif}^2}{\omega_{if}} \frac{i_{if}}{i_o} - \frac{1}{2v_o}\left[v_a \left(\frac{dv_b}{dz}\right)^* + \frac{dv_a}{dz} v_b^* - j \frac{\omega_{if}}{v_o} v_a v_b^* \right] \quad (1)$$

$$\frac{di_{if}}{dz} = j \frac{\omega_{if}}{v_o^2} i_o \left[-v_d + \frac{1}{2i_o} (i_a v_b^* + v_a i_b^*) + \frac{v_a v_b^*}{v_o} \right] \quad (2)$$

where i_o, v_o - DC current and velocity respectively,

i_a, v_a - current and velocity at the frequency ω_a

i_b, v_b - current and velocity at the frequency ω_b

ω_{qif} - reduced plasma frequency at ω_{if}.

The current and velocity at the frequencies ω_a and ω_b are assumed to be independent of each other but both depend on the applied fields. The interaction between the waves on the slow wave structure and those on the electron beam can be best described with the aid of coupled wave theory. It is convenient therefore to use the amplitudes of space charge waves as new variables. The relationship between the old and new variables is as follows :-

$$v = - \frac{\eta}{v_o \sqrt{2W}} (A_s + A_f) \quad (3)$$

$$i = - \sqrt{\frac{2}{W}} (A_s - A_f) \quad (4)$$

where A_s, A_f - amplitudes of slow and fast space charge waves respectively

$W = - \frac{2V_o \omega \eta}{\omega i_o}$,

V_o - DC voltage,

η - electron charge to mass ratio.

Restricting subsequently the analysis to the case when $\omega_{if}/\omega_a \ll 1$ and $\omega_q/\omega_a \ll 1$ (both fulfilled in practical applications) the differential equation system can be easily solved. Substituting for the current and velocity from Eqn (3) and (4) we get :-

$$i_{if}(z) = j \frac{\omega_{if}}{\omega_a} \frac{\beta_{ea}}{v_o} \int_o^z (A_{sa} A^*_{sb} - A_{fa} A^*_{fb}) \, dz \qquad (5)$$

where $\beta_{ea} = \omega_a/v_o$.

Thus if the amplitudes of the space charge waves are known a simple integration yields the i-f current.

a. Comparison of high QC and low QC thories for the one-circuit BWC

A simplified diagram of the one-circuit arrangement can be seen in **Fig.** 20(b). The oscillator is working at ω_a, the frequency of the input signal is ω_b and it is amplified by backward wave amplification using the same circuit. The i-f current can be extracted from the collector circuit.

Since both the BWO and the BWA are working on the same principle and ω_a and ω_b are assumed to be very near to each other the spatial variations of the space charge waves can be taken as identical. This will permit writing Eqn (5) in the following form :-

$$i_{if}(L) = j \frac{\omega_{if}}{\omega_a} \frac{\beta_{ea}}{v_o} B_b B_a g \int_o^L \left[\left| f_s(z) \right|^2 - \left| f_f(z) \right|^2 \right] dz \qquad (6)$$

where B_a, B_b - amplitudes of input signal and local oscillator signal respectively

g - gain of the BWA,

L - length of the interaction region

$f_s(z)$, $f_f(z)$ - normalised functions representing the spatial variation of the slow and fast space charge waves respectively.

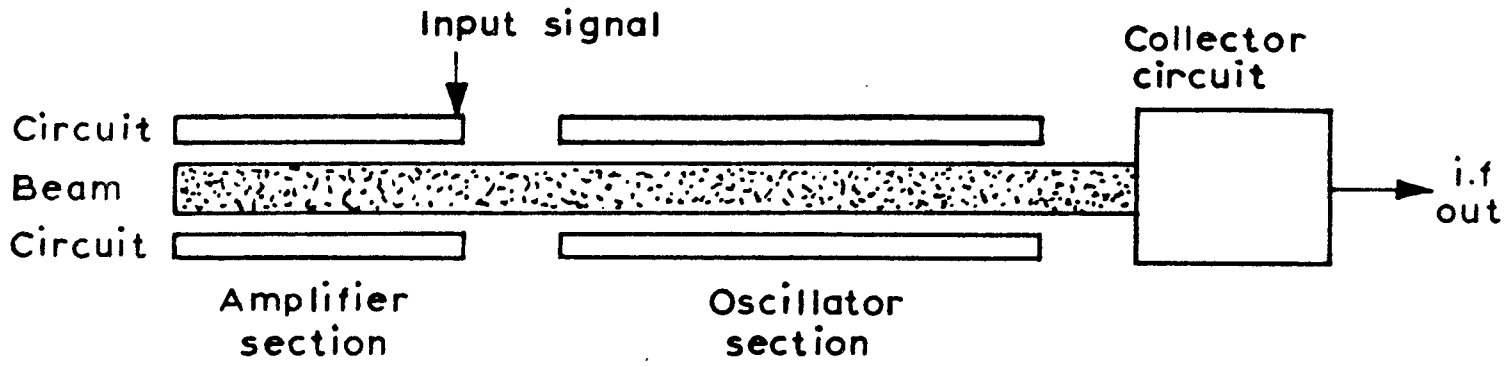

FIGURE 20 (a) Two Circuit B.W.C.

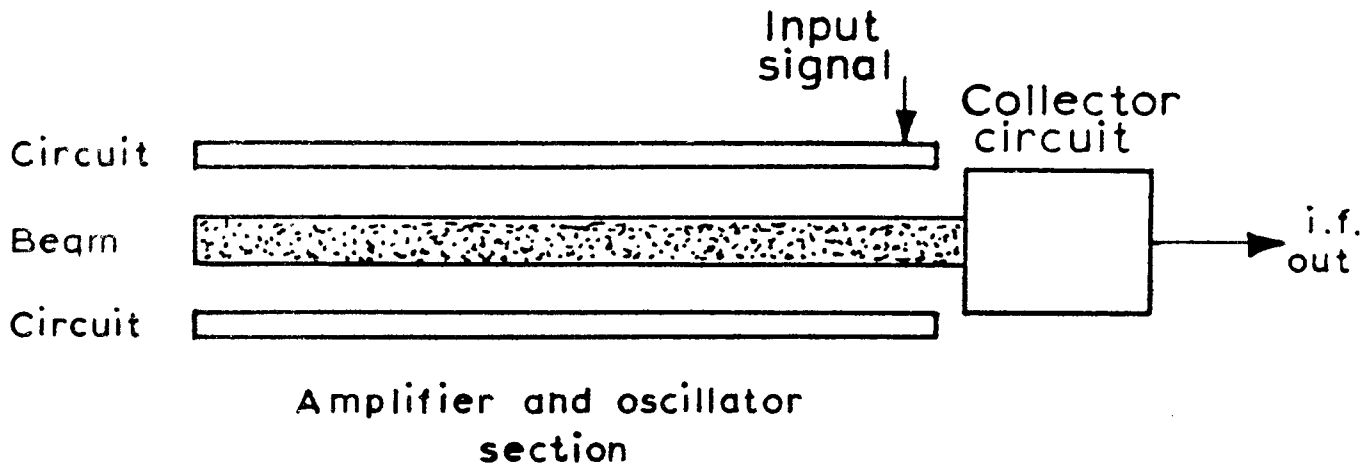

FIGURE 20 (b) One Circuit B.W.C.

Assuming for the moment no losses (the effect of losses will be treated in the next Section) the conservation of energy implies that :-

$$\left| f_s(z) \right|^2 + \left| f_c(z) \right|^2 - \left| f_f(z) \right|^2 = 1 \qquad (7)$$

where f_c is representing the variation of circuit wave, and $f_c(0) = 1$.

Thus in the absence of losses only the circuit wave appears under the integral sign.

Our next aim is to calculate Eqn (6) both for the 3-wave case (treated so far) and for the 2-wave case when the fast space charge wave is omitted. Generally both space charge waves are necessary for describing a beam type amplifier but if QC is sufficiently large (Pierce's space charge parameter) the operation of the BWO and the BWA can be explained by the interaction of the circuit wave and that of the slow space charge wave. The advantage of the 2-wave approach is that both the oscillation conditions and the amplification parameters can be analytically determined showing clearly the effect of different factors.

In order to satisfy ourselves how good the high QC approximation is, we compare the relevant expressions with those obtained from low QC theory (detailed calculations can be found in Appendices III and IV). Writing the gain of the BWA in the following approximate form :-

$$g \simeq \frac{1}{\frac{\omega_{if}}{\omega_a} K} \qquad (8)$$

the variation of K is plotted in Fig 21 and 22 against QC for $(1 + \alpha_1)/C = 10$ and 100 ($\alpha_1 = v_o/v_g$ where v_g - group velocity). It may be seen that if QC > 0.75 the discrepancy between the theories is negligible. For QC = 0 the high QC approximation obviously breaks down. If we chose, however, a value like QC = 0.25 the value of K deviates little from that given by 3 wave theory for QC = 0. (We have to note here that a 50% deviation is regarded in this context as "little" since a few db accuracy in determining the i-f current would be sufficient.)

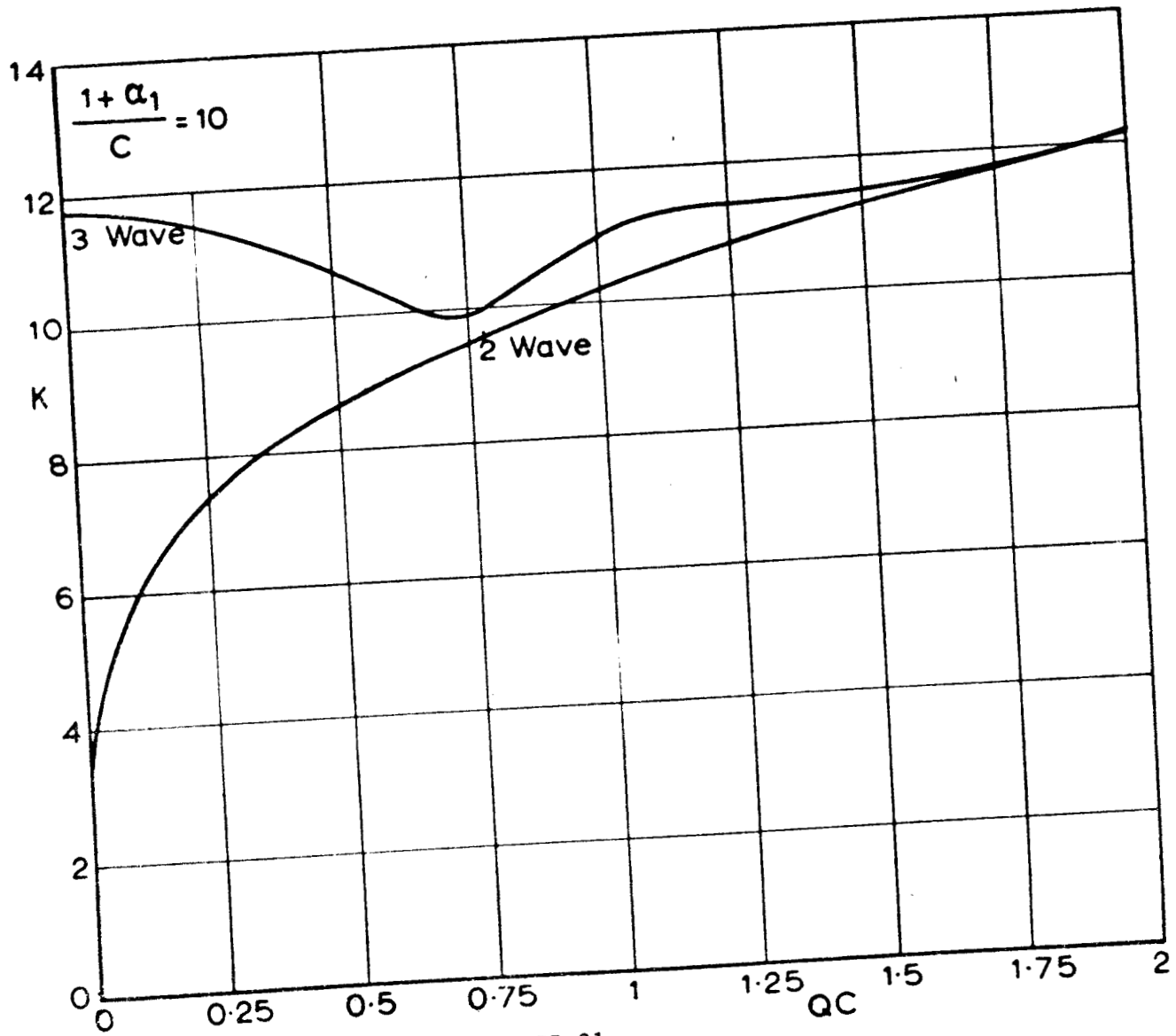
$\frac{1+\alpha_1}{C} = 10$
3 Wave
2 Wave
K
QC
14
12
10
8
6
4
2
0
0
0·25
0·5
0·75
1
1·25
1·5
1·75
2

FIGURE 21

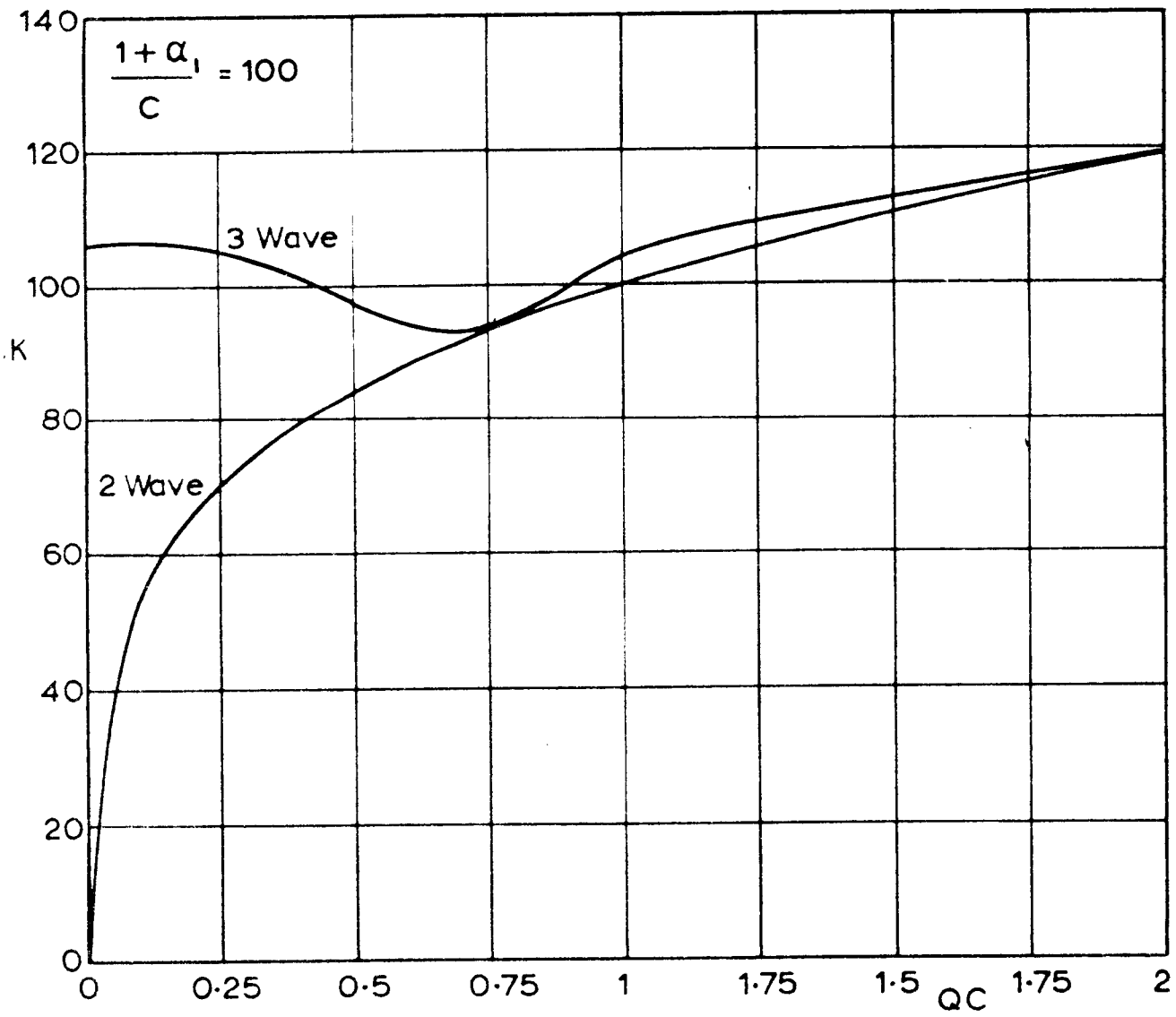
140
120
100
80
60
40
20
0
K
$\frac{1+\alpha_1}{C} = 100$
3 Wave
2 Wave
0
0·25
0·5
0·75
1
1·75
1·5
QC
1·75
2

FIGURE 22

Similarly if we plot the variation of the circuit wave amplitude square for QC = 0 and for high QC we can see (Fig 23) that they are fairly close to each other. Taking further into account that at QC = 0.25 the value of CN resulting in oscillation differs only by 10% from its value at QC = 0, we can safely come to the conclusion that high QC theory will be sufficiently accurate for the present calculations.

b. High QC calculations for a lossy structure

As derived in Appendix IV the i-f current is given by the following expression :-

$$i_{if} = \frac{B_{sa} B_{cb}}{V_o} F(\alpha L, \alpha_1, h) \qquad (9)$$

where α - attenuation coefficient of the circuit wave and $h = C^2 \sqrt{QC}$. It is worthwhile to note that Eqn (9) is independent of ω_{if}/ω_a. This is characteristic to the one circuit convertor where conversion is proportional to ω_{if}/ω_a while BWA gain is inversely proportional to it, as seen in Eqn (8). Plotting F against $\Omega \simeq 8.68\ \alpha L$ (total circuit loss) in db-s for several values of α_1 and h it can be seen (Fig 24) that low loss, low value of h, and low value of α_1 are preferable but as the function is rather slowly varying none of the parameters are critical. The effect of losses on the length (or starting current) of the BWO are shown by the dotted lines. A further conclusion emerging from Eqn (9) is that by reducing DC voltage the i-f current can be increased. The relationship is, however, not simply inversely linear because α_1 and h are also functions of the DC voltage.

The analysis for a 2-circuit BWC is very similar as can be seen in Appendix IV. The only points which have to be remembered here are that the gain can be adjusted separately and conversion gain is proportional to i-f frequency.

c. Comparison of the one-circuit and two-circuit BWC

A qualitative comparison is given in Table 1, the + and - signs denoting advantage and disadvantage respectively. The one-circuit BWC can be used only if the required i-f frequency is well within the amplification region of the BWA. In this case, however, larger gain can be achieved because instability is no longer a danger. If we assume identical gain the i-f currents obtained by the two different arrangements compare as follows

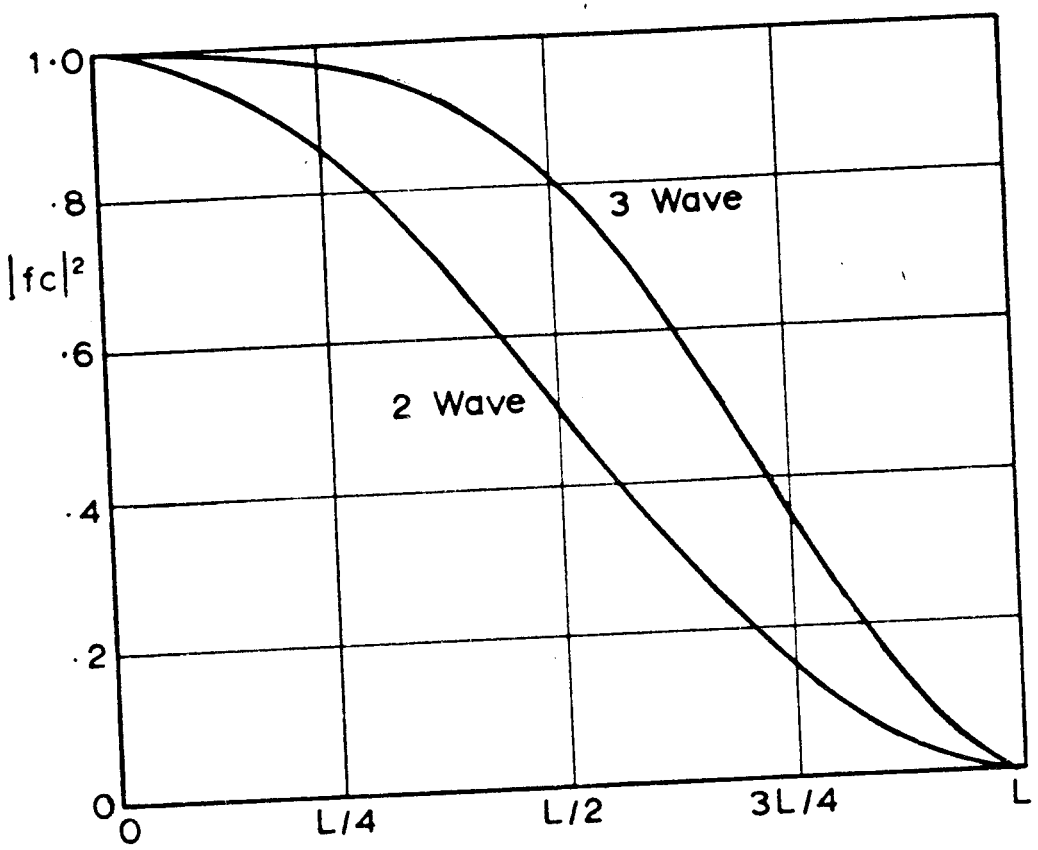

FIGURE 23

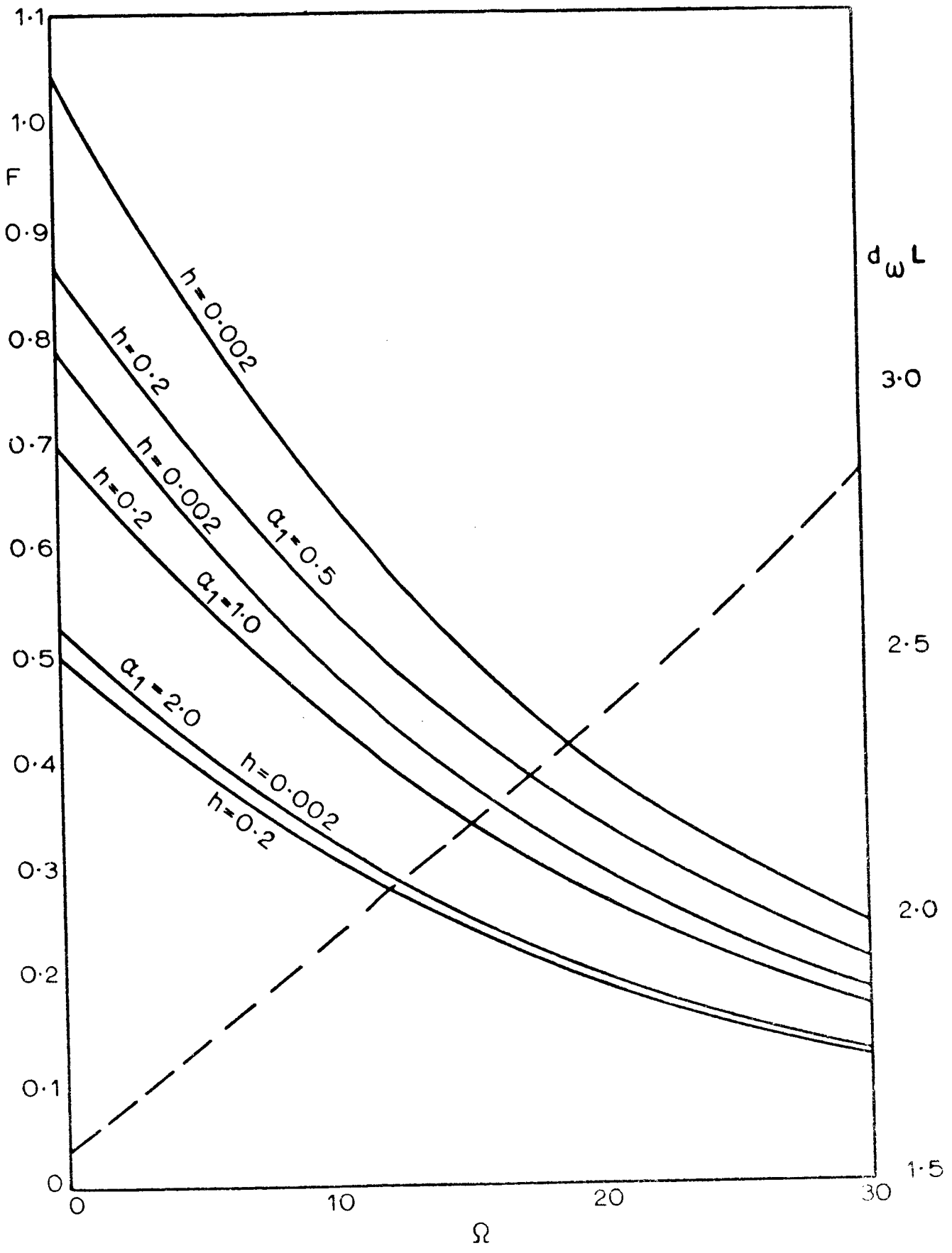
1·1
1·0
F
0·9
0·8
0·7
0·6
0·5
0·4
0·3
0·2
0·1
0
0
10
20
30
Ω
$d_\omega L$
3·0
2·5
2·0
1·5
h=0·002
h=0·2
h=0·002
h=0·2
h=0·002
h=0·2
α_1=0·5
α_1=1·0
α_1=2·0

FIGURE 24

$$\frac{\text{i-f current two-circuit}}{\text{i-f current one-circuit}} = \frac{\sqrt{1-y^2} + 2\, e^{\frac{\alpha L}{2}}\, y \sin \sqrt{1-y^2}\, d_{cs} L}{\frac{1}{4}\left\{\frac{1}{y}\left(e^{\alpha L}-1\right) - y\left[\left(4y^2-3\right)\, e^{\alpha L}-1\right]\right\}} \qquad (10)$$

where $y = \frac{\alpha}{2d_{cs}}$

Plotting Eqn (12) in Fig 25 against Ω it can be seen that for a lossless structure the two-circuit arrangement is somewhat better but as the losses increase the situation is reversed.

TABLE 1

	length	weight	image rejection	freedom for choosing the i-f frequency	stability	noise
one-circuit	+	+	-	-	+	-
two-circuit	-	-	+	+	-	+

3. Ballistic Analysis

An approximate analysis of the backward wave converter was obtained by Dr. Murray Sirkis using a simple ballistic analysis. This was presented as Appendix I of Bimonthly Report No. 2. The simple analysis was then expanded by investigating the parameter χ and the dependence of current amplitude on the position along the trajectory which were presented as Appendices I and II of Bimonthly Report No. 3. The analysis was then further extended to include the effects of space-charge and of the cosinusoidal envelope of the electric field. These extensions are included as Appendices I and II of this report and will not be expanded upon further in this section.

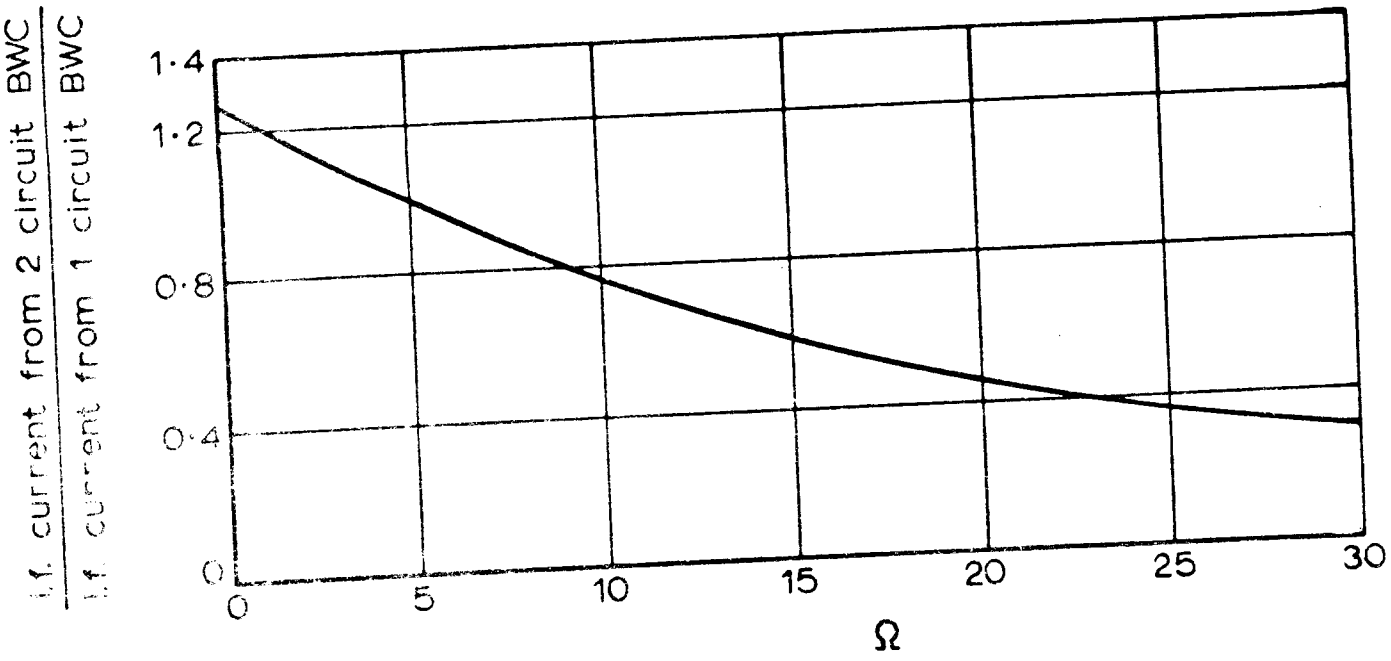
i.f. current from 2 circuit BWC
i.f. current from 1 circuit BWC
1·4
1·2
0·8
0·4
0
0
5
10
15
20
25
30
Ω

FIGURE 25

4. Comparison of space charge wave and ballistic analyses

Space charge wave theories have been very successful in predicting the low level operation of electron beam devices and even nonlinear phenomena can be tackled by using higher order perturbations. The first effect of non-linearity can be relatively easily obtained but the disadvantage of this method is that it fails to predict saturation effects. A second order theory is possible but analytically intractable. Thus it is much more convenient to employ a ballistic analysis for this purpose as done in Appen. I & II. Further advantage of ballistic theory that the conclusions are not restricted to start of oscillation conditions. It is, however, less flexible which means that two separate analyses would be needed for the one-circuit and two-circuit BWC.

The i-f currents given by the two different theories for a lossless two-circuit BWC are as follows :-

$$I_{if} = -\frac{kI_o}{4\eta}\,\frac{\omega_{if}}{\omega}\,\frac{\omega^2\ \sqrt{2KP}\ \ell^2}{\pi^3 V_o^2}\ \sqrt{4+\pi^2}$$

from ballistic theory and

$$i_{if} = \frac{\omega_{if}}{\omega_a}\ g\ \frac{4N}{V_o}\ B_{sa}\ B_{sb}$$

from Eqn (A.16) of space charge wave theory substituting $\alpha = 0$.

The two expressions do not seem to agree at first sight but this is due to the unfortunate fact of different notations and different variables. If we take into account that

$$I_{if} = i_{if}, \quad I_o = i_o, \quad \ell = L, \quad B_{sa} = \sqrt{P}$$

and

$$\kappa I_o = g B_{sb} \sqrt{\frac{\alpha I_o}{\omega_q V_o}}$$

it can be easily shown that the two formulae are identical but for a constant factor which is

$$\frac{\pi}{\sqrt{4 + \pi^2}} = 0.875$$

This agreement is very encouraging and gives confidence in the validity of both theories.

B. Slow Wave Structures

1. Choice of Slow-wave Structure

In considering the most suitable type of slow wave structure for the convertor we have to bear in mind that the requirements of over-riding importance are low noise and high efficiency; other desirable features are small size and low weight. To these, the designer of a millimeter tube must add the desirability of a structure which is easy to fabricate.

The efficiency of a backward wave oscillator under the low space charge conditions occurring in millimeter tubes is proportional to the Pierce parameter C^1 where $C3 = \frac{K V_o}{4I_o}$ and K is the interaction impedance of the space harmonic in use, V_o is the beam voltage and I_o the beam current. The theoretical analysis of convertor operation suggests that V_o should be kept as low as possible and hence to obtain as high an efficiency as possible K should be as high as possible.

Of the circuits which have been studied the helix and ladder type circuits all have high interaction impedances compared with the coupled cavity circuit. The latter, therefore, although it has been used successfully for backward wave oscillators is not very suitable for this application, especially as it may not be possible to take advantage of one of its important properties, high heat dissipation, because the low noise requirement may necessitate small interception of the beam by the circuit if a single circuit is used in the convertor.

The simple helix is a very good circuit in theory but at millimeter wavelengths is very small and difficult to make and, unless unconventional methods are used to support it, has very poor heat dissipation indeed. The same objections hold, with stronger force, in the case of the bi-filar helix. The ring and bar structure is more rugged but it has the property, exploited when used for high power forward wave amplifiers, that the fundamental forward wave is increased at the expense of the harmonics.

The ladder type structures considered are the interdigital line, the Karp and Anti-Karp structures and the ridge loaded meander line. The interdigital line involves the problem of intermeshing two structures, as does the bi-filar helix. This is not only a difficult constructional problem in itself but it makes all the more difficult the attainment of the symmetry required to avoid a stop band at $\beta \ell = \pi$ in these bi-periodic structures. The interdigital line, anti-Karp structure and the bi-filar helix have backward fundamental space harmonics, which

1. Grow, R.W., Watkins, D. A., "Backward Wave Oscillator Efficiency" Proc. IRE 43, P848, July 1955.

results in a high impedance but also makes them impossibly small at millimeter wavelengths, especially if V_o has to be kept low. On the other hand the next backward harmonic would have too low a value of K. At these frequencies the use of the first backward harmonic of a forward fundamental seems optimum.

This leaves the Karp structure and the ridge loaded meander line as being the most promising circuits for use in a millimeter backward wave convertor, because of their relatively high impedance, reasonably good heat dissipation, large size and ease of construction. A detailed analysis has therefore been made of these two structures and the results are discussed below.

The Karp Structure and the Ridge Loaded Meander Line

The ridge loaded meander line is shown diagrammatically in Fig. 26, which defines the physical parameters. Dispersion curves and curves of the impedance of -2 space harmonic, which is the space harmonic suitable for backward wave operation were calculated and presented in Bimonthly Report No. 2. These were plotted as the normalized frequency f' against , the phase change per bar and the -2 space harmonic impedance Z_{-2} against f'. $\frac{W_2}{P}$, $\frac{d}{q}$ and α are parameters and

$$f' = f/f_o$$

f is the frequency

$$f_o = \frac{c}{4b}$$

c is the velocity of light

$$\alpha = a/b$$

The Karp structure is shown diagrammatically in Fig 27 and Fig 28- 42 are curves of the dispersion and the impedance of the -1 space harmonic which is the harmonic in this structure most suitable for backward wave operation. The curves are presented in the same form as those for the ridge loaded meander line.

Examination of the curves shows that with both circuits, as the ridge is brought closer to the line (i.e. as $\frac{W_1}{P}$ is decreased) the bandwidth increases.

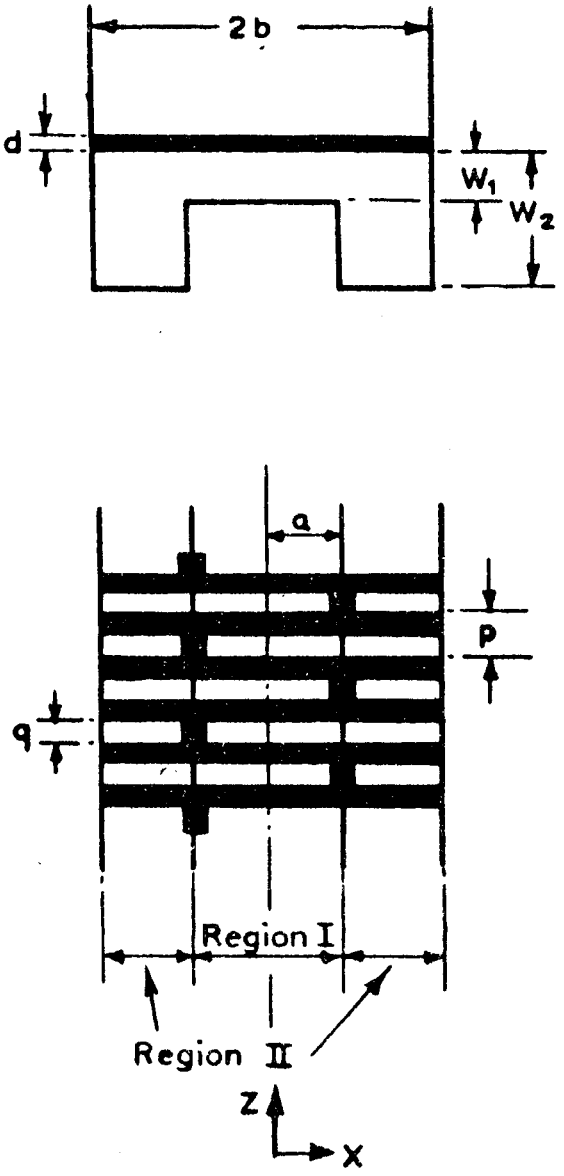

Figure 26

Ridge Loaded Meander Line

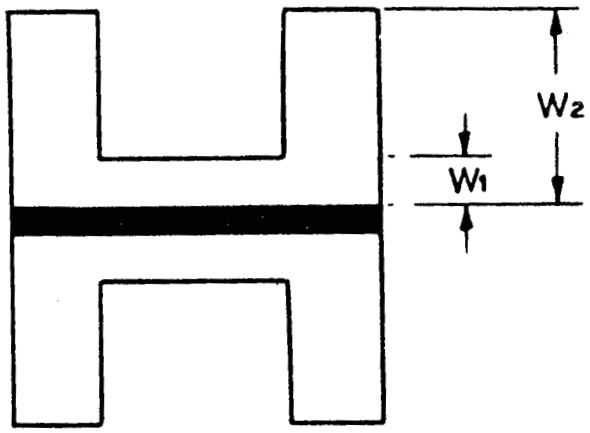

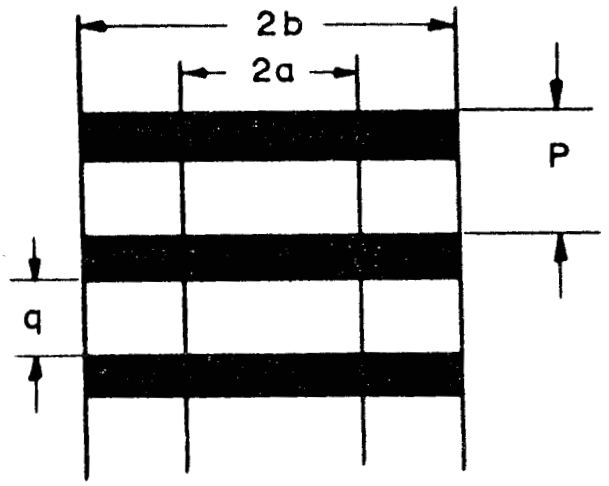

Symmetrical Karp Structure

Figure 27

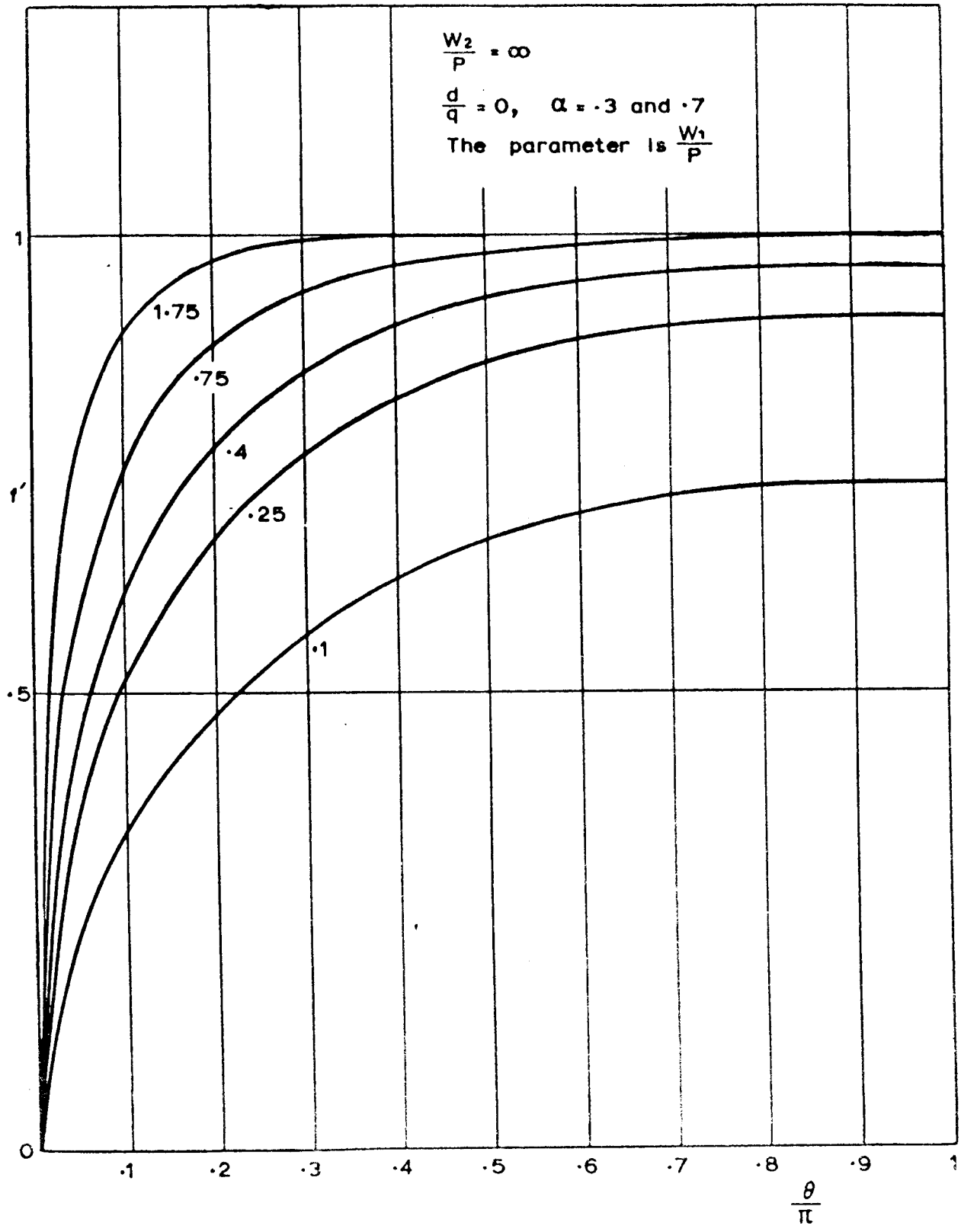
$\frac{W_2}{P} = \infty$
$\frac{d}{q} = 0$, $\alpha = \cdot 3$ and $\cdot 7$
The parameter is $\frac{W_1}{P}$
1·75
·75
·4
·25
·1
f'
1
·5
0
·1
·2
·3
·4
·5
·6
·7
·8
·9
1
$\frac{\theta}{\pi}$

Figure 28

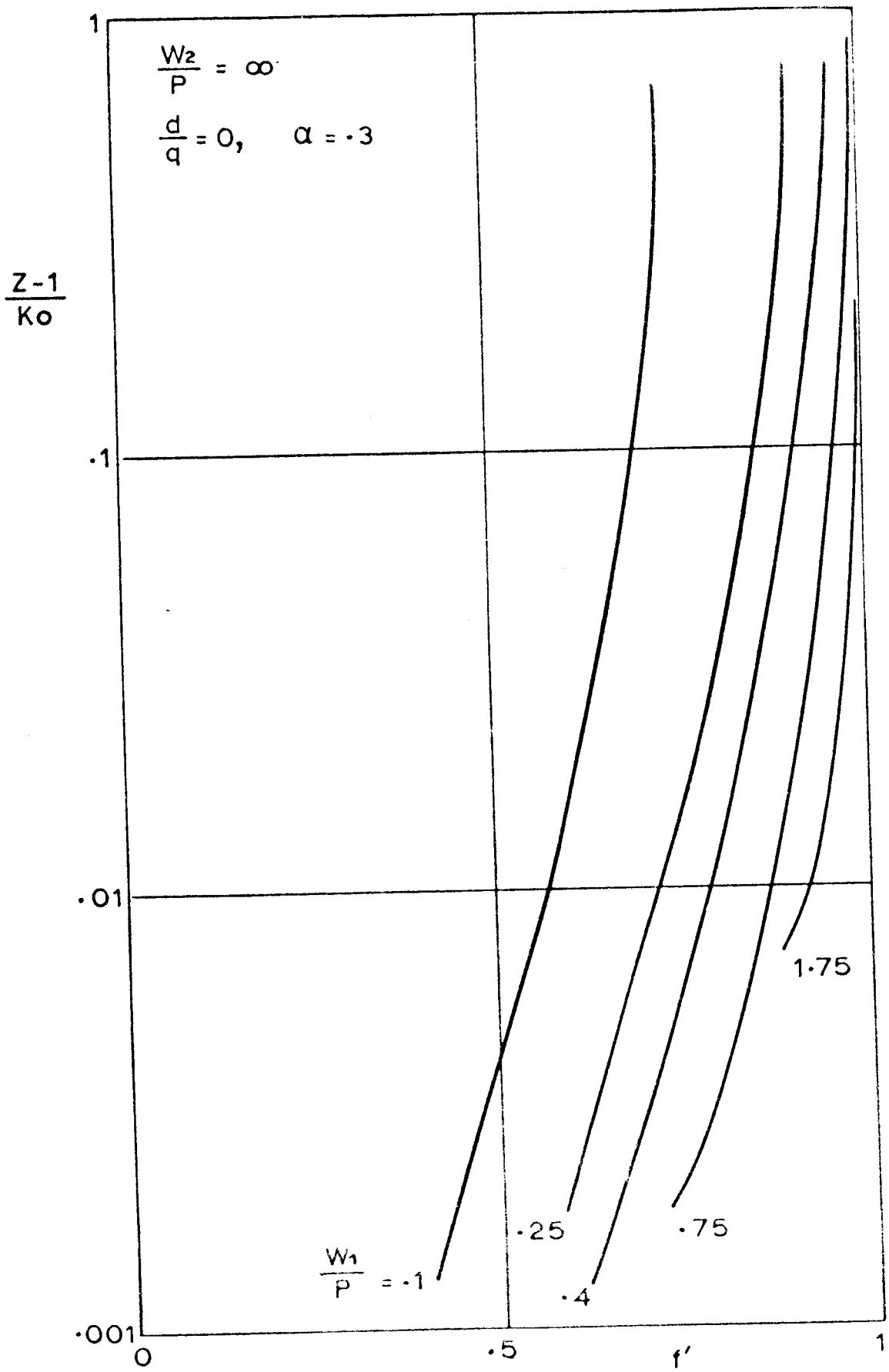
$\frac{W_2}{P} = \infty$
$\frac{d}{q} = 0, \quad \alpha = \cdot 3$
$\frac{Z-1}{K_o}$
1
·1
·01
·001
0
·5
1
f'
$\frac{W_1}{P} = \cdot 1$
·25
·4
·75
1·75

Figure 29

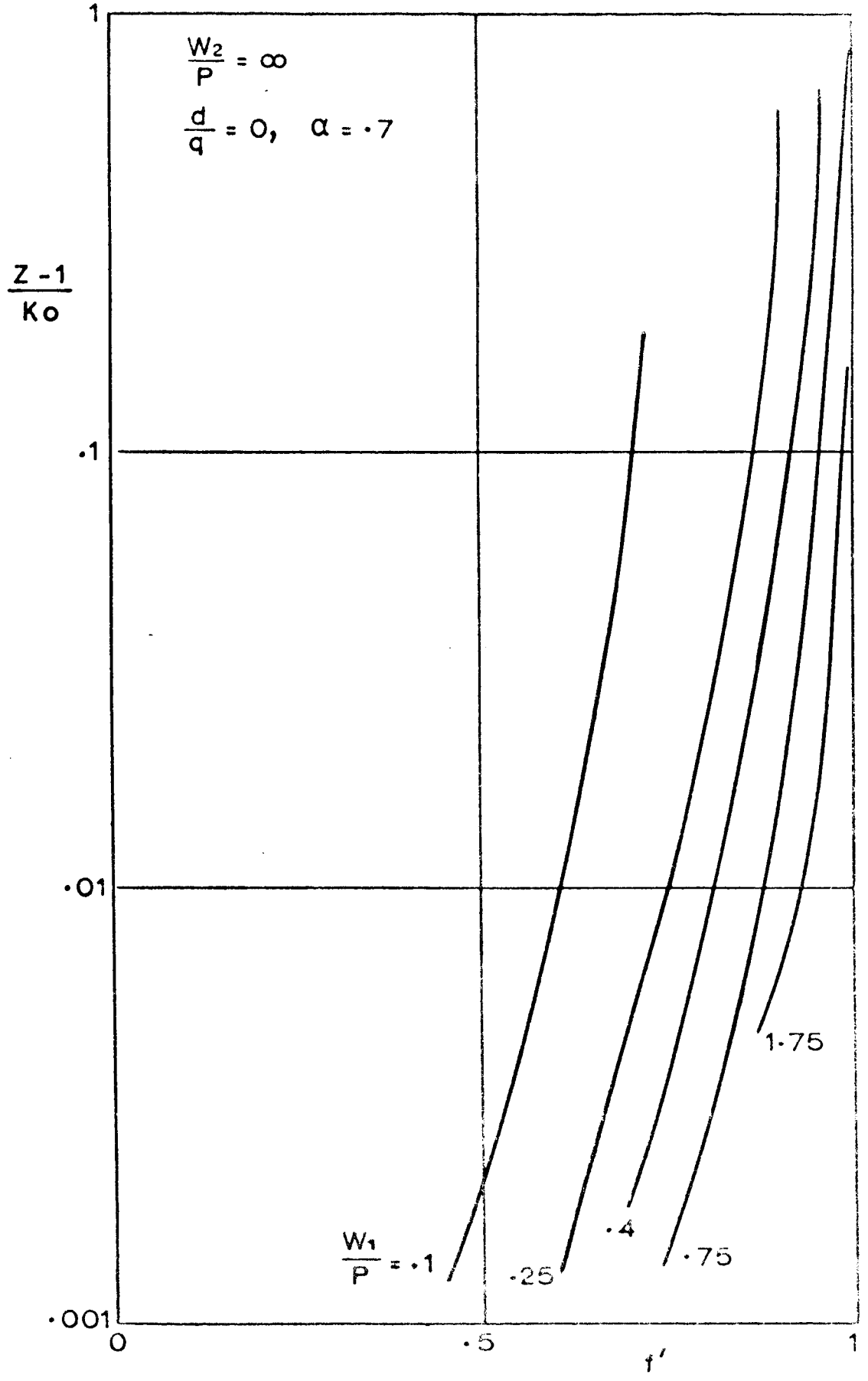
$\frac{W_2}{P} = \infty$
$\frac{d}{q} = 0, \quad \alpha = \cdot 7$
$\frac{Z-1}{Ko}$
1
·1
·01
·001
0
·5
1
f'
$\frac{W_1}{P} = \cdot 1$
·25
·4
·75
1·75

Figure 30

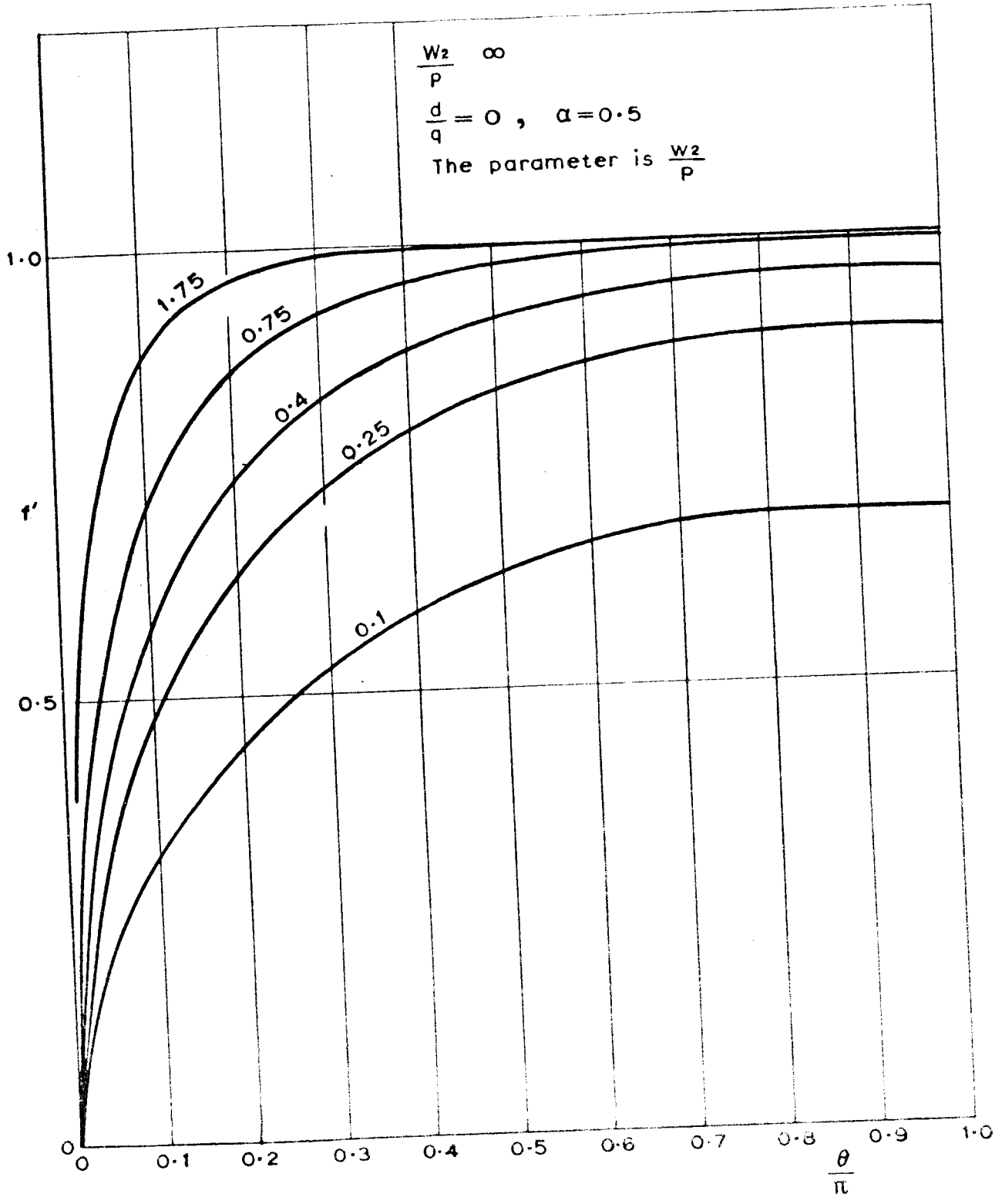
W2/P ∞
d/q = 0 , α=0·5
The parameter is W2/P
1·75
0·75
0·4
0·25
0·1
f'
1·0
0·5
0
0
0·1
0·2
0·3
0·4
0·5
0·6
0·7
0·8
0·9
1·0
θ/π

Figure 31

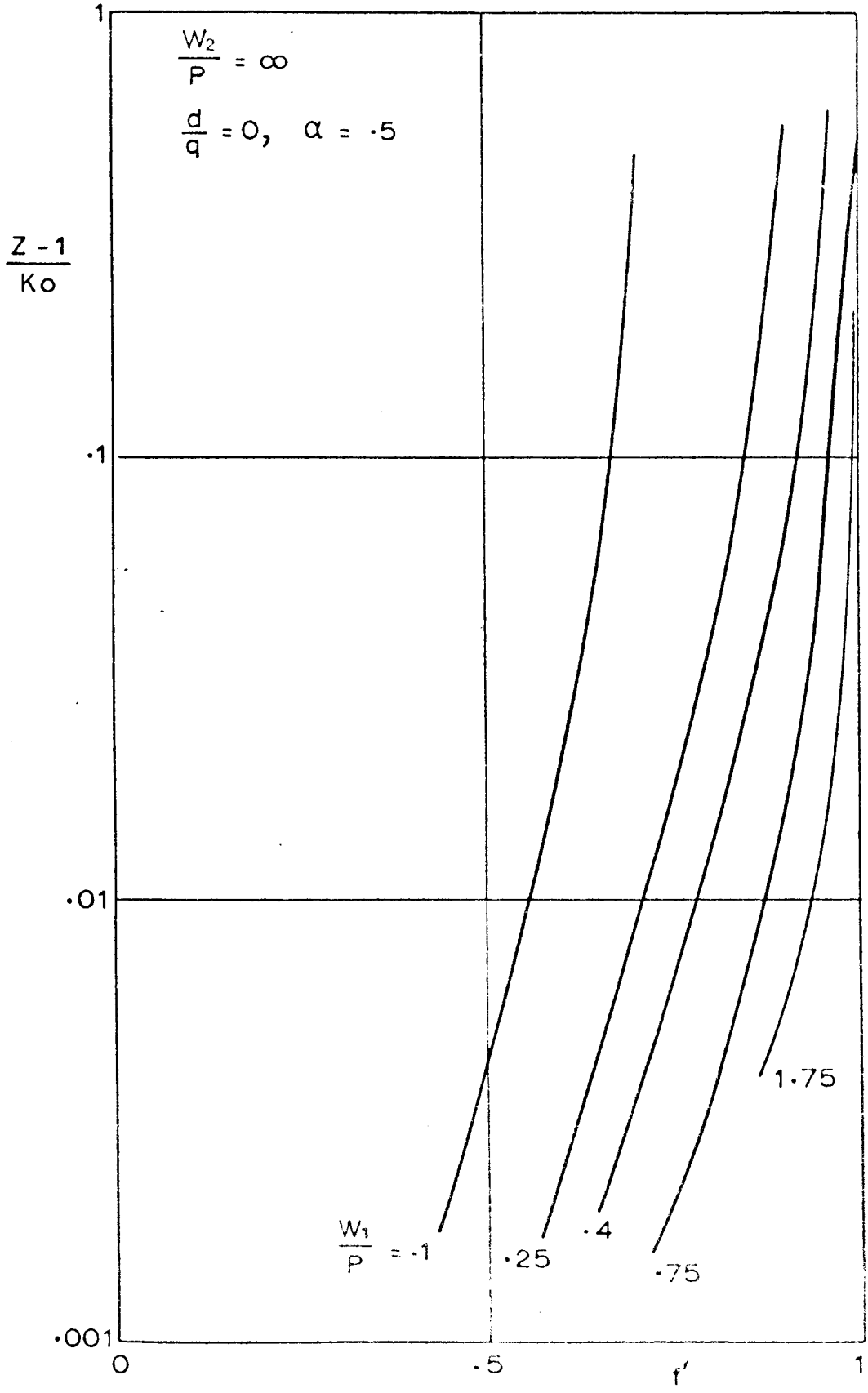
$\frac{W_2}{P} = \infty$
$\frac{d}{q} = 0, \quad \alpha = .5$
$\frac{Z-1}{Ko}$
1
.1
.01
.001
0
.5
1
f'
$\frac{W_1}{P} = -.1$
.25
.4
.75
1.75

Figure 3.2

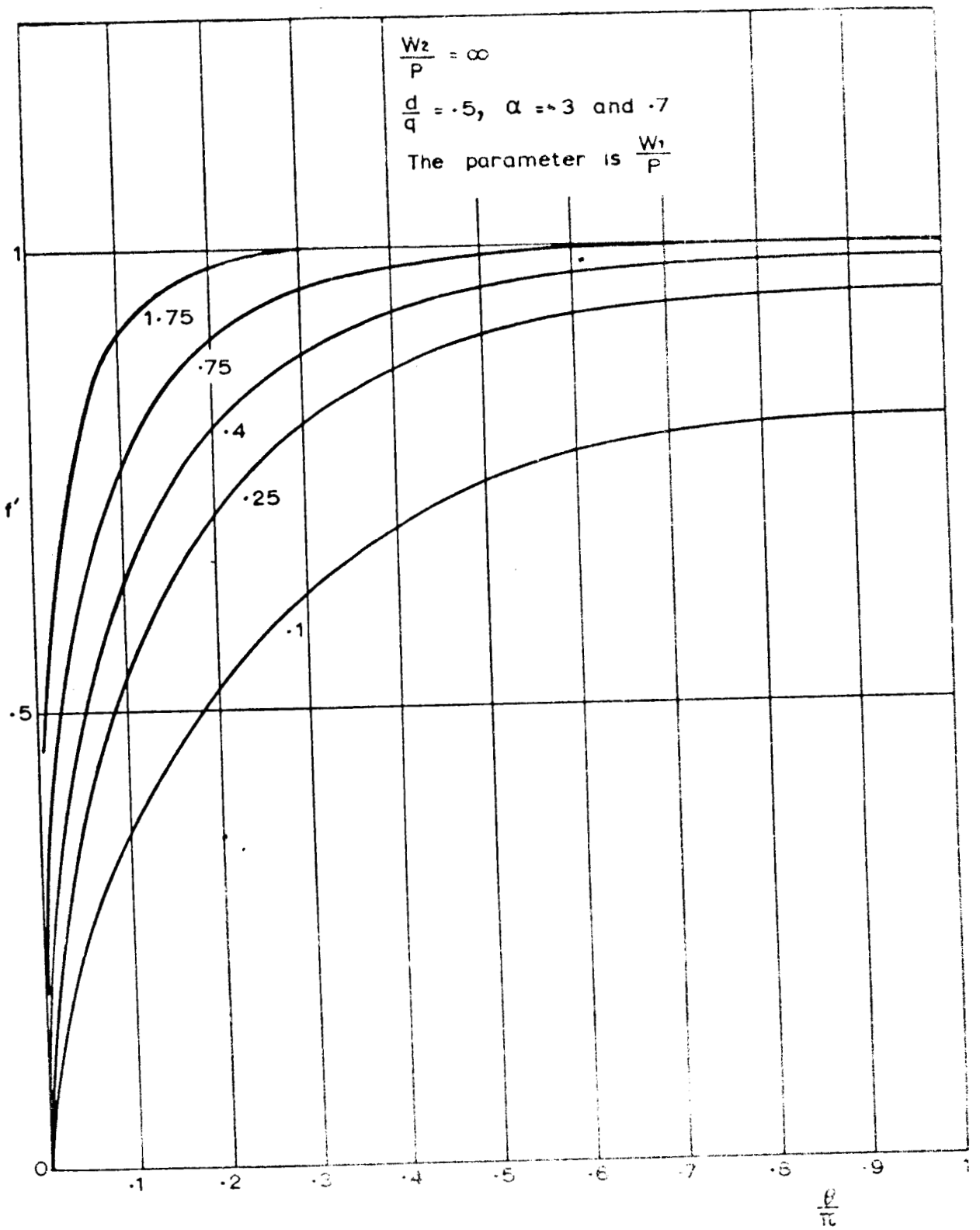
W2/P = ∞
d/q = ·5, α = ·3 and ·7
The parameter is W1/P
1·75
·75
·4
·25
·1
f'
1
·5
0
·1
·2
·3
·4
·5
·6
·7
·8
·9
θ/π

Figure 3

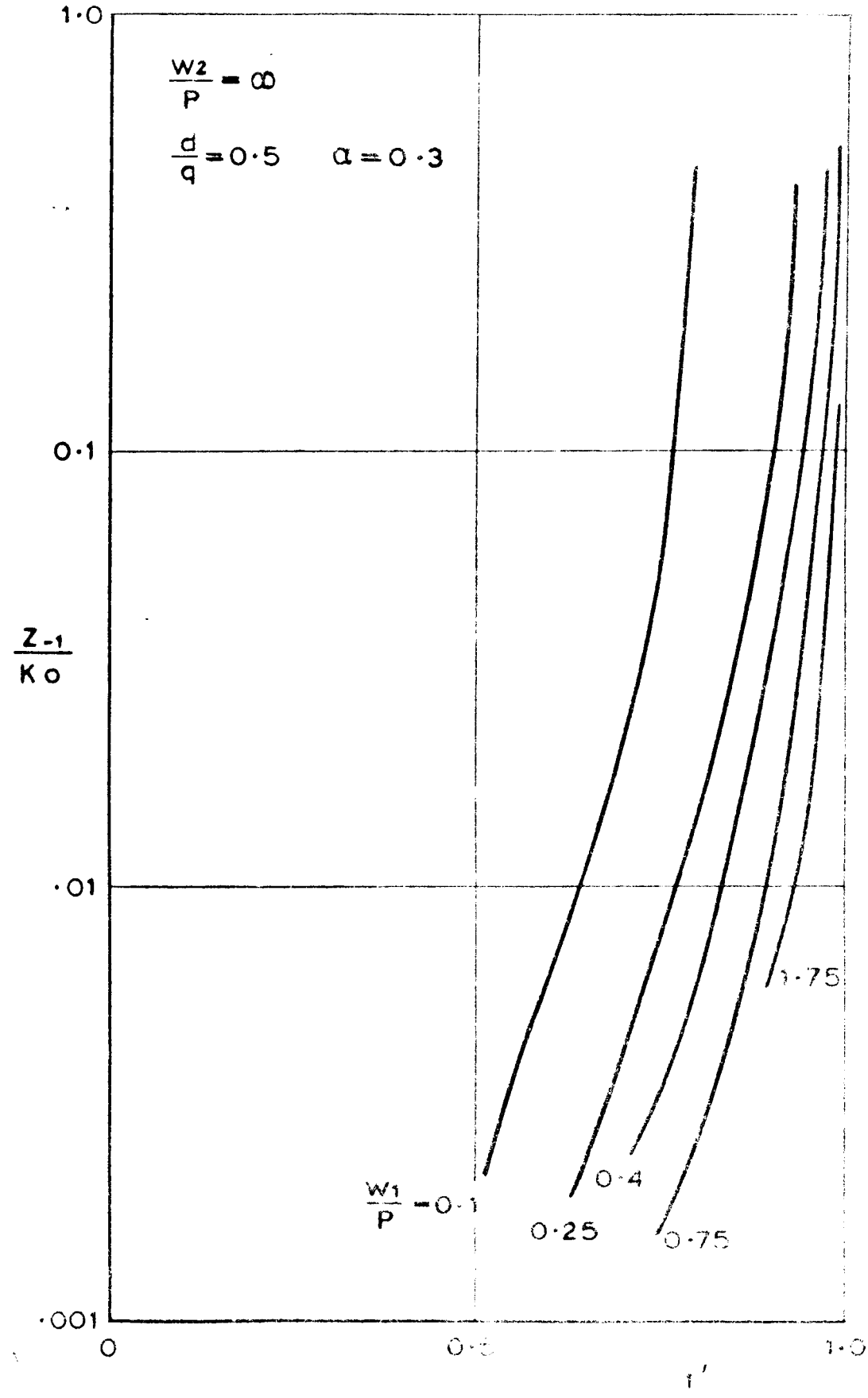
1·0
$\frac{W_2}{P} = \infty$
$\frac{d}{q} = 0·5$ $\alpha = 0·3$
0·1
$\frac{Z_{-1}}{K_0}$
·01
·001
0
0·5
1·0
1'
1·75
0·4
$\frac{W_1}{P} = 0·1$
0·25
0·75

Figure 3a

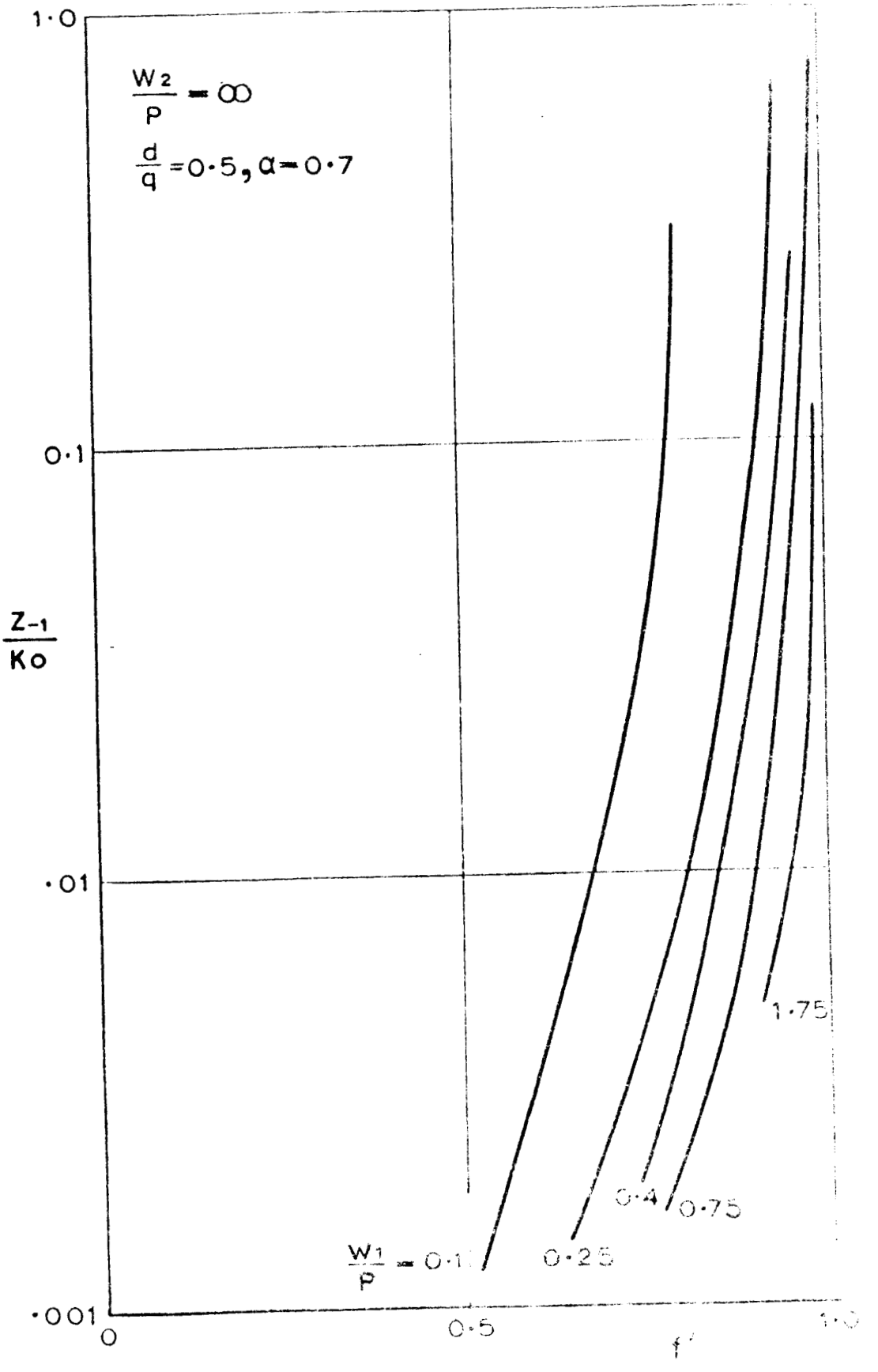
1·0
$\frac{W_2}{P} = \infty$
$\frac{d}{q} = 0·5, \alpha = 0·7$
0·1
$\frac{Z_{-1}}{K_0}$
·01
·001
0
0·5
1·0
f'
1·75
0·4
0·75
$\frac{W_1}{P}$ = 0·1
0·25

Figure 5.

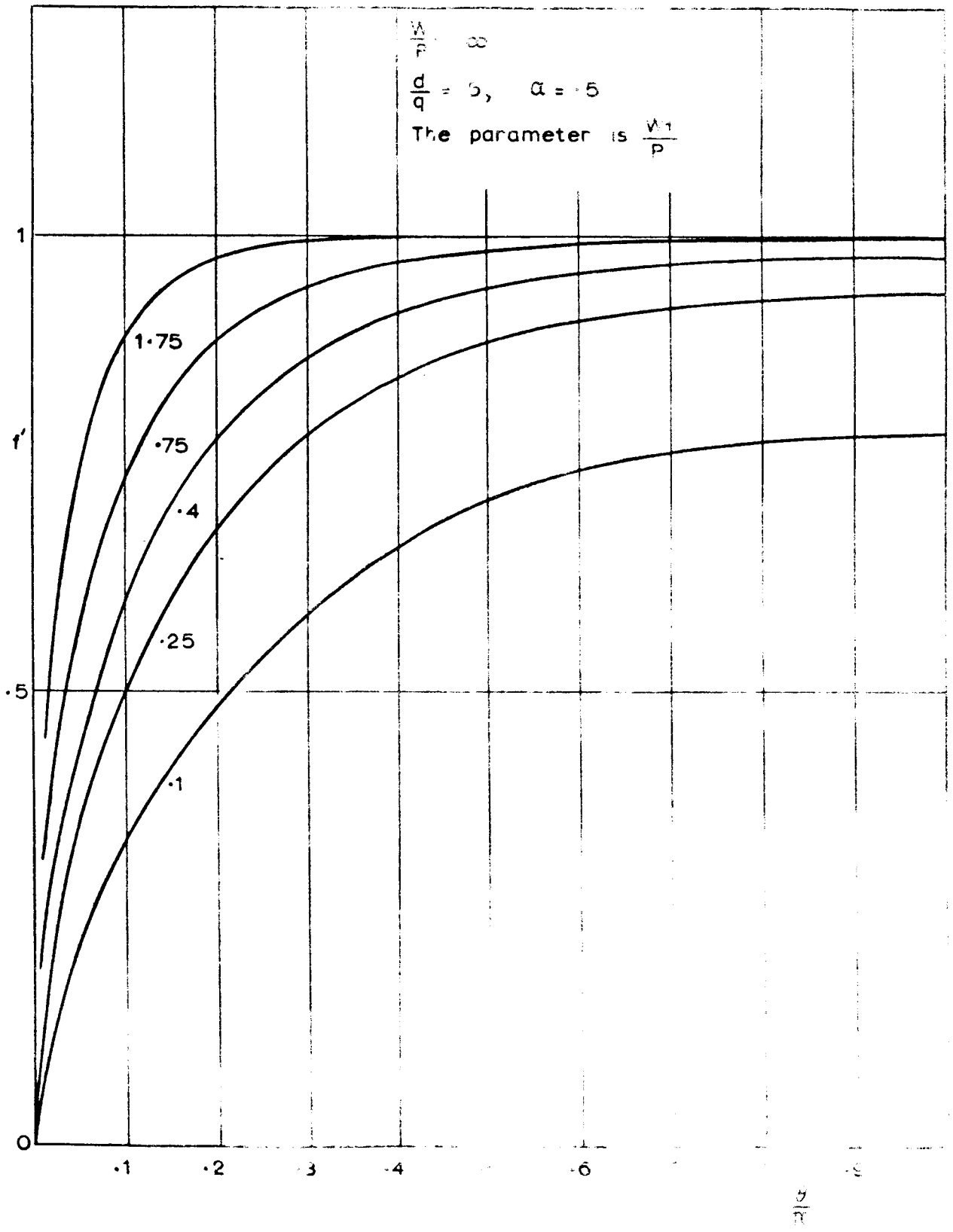
$\frac{W}{P}$ ∞
$\frac{d}{q}$ = 5, α = ·5
The parameter is $\frac{W_1}{P}$
1
·5
0
f'
1·75
·75
·4
·25
·1
·1
·2
·3
·4
·6
$\frac{y}{h}$

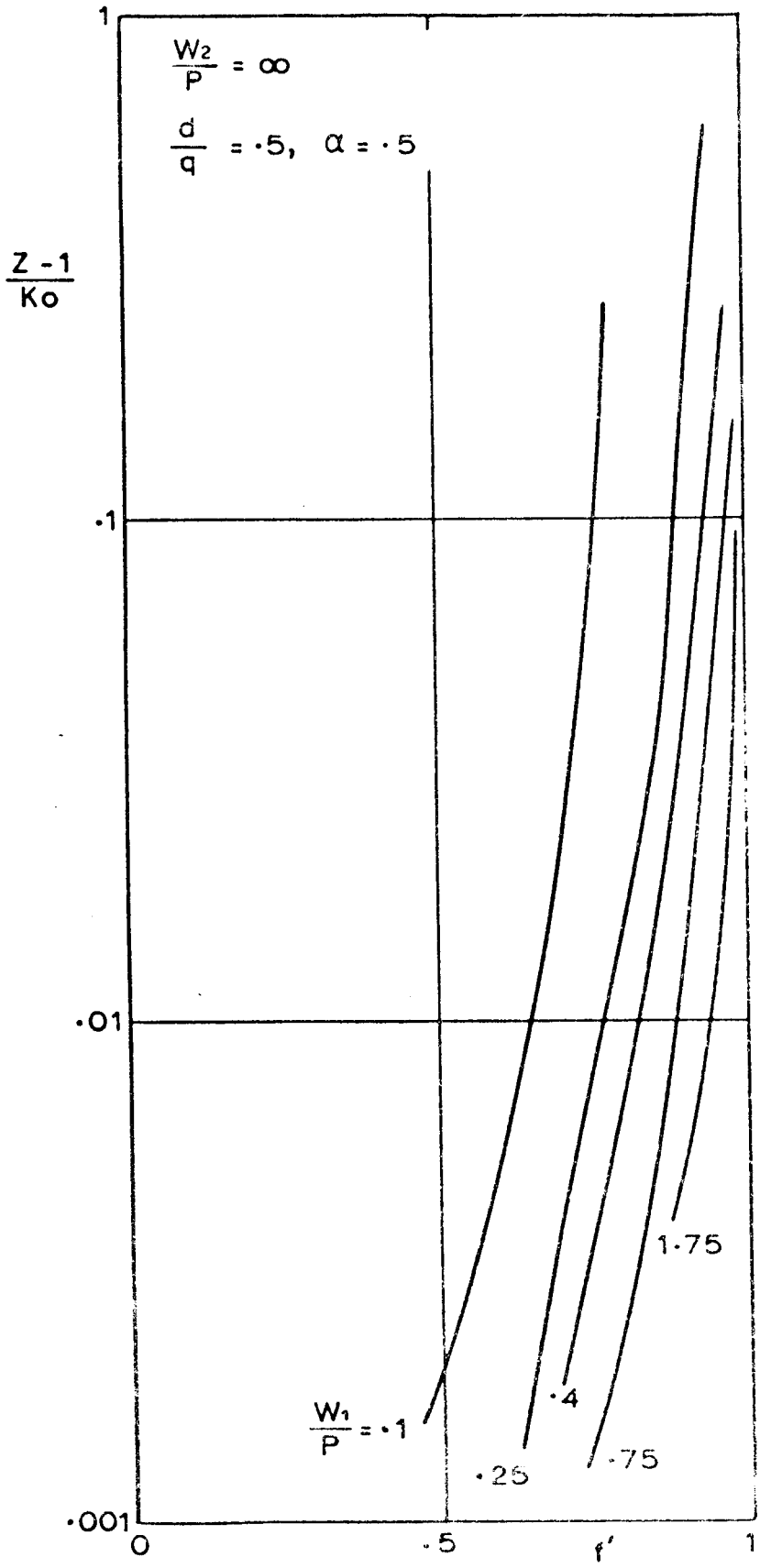
1
$\frac{W_2}{P} = \infty$
$\frac{d}{q} = \cdot 5, \ \alpha = \cdot 5$
$\frac{Z-1}{Ko}$
·1
·01
·001
0
·5
f'
1
$\frac{W_1}{P} = \cdot 1$
·25
·4
·75
1·75

Figure 37

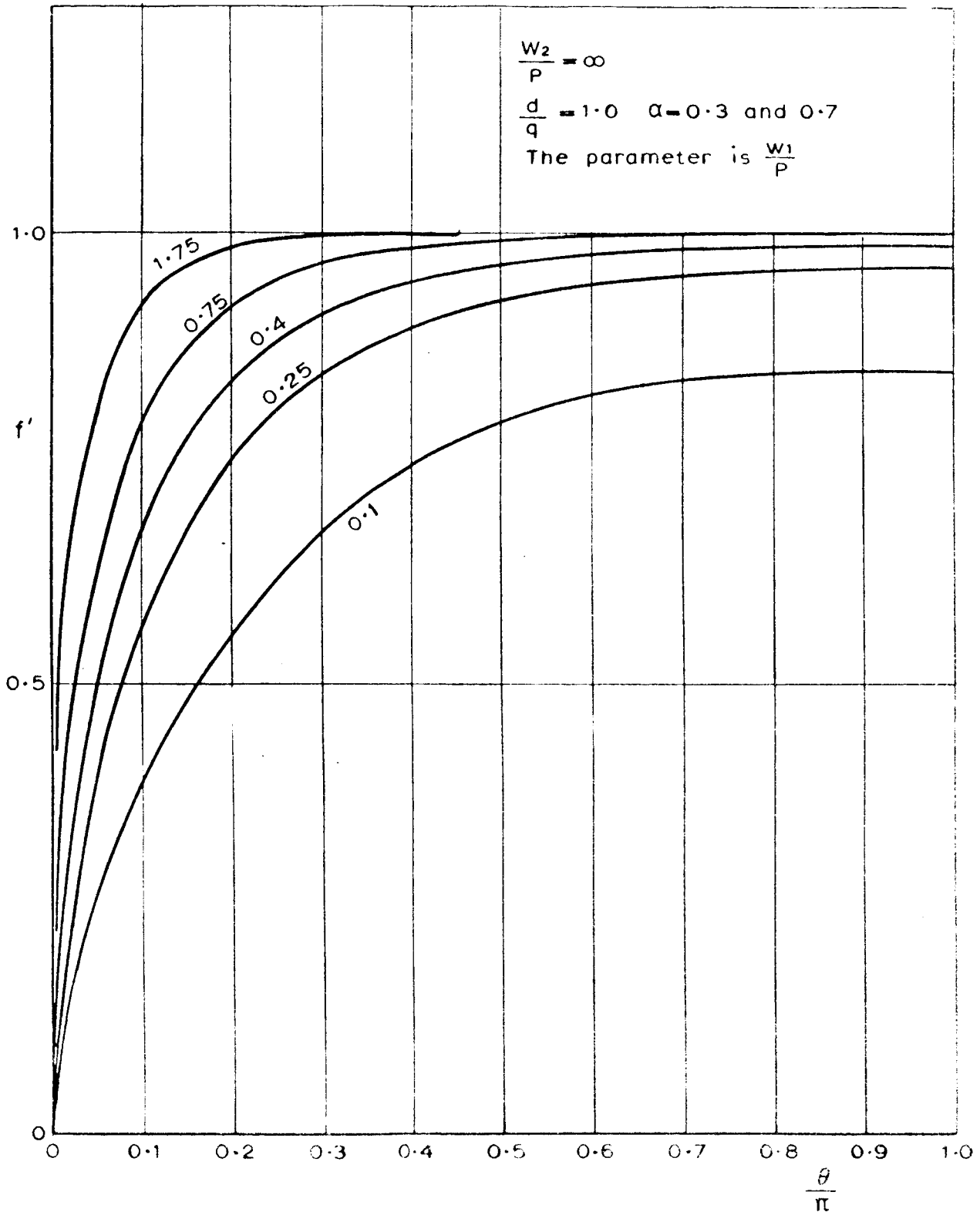
$\frac{W_2}{P} = \infty$
$\frac{d}{q} = 1{\cdot}0$ $\alpha = 0{\cdot}3$ and $0{\cdot}7$
The parameter is $\frac{W_1}{P}$
1·75
0·75
0·4
0·25
0·1
f'
1·0
0·5
0
0
0·1
0·2
0·3
0·4
0·5
0·6
0·7
0·8
0·9
1·0
$\frac{\theta}{\pi}$

Figure 38

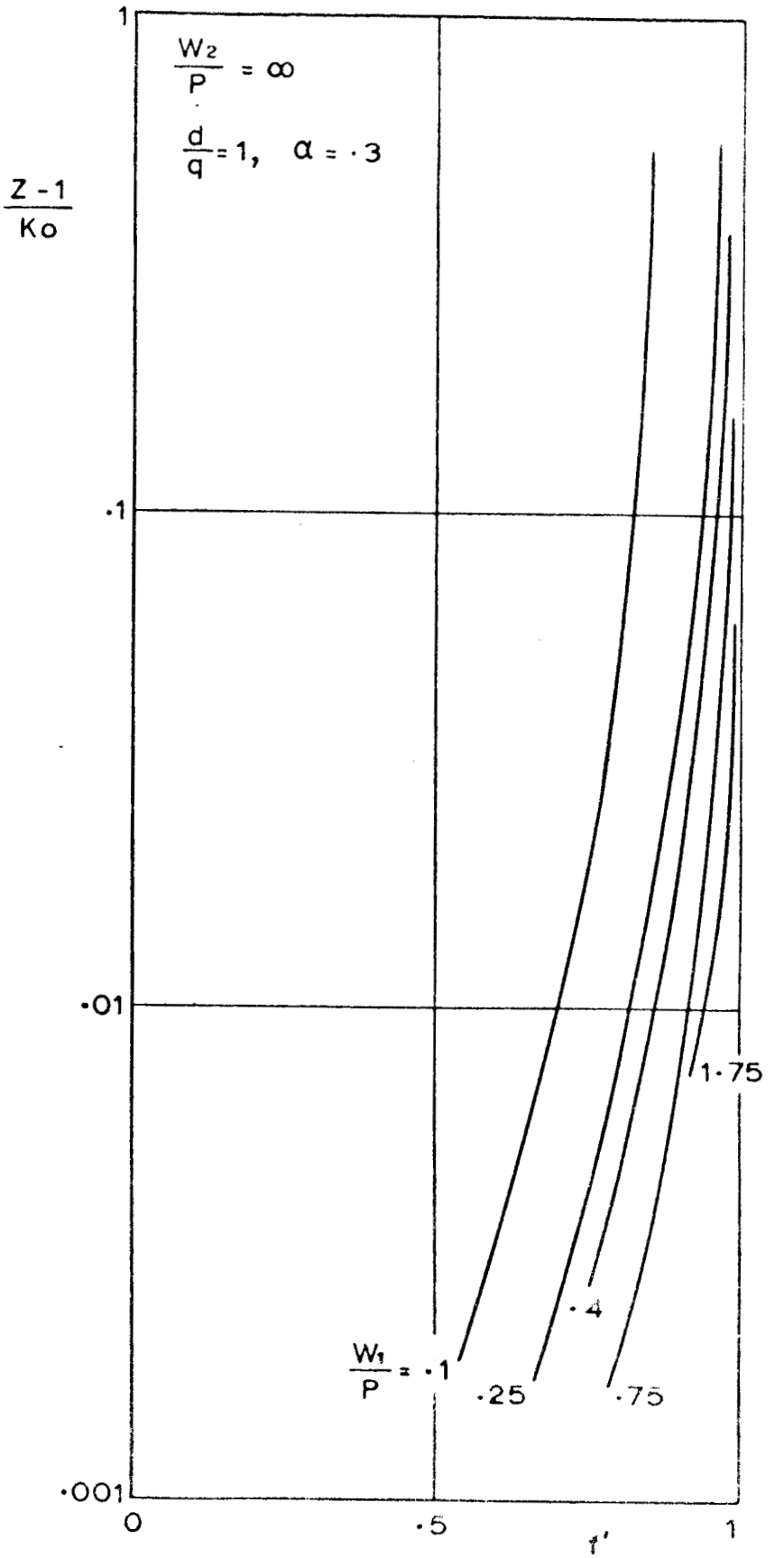
$\frac{W_2}{P} = \infty$
$\frac{d}{q} = 1, \quad \alpha = .3$
$\frac{Z-1}{Ko}$
1
.1
.01
.001
0
.5
1
f'
$\frac{W_1}{P} = .1$
.25
.75
.4
1.75

Figure 39

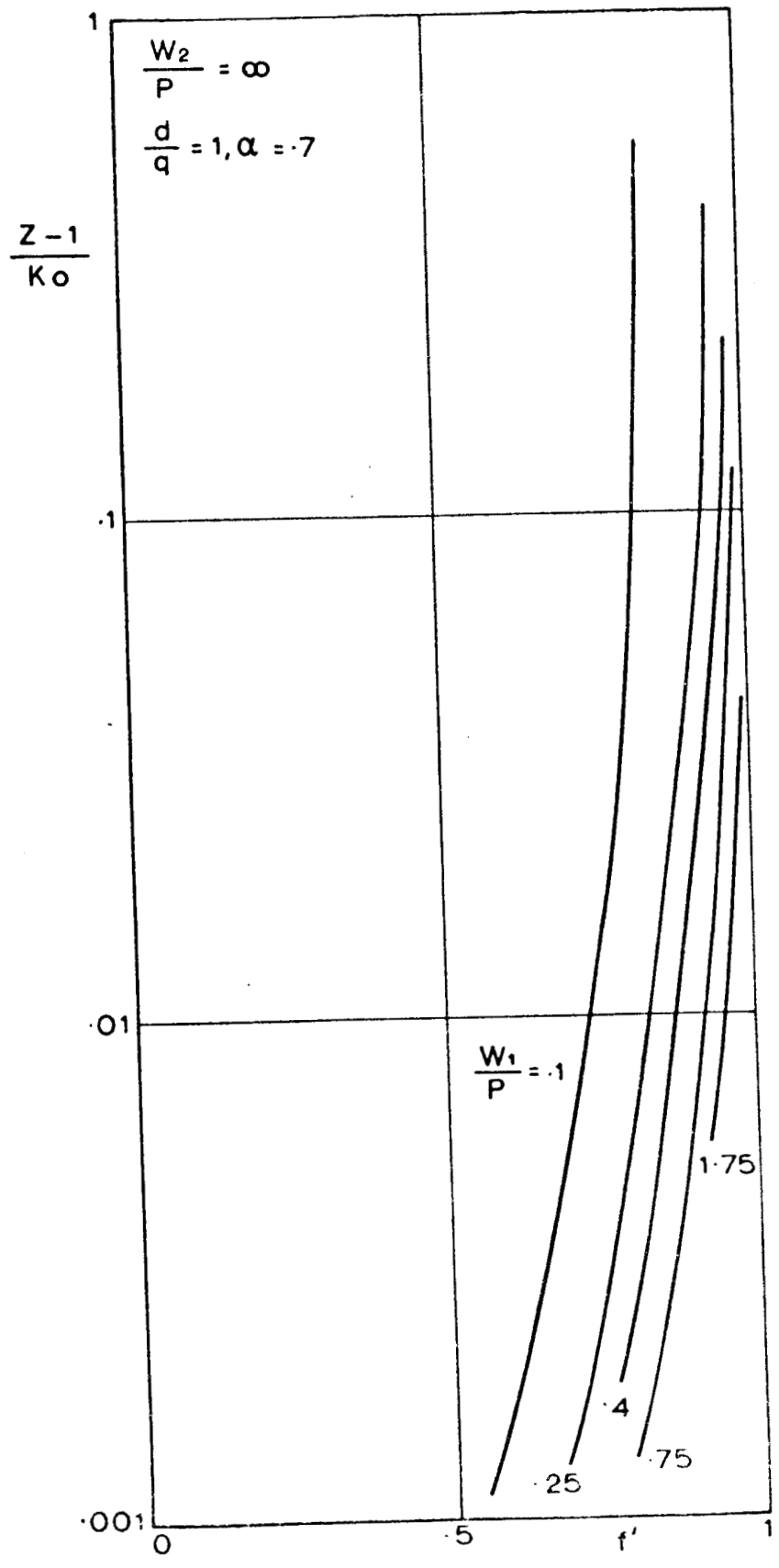

Figure 40

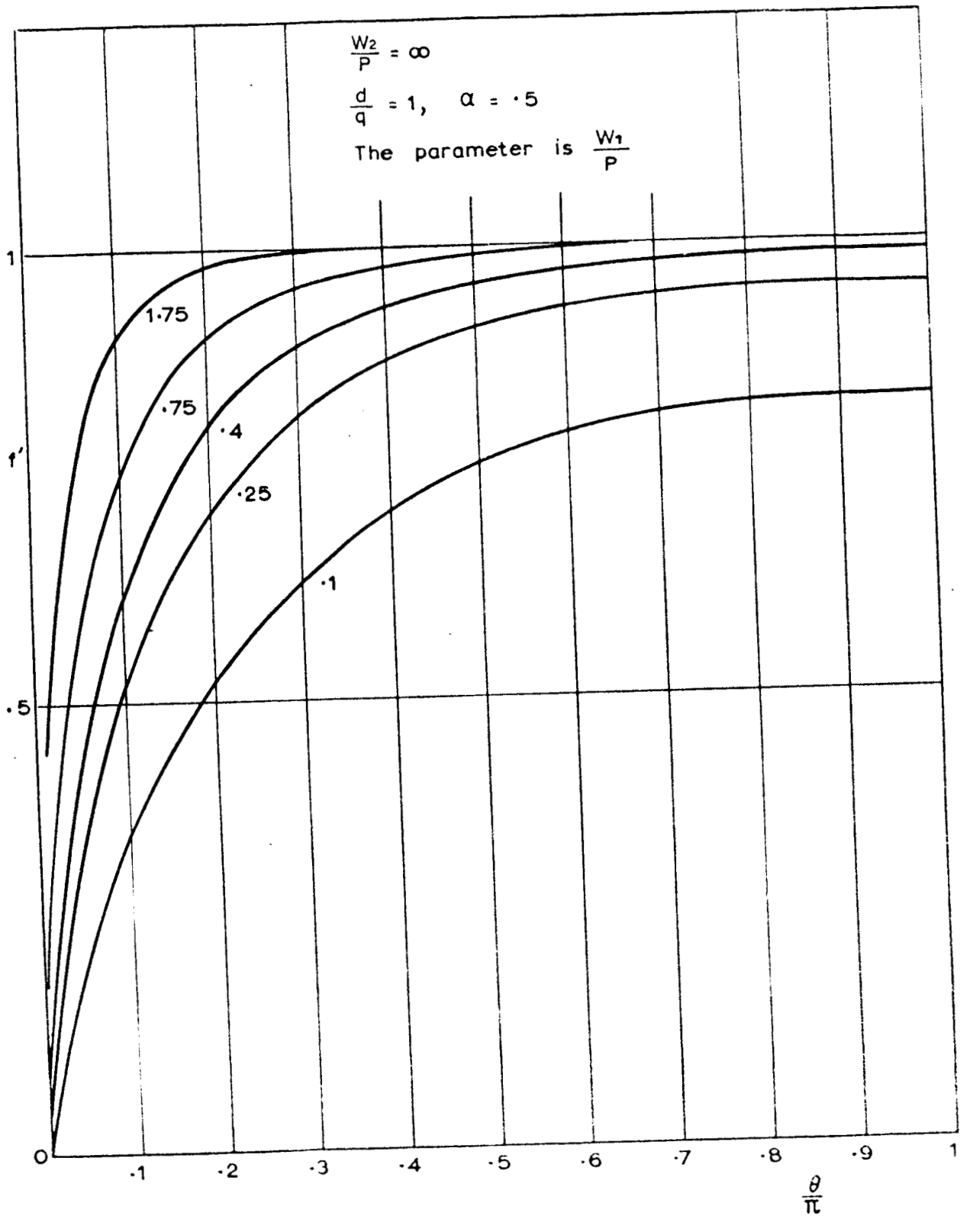
$\frac{W_2}{P} = \infty$
$\frac{d}{q} = 1, \quad \alpha = \cdot 5$
The parameter is $\frac{W_1}{P}$
1
f'
·5
0
1·75
·75
·4
·25
·1
·1
·2
·3
·4
·5
·6
·7
·8
·9
1
$\frac{\theta}{\pi}$

Figure 41

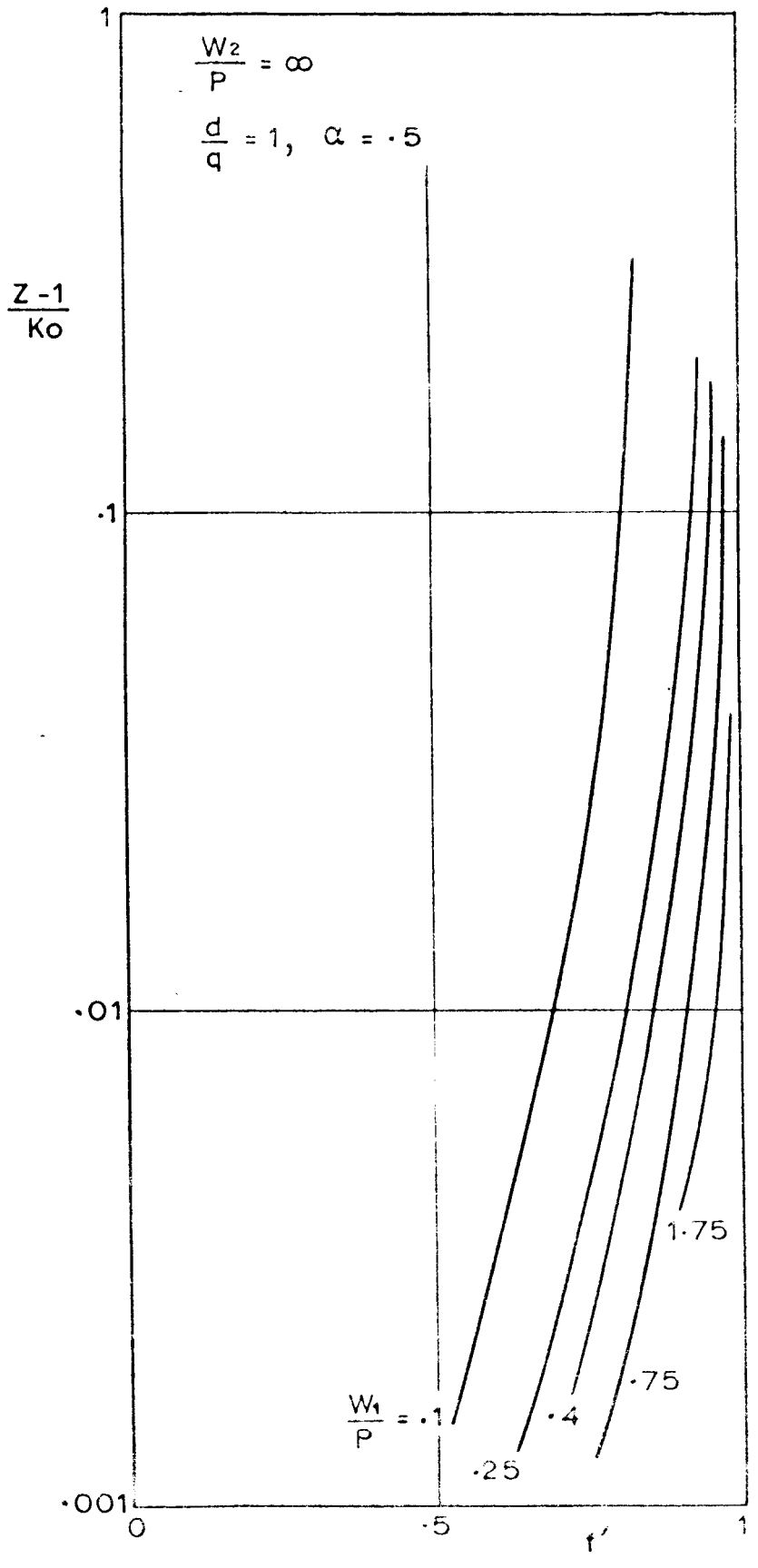
$\frac{W_2}{P} = \infty$
$\frac{d}{q} = 1, \quad \alpha = \cdot 5$
$\frac{Z-1}{Ko}$
1
·1
·01
·001
0
·5
1
f'
$\frac{W_1}{P} = \cdot 1$
·25
·4
·75
1·75

However, when $\frac{W_1}{P}$ is very large, the Karp circuit has very little bandwidth, while that of the ridge loaded meander line is still quite considerable. In fact, if there is no ridge at all, the bandwidth of the Karp circuit is zero while that of the meander line is 67% (one octave frequency coverage). On the other hand, as the ridge is brought nearer to the circuit the impedance of the ridge loaded meander line falls but that of the Karp circuit remains relatively unchanged although the value of f' at the centre frequency falls in the Karp circuit, thus reducing the width of the circuit and hence the available beam cross-section. Thus while the value of f' at the center frequency is typically 1.5 for the ridge loaded meander line, whatever the degree of loading, for a broad band Karp circuit it might be as low as 0.8 and hence the former circuit would have almost twice the width of the latter.

For the Karp structure α is a measure of the width of the ridge. Variation of α has very little effect; $\alpha = 0.5$ gives the optimum bandwidth and the impedance decreases slowly as α increases. In making calculations on the ridge loaded meander line the separation of the connecting links has been taken equal to the width of the ridge, although it is not essential that this be so. In this case variation of α has much more effect. As α is increased the impedance increases considerably. Also, as α rises above 0.5 the bandwidth falls sharply. From calculations and measurements made on the unloaded meander line it is known that the input match has the broadest band when $\alpha = 0.4$. This is therefore the most suitable value for α unless bandwidth has to be sacraficed to obtain the highest values of impedance.

Increase of the parameter $d/_q$ lowers the impedance in both cases. In the case of the ridge loaded meander line it reduces the bandwidth as well but it seems to have little effect on the bandwidth of the Karp circuit. Choice of this parameter depends on practical considerations. If it is kept too small, the circuit will be difficult to construct, fragile and have poor heat dissipation. On the other hand it is difficult to make circuits by photographic etching with α greater than 0.5, although there is no such limitation if spark machining is employed. The simplified theory used in the analysis suggests that the circuit loss will increase steadily as $\frac{d}{q}$ is increased but it does not deal adequately with effects at the bar corners and it is possible that there is value of $d/_q$ which will give minimum circuit loss. Until this point is established, either theoretically

or experimentally, the value of 0.5 will serve as a reasonable compromise on grounds of mechanical strength and thermal dissipation.

In order to reduce the number of variables, $\frac{W_2}{P}$ has been made ∞ in all cases. This means that in theory the circuits operate down to zero frequency but in practice the impedance has dropped to a very low value in this region. In a practical case where W_2 is finite the lower cut off may be found from the expression

$$\frac{W_1}{W_2} = \tan ka \tan k(b-a) \qquad \text{where} \quad k = 2\pi/\lambda_o$$

Where $\frac{W_2}{P}$ is 5 or greater the useful part of the dispersion and impedance plots will not differ greatly from those given.

For our purposes the optimum parameters for the ridge loaded meander line may be taken as $\alpha = 0.4$, $d/_q = 0.5$ and for the Karp circuit, $\alpha = 0.5$, $d/_q = 0.5$ (**Figures 36 and 37**). For the Karp circuit, if we consider that $W_1/_P = 0.25$ brings the ridge as close to the line as is practicable, then a bandwidth of 20% can be obtained if somewhat arbitrarily we require that the variation of impedance over the band should not exceed 10:1. A reasonable target for bandwidth is that of a normal waveguide, i.e. 40%. To obtain this a value of $W_1/_P$ of 0.1 would be required making the clearance between line and ridge of the order of 0.001 in. at 50 kMc. Using the ridge loaded meander line circuit a 40% bandwidth could be obtained with an impedance ratio of 100 at a ridge separation of $W_1/_P = 1.75$ although the impedance values would be lower than for the Karp circuit by a factor of 2 or so. This is not a large factor when it is remembered that C is proportional to the cube root of impedance. Also, whereas the impedance of the Karp circuit is a steeply rising function of frequency over the whole range, the impedance of the ridge loaded meander line reaches a maximum and then falls again. Hence there is a frequency range over which the impedance is fairly constant and this can be increased, at the expense of a further fall in impedance, by reducing W_1.

It should be mentioned here that the high impedances predicted for the Karp circuit occur close to the high frequency cut off, where the theory is less

reliable and therefore results in this region have to be treated with caution. This does not apply to the ridge loaded meander line where the highest impedances occur well away from the cut-off frequency.

To summarise, the Karp circuit has the highest impedance but has small bandwidth with the impedance varying rapidly over the band. The lateral dimensions of the circuit are small, restricting the beam area. The ridge loaded meander line has lower impedances but a broader bandwidth with the impedance more constant over the band. This is an important point if we wish to hold the conversion efficiency constant over the band. It has great flexibility because constancy of impedance can be traded against magnitude over a wide range by the choice of ridge to circuit separation. In addition, the circuit has greater lateral dimensions, giving a greater beam area. It is therefore considered the more suitable circuit except possibly for applications where the highest efficiency is required at whatever cost in bandwidth.

2. Circuit Loss

Circuit loss is known to be important in the operation of millimeter backward wave oscillators and the theoretical analysis of the convertor also indicates the importance of keeping circuit loss to a minimum. The calculation of loss for the various types of circuit is a difficult problem but some approximate calculations have been made which indicate that the loss does not vary very greatly between one type of circuit and another. However, the measured loss of structures is found to be many times greater than the calculated values. Some part of this discrepancy is undoubtedly due to the difference between bulk and surface conductivity and the presence of braze materials etc, but the greater part must arise from irregularities of construction. Pitch irregularities are probably the most important source of loss in millimeter slow wave circuits and therefore it is important that they be kept to a minimum.

3. Construction of Circuits

A meander line circuit suitable for a backward wave tube at 50 KMc/s has been produced by spark machining using a technique which eliminates all periodic errors of pitch. Random errors of pitch do not exceed $\pm$ 1%. Loss measurements are not yet available for this circuit but similar circuits have been made by the photographic etching process (Fig 16). These have about 2% of periodic error and a rather high amount of random error. Such circuits have been gold brazed between side walls containing input and output transitions (Figs 17 and 18). No ridge loading was used. The input and output VSWR and the insertion loss of one such circuit are shown in Fig 19. It is reasonable to expect much improved results from the spark machined circuits.

C. Electron Beam Considerations

1. The Electron Beam

The Karp structure and the ridge loaded meander line are, in their simple form, planar structures and as such provide a large interaction cross-section, particularly the ridge loaded meander line which has a greater width than the Karp structure. This is an important point because at these frequencies the fields fall off very rapidly away from the structure while, to achieve low noise operation, some clearance must be left between the beam and the circuit to avoid interception. It would therefore appear that planar circuits using strip beams are ideal for this application. There are difficulties however. There is not a great deal of experience in the design of strip beams and problems may arise in constraining the edge of the beam in the gun region and in preventing twist of the beam and consequent interception on the circuit.

The usual arrangement is for the strip beam to lie on one side of the circuit (Fig. 43A). In order to allow greater clearance between the beam and the circuit it may be preferable to have two circuits with the beam in between them (Fig. 43B). If, however, it is desired to take advantage of the advanced technology of circular beams this could be done by making a further modification (Fig. 43C). However, if it is the ridge loaded meander line we are considering, the circuit is now very similar to a stub supported ring and bar circuit in which, as we have already discussed, the fundamental is increased at the expense of the harmonics. Thus we may find that our modifications of the simple circuit have successively reduced the impedance of the desired harmonic. This subject requires further study before the relative importance of the various factors can be assessed.

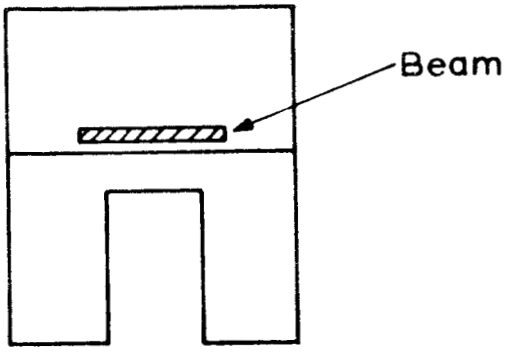

(A)

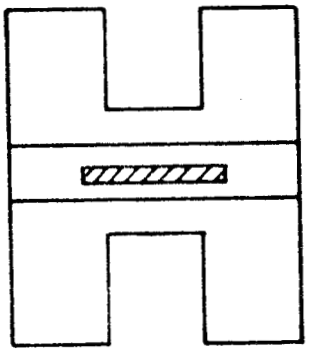

(B)

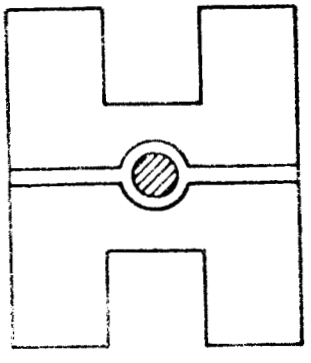

(C)

Figure 43

Alternative Dispositions of Electron Beam

2. Noise

The noise performance of the BWC is of critical importance in most of the projected applications. A detailed theory of all the noise conversion processes in a BWC would be very involved, the effect of the non-linearity being to permit contributions to the output noise from a large number of frequency bands. Experience in the past, particularly with the longitudinal space charge wave amplifier has taught the lesson that the neglect of higher order side bands may, in certain circumstances, lead to entirely erroneous conclusions. Nevertheless we feel that in this case simple considerations involving only signal, local oscillator and i.f. frequencies do lead to a correct understanding of the behavior, and experiments which have been conducted on low frequency tubes support this view.

In discussing the noise behavior, we will consider the single circuit and two circuit BWC separately. The situation in the latter is inherently simpler and will be discussed first.

a. The 2 Circuit BWC

The first part of the BWC consists of a conventional BWA, and the theory of the noise in this case has been very fully worked out. The classical theory predicts that noise temperatures of the order of the cathode temperature can be achieved, and a considerable body of more recent work has shown that by the use of suitable drift regions, in the very low velocity region in the immediate vicinity of the potential minimum, there is no fundamental limit to the extent to which the noise can be reduced. Provided the gain in the BWA section is sufficiently large, it is at once clear that the over-all noise figure of the BWC will be that of the BWA. In practice, however, the gain may not be sufficiently great, and other effects, particularly the presence of noise at the i-f frequency originating at the cathode, must be considered. Even before doing so, we must however bear in mind that the best performances for low noise BWA's and TWT's are invariably obtained using very low beam currents, a course which is not open to us in that the beam current must be sufficiently

large to bring the oscillator section to a region of efficient oscillation. It should be emphasized that there is no fundamental reason why the current must be very low. The reason for the choice of a low current lies in the need to obtain a particular potential profile in the gun region, which implies a relatively low first anode voltage. There is no reason to expect that the change to substantially larger currents than normally used in a low noise tube should have a drastic effect on the noise performance. Experiments carried out at .5 kmc on a two circuit BWC have in fact led to noise figures around 8 db.

In considering the additional noise arising from a limited amount of gain in the BWA section we must consider the noise introduced directly at the i-f frequency and also noise at the local oscillator frequency. Fortunately it turns out that the latter is a second order effect, and that on the basis of known BWO noise behavior is entirely negligible. We turn, therefore, to a consideration of the noise in the i-f channel.

Let N_s be the effective beam noise at the signal frequency at the gun end of the tube

and

N_{if} the effective noise at the i.f.

It is usual to relate this noise to the cathode temperature T_c (even though its physical nature is quite distinct from Johnson noise), and can be expressed in the form

$$N_s = k\gamma^2 T_c \, df$$

and

$$N_{if} = k\Gamma^2 T_c \, df$$

The Γ^2 factor is the space charge smoothing factor used in the noise theory of grid controlled low frequency tubes. The numerical value of this factor is not easy to predict accurately, but in typical low frequency conditions lies in the range 0.05 to 0.15. In the following we will adopt a figure of 0.1. Low frequency here means up to $\sim$ 100 mc. At higher frequencies Γ^2 rises until it approaches unity at low microwave frequencies.

The γ^2 factor will be greater than unity as a result of loss, partition noise, and defects in the space charge wave matching region. The practical figures which emerge are well known from experience with ordinary BWA's and TWT's, and depend mainly on the frequency. The use of guns which provide a suitable drift region immediately in front of the cathode potential minimum can lead to γ^2 less than unity,--the best performance at relatively low microwave frequencies being of the order of 0.2. However, combining all these (physically quite distinct) factors, the values which can be anticipated at millimeter wavelengths are of the order of 10.

The noise figure of an amplifier can be defined as the noise output related to the noise output for an idealized amplfier of the same gain, which does not itself contain any sources of noise. It is usual to define the noise figure in terms of a signal source at an ambient temperature of T = 300°K. It should, of course, be appreciated that if the amplifier is used in "cold sky" applications where the effective source noise may correspond to a very low noise temperature, the noise figure as defined above, does not directly reflect the effective sensitivity of the converter. It should be noted that in an application where the sun is used as the effective signal source the source noise, where "noise" is now defined as <u>undesired</u> random signals, may again be very low.

We can write the noise figure NF in the form,

$$NF = (GN_s + GkTdf + N_{if})/GkTdf$$

where G is the over-all converter gain (expressed as a power ratio). Writing the noise terms in the form used above, we have

$$NF = 1 + \frac{T_c}{T}\left(\gamma^2 + \frac{\Gamma^2}{G}\right)$$

This relationship shows that the point where insufficient gain has a seriously deleterious effect on the noise performance depends in the first instance on the relative values γ^2 and Γ^2. In the case of a low i.f. and a typical BWA in the millimeter region, the conversion gain could probably

sink to -15 db before the i-f signal makes a serious contribution. However, for a substantially higher i.f., where Γ^2 might be of the order of 0.5 and a BWA using an ultra low noise gun where γ^2 might possibly be as low as 8, the i-f noise would begin to make a noticeable contribution, for a conversion gain which was only negative by a few db. This example is not intended to indicate our conclusion on optimum design (the higher i-f frequency might for example lead to an improvement in G which would outweigh the increase in Γ^2), but serve merely to illustrate the above results.

b. The Single Circuit BWC

In the case of the single circuit converter, the gain and frequency conversion functions are no longer separate. However, with the assumption, already discussed in the case of the two circuit converter, that the noise introduced by the oscillator can be neglected, the noise situation will be very similar, with one significant exception. The single circuit converter has no discrimination against the image frequency, so that noise entering on this band will make an equal contribution to the ultimate i-f noise. The equation for the noise figure then becomes,

$$NF = 1 + \frac{2T_c}{T}\left(\gamma^2 + \frac{\Gamma^2}{G}\right)$$

The deterioration of the noise figure by 3 db relative to the two circuit converter is fundamental, and is the price which must be paid for the greater simplicity.

It should be emphasized that there are many sources of noise, such as interception noise, secondary emission noise etc. which have not been considered above.

To illustrate the above result it is of interest to consider an example. Suppose we have a single circuit BWC which, acting as a conventional backward wave amplifier would have a noise figure of 10 db. Figure 44 then shows how the conversion gain of the device affects the noise figure. It is seen that provided that the conversion gain does not fall below around -10db, the deterioration of the noise figure as a result

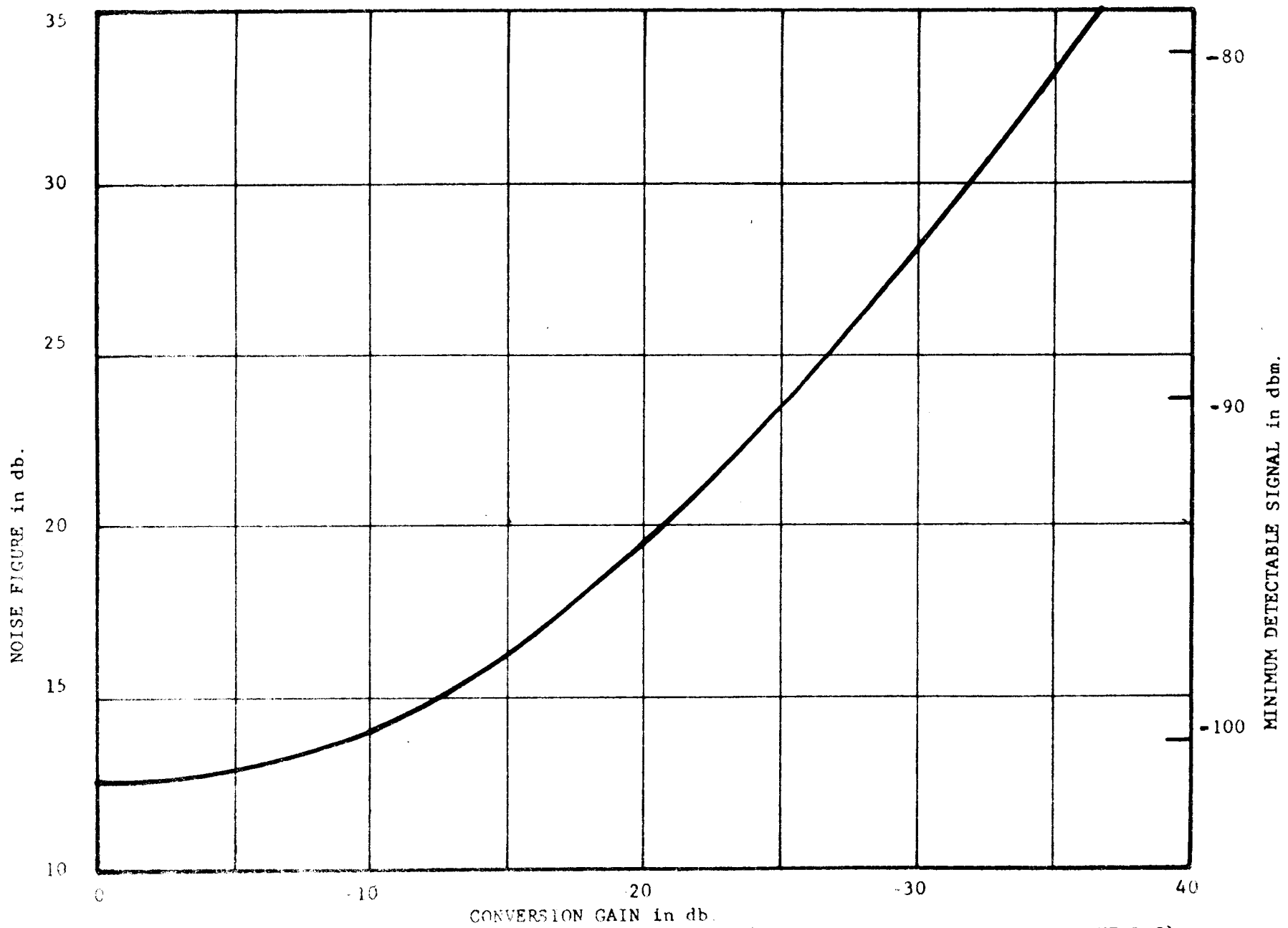

FIGURE 44. INCREASE IN NOISE FIGURE AND MINIMUM DETECTABLE SIGNAL(DUE TO NOISE GENERATED WITHIN THE BVC) VERSUS CONVERSION GAIN

of internally generated i-f noise is relatively slight. However, as the conversion gain becomes smaller the deterioration becomes more marked, until atvery low conversion gains, the noise figure increases directly with the magnitude of (negative) G. This example shows the importance of achieving conversion gains not too far below unity in a single circuit BWC. This point will be discussed further in connection with the proposed choice of i-f frequency for the single circuit.

c. Minimum Detectable Signal

In a single frequency low noise TWT, a knowledge of the noise figure suffices to compute the minimum detectable signal. In the case of the BWC it turns out that this is not strictly true under conditions when the i-f noise is significant. The reason lies in the fact that the conversion gain G as used above relates to the internal conversion gain (e.g., the increase in the effective r-f current squared), and is not the quantity measured, which depends also on the effective i-f impedance. It is, nevertheless, of some interest to compute the order of magnitude of the minimum detectable signal, on the assumption that the observed and true internal conversion gains do not differ in order of magnitude.

We can return to the same example considered in Fig. 44. Assuming that the i-f bandwidth is 2 mc, we obtain the minimum detectable signal, assuming that this lies 3 db below the noise level.

The above considerations are of a general nature, and the noise problem is certainly one which requires further and more detailed study. However, the conclusion based on these considerations is that, provided that the conversion gain of a single circuit BWC can reach values no less than -10 db, a minimum detectable signal of the order of -100 dbm should represent an attainable target at millimeter wavelengths.

IV. CONCLUSIONS AND RECOMMENDATIONS

A. Estimated Power and Magnetic Field Requirements

It is estimated that a tube using the ridge loaded meander line and operating over the range 50 - 75 kMc/s will require a current of 10 mA at a maximum voltage of 4.5 kV and hence a maximum beam power of 45 watts. To this will have to be added some allowance for heater power. This calculation assumes two strip beams, one on either side of the circuit, having a current density of 1 amp/cm^2 which does not require a convergent gun. The circuit will be 1 in. long and the gun will probably be of equal length.

If we consider the space charge forces on an electron on the surface of a strip beam, it has a trajectory given by the expression :-

$$\left(\frac{dY}{d\beta_p z}\right)^2 = - \frac{\omega_H}{\omega_p} \left[Y^2 + \frac{1}{Y^2} - 2 \right] + 2 \log_n Y + Y_o'^2$$

where $Y = y/y_o$, the ratio of the distance of the electron from the mid plane to that of the unperturbed electron. The remaining symbols are defined by Brewer [1]. This expression can be integrated to give the limits of the excursion of the electron. It is found that, for the beams considered, which have a thickness of 0.006 in. a field of 200 gauss is sufficient to keep the excursion within 0.001 in. if the beam if launched parallel to the structure.

The excursion of electrons due to thermal velocities however is given by the expression

$$r = 3.37 \, V^{\frac{1}{2}}/B$$

where B is the field in gauss, V the thermal energy of the electrons in volts and r the radius of the electron orbit in cms. This shows that the field required to reduce the radius of the electron orbits to 0.0005 in., assuming thermal energies of 0.1 volts from a non-convergent electron gun is 900 gauss.

These are theoretical figures, and it is usually assumed that in practice a considerably larger field than the theoretical will be required. However this is because calculations of field are usually based on space charge considerations alone and do not take into account thermal velocities or gun inaccuracies which prevent the beam being launched in a truly parallel manner. If we assume a field of 900 gauss will be required this will not only take thermal velocities into account but will also leave a wide margin of safety for inaccurate launching.

Methods of correcting radial velocities arising from the lens action of gun electrodes which are effective over wide ranges of voltage have been discussed by King[2] and others. These are expensive in magnetic field but it is reasonable to hope that a sufficient degree of correction could be obtained without exceeding the value of field quoted above.

A further improvement could be obtained by the use of an additional, variable voltage anode. In operation this would have to be "tracked" with the circuit voltage. Further investigation would be required to assess whether the improvement in beam launching, and the consequent reduction in magnetic field, which could be obtained in this way is justified when balanced against the additional external circuit complications.

B. Estimation of Magnet Weight

In general there are three basic methods of magnetically focusing O-type traveling wave devices; namely, the electromagnet, the permanent magnet, and the periodic permanent magnet. From the considerations of the previous section, the magnetic field was estimated to be at least 900 gauss over a two-inch length. From a physical viewpoint we estimate that a 50 Gc backward wave converter will have an outside diameter of one-half inch. For an electromagnet this would mean that at least 100 watts of power would have to be supplied to the magnet and in addition cooling would be required. For a device to be used in a space probe this is obviously undesirable and therefore the use of an electromagnet has been ruled out. Since the backward wave converter is a voltage tunable device, the use of a periodic permanent magnet must also be ruled out as these two conditions are not compatible. We are therefore left with the choice of permanent magnet structures.

Many types of permanent magnet configurations have been devised to focus beam type traveling wave devices. For this discussion, however, we will limit ourselves to a tubular arrangement as shown in Figure 45, since straightforward design procedures have been devised by Glass[3]. With a

1. Brewer, G.R., "Some Characteristics of a Cylindrical Electron Stream in Immersed Flow". Trans. IRE ED4 p 134, April 1957.
2. King, P.G.R., "Electron Guns for Traveling Wave Tubes", SERL Technical Journal, 4 , p 9, 1954.
3. Glass, M.S., "Straight-Field Permanent Magnets of Minimum Weight for TWT Focusing-Design and Graphic Aid in Design", Proc. IRE, Vol. 45, No. 8 August 1957.

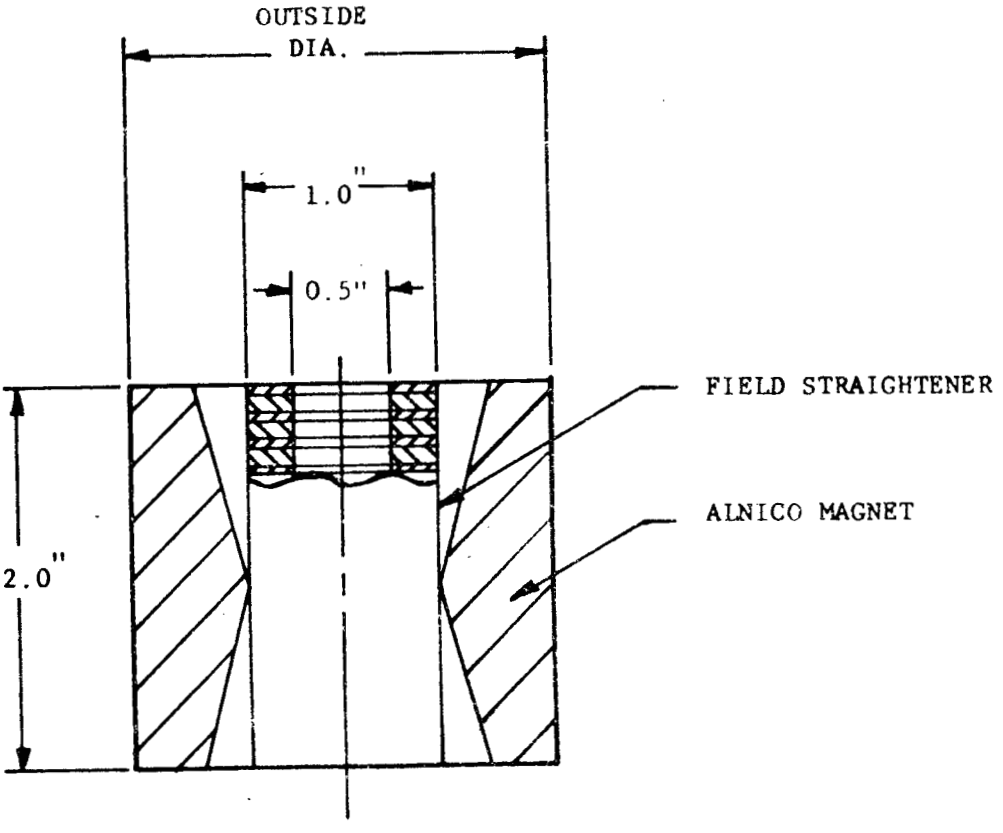

FIGURE 45

FOCUSING MAGNET FOR A 50GC. BACKWARD WAVE CONVERTER

With a permanent magnet focusing scheme it is usually necessary to suppress any radial components of magnetic field. This can be done with field straighteners of the type illustrated. In general the straighteners consist of a series of thin magnetic discs separated by non-magnetic spacers. With a good straightener the radial field components can be reduced to the order of one gauss while having negligible effect on the axial field. In following the procedures of Glass it is necessary to specify three quantities, the length and inside diameter of the magnet and the required magnetic field. With a tube diameter of one-half inch it was decided to set the inside diameter of the magnet at one inch in order to permit room for a straightener. From here the outside diameter and weight for a given magnet material may be readily determined. Several trial designs have been worked out for various field values and the results are as follows.

Magnetic Field	Material	Outside Diameter	Weight
900 Gauss	Alnico 7	3 in.	3.25 lbs.
1200 Gauss	Alnico 8 (Improved)	2.22 inc.	0.81 lbs.
2000 Gauss	Platinum-Cobalt	3 in.	6.8 lbs.

The platinum-cobalt figures have been included to illustrate that if necessary, a 2000 gauss field could be obtained; however, the basic cost of the magnetic material would be considerable. From the table it is seen that a very reasonable design appears possible with Improved Alnico 8. If we take a most pessimistic viewpoint and say the magnet would have to be larger and an order of magnitude heavier, the end result would still be reasonable. For information purposes, Figure 45 has been drawn to full scale for the Alnico 8 values tabulated.

C. Program Recommended for Next Phase

The above discussions have been largely concerned with ladder lines, for which the natural beam shape would correspond to a strip geometry. Although successful high and low power tubes have been built at millimeter wavelengths, in the case of a tube where it is vital to restrict the beam interception to

the lowest possible value in order to avoid interception noise, there are many advantages in favor of using a circular solid or hollow beam. In particular the problem of preventing any twist of the strip beam is avoided.

If we start with a double ladder circuit, as indicated in Figure 46 (a), there are two ways in which we can make a modification which will permit the use of an interacting beam having circular symmetry. Figure 46 (b) shows the first of these possibilities; the main disadvantage is that we have incurred a substantial reduction in available beam area. Experiments have shown that the dispersion curve of this structure is indistinguishable from that of Figure 46 (a). The change in impedance has not as yet been investigated, but is also likely to be insignificant.

In the circuit of Figure 46 (c) we are not faced with any reduction of beam area, and we can use a high perveance annular beam. The dispersion curve and impedance is substantially that of a single ladder structure. In both cases, a ridge (shown dotted) can be introduced in order to achieve a wider pass band. In both cases matching is effected by combining one lead-out-bar from each structure, and the results obtained are very similar to those shown (Figure 19) for a single ladder.

The advantages of the structure of Figure 46 (c) appear to be dominant. It is this structure which we would propose to use in the first operating BWC at millimeter wavelengths.

We therefore recommend that the work on the millimeter wave converter tube be continued and propose that the next logical phase in this program is to build an operating tube that will operate in the lower millimeter range of frequencies. A tube that will operate from 50 to 60 kmc (or some similar bandwidth with a slightly higher center frequency) which has a circuit as shown in Figure 46 (c) is a logical starting place.

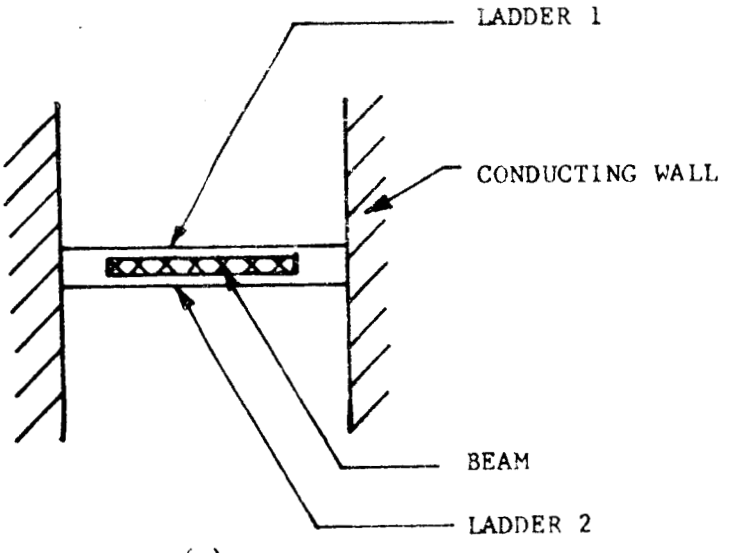

(a)

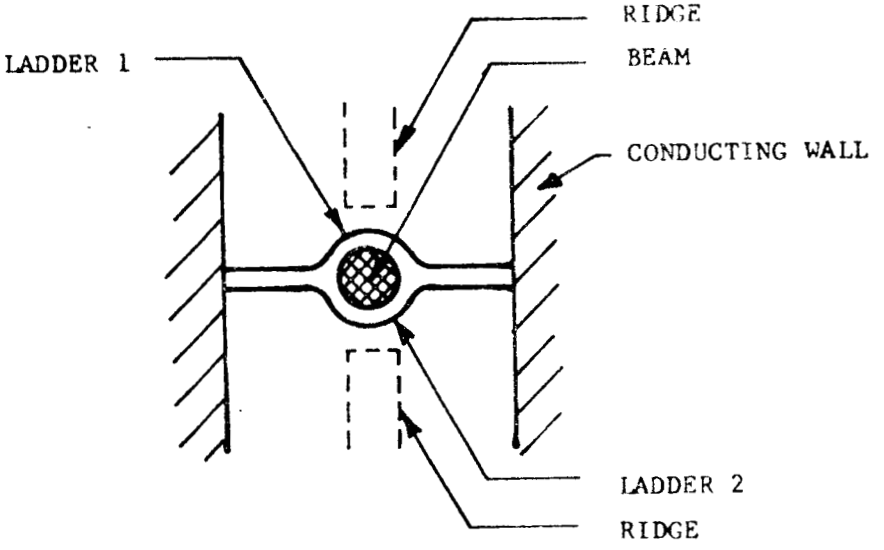

(b)

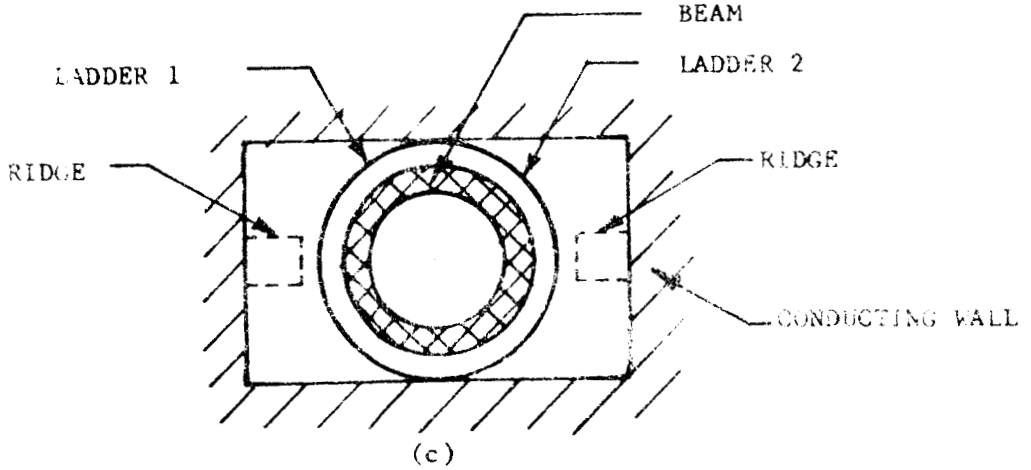

(c)

FIGURE 46. ALTERNATE CIRCUIT CONFIGURATIONS

From evidence presented above it can be seen that the device is practical. The theory of operation has been determined by two different methods which agree close enough so that the operation can be predicted. The r-f structures required have been studied and broadband structures have been arrived at which can be fabricated by methods for which the required skills and techniques. The electron gun and cathode requirements are readily available within the present state of the art, the noise figure of the tube should be no more than 15 db, and the weight and power requirements of the device are reasonable for use in a planetary spacecraft.

APPENDICES

APPENDIX I

BWC BALLISTIC ANALYSIS MODIFICATION TO INCLUDE COSINE TERM

The approximate analysis previously presented has been modified to include the effect of the cosinusoidal variation of the envelope of the accelerating electric field. The analysis proceeds along the same lines as before, and it turns out that the cosinusoidal variation does not complicate the analysis to any significant extent. Likewise, the results do not differ greatly from those obtained previously for the constant amplitude case.

The symbols that will be used in the analysis that follows are defined below:

- e -- electronic charge
- m -- electronic mass
- η -- electronic charge to mass ratio = e/m
- ω -- angular frequency
- v_0 -- d.c. beam velocity
- V_0 -- d.c. beam voltage
- v_ϕ -- wave phase velocity
- β -- propagation constant = ω/v_ϕ
- z -- coordinate along beam
- t -- time
- t_1 -- time of entrance at $z = 0$
- α -- time of entrance in radians = ωt_1
- t_2 -- time of exit at $z = \ell$
- ϕ -- transit angle = $\omega(t_2 - t_1)$
- ϕ_0 -- d.c. transit angle = $\omega\ell/v_0$
- E_0 -- electric field amplitude
- g -- normalized velocity difference = $1 - (v_0/v_\phi)$
- Ω -- effective frequency associated with envelope variation = $\pi v_0/(2\ell)$
- ℓ -- length of interaction region
- I -- current
- Φ_0 -- $g\phi_0$

We assume that the electric field with which the electron beam interact may be represented by the real part of the complex expression

$$E(z,t) = E_0 \cos(\pi z/2\ell)\, \varepsilon^{j(\omega t - \beta z)}$$

For an electron which enters the interaction region at the time $t = t_1$, we may write

$$z = v_0(t - t_1)$$

provided that the amplitude of the electric field is not too large. With this assumption the equation of motion may be written as

$$\frac{d^2z}{dt^2} = \eta E_0 \left[\frac{\pi v_0 (t-t_1)}{2\ell}\right] \varepsilon^{j[\omega t - \beta v_0 (t-t_1)]} \tag{1}$$

To eliminate possible confusion the parameter previously designated as ρ will henceforth be denoted by g ; i.e.,

$$g = 1 - (v_0/v_p) \tag{2}$$

We note that

$$\omega t - \beta v_0 t = \omega t\left(1 - \frac{\beta v_0}{\omega}\right) = \omega t\left(1 - \frac{v_0}{v_p}\right) = g\omega t$$

Consequently the equation of motion may be written in the form

$$\frac{d^2z}{dt^2} = \eta E_0 \cos\left[\frac{\pi v_0 (t-t_1)}{2\ell}\right] \varepsilon^{j\beta v_0 t_1} \varepsilon^{jg\omega t}$$

With the introduction of the effective frequency Ω , defined by

$$\Omega = \pi v_0/(2\ell)$$

the equation becomes

$$\frac{d^2z}{dt^2} = \eta E_0 \left\{\cos\Omega t \cos\Omega t_1 + \sin\Omega t \sin\Omega t_1\right\} \varepsilon^{j\beta v_0 t_1} \varepsilon^{jg\omega t} \tag{3}$$

Integration of this equation twice leads to an expression for the exit angle (ωt_2) as a function of the entrance angle ($\alpha = \omega t_1$).

$$\omega(t_2 - t_1) = \frac{\omega\ell}{v_0} - \frac{\omega\eta}{2v_0} E_0 \varepsilon^{j\omega t_1} \left\{\frac{\varepsilon^{j(\omega g + \Omega)(t_2 - t_1)}}{-(\omega g + \Omega)^2} + \frac{\varepsilon^{j(\omega g - \Omega)(t_2 - t_1)}}{-(\omega g - \Omega)^2} \right.$$

$$\left. + \frac{j(t_2 - t_1)}{\omega g + \Omega} + \frac{j(t_2 - t_1)}{\omega g - \Omega} + \frac{1}{(\omega g + \Omega)^2} + \frac{1}{(\omega g - \Omega)^2}\right\}$$

We define

$$\omega' = E_0 \ell \left[2 v_0 \frac{\omega\ell}{v_0} g\right]^{-1} \tag{4}$$

and set $\omega g(t_2 - t_1) = \phi_0$ in the formula in two places. Then taking only the real part, we obtain

$$\phi = \phi_0 + \frac{\omega'}{2g}\left\{\cos\alpha\left[\frac{\cos(1+\Omega/\omega g)\phi_0}{(1+\Omega/\omega g)^2} + \frac{\cos(1-\Omega/\omega g)\phi_0}{(1-\Omega/\omega g)^2}\right.\right. \tag{5}$$

$$\left. - \frac{1}{(1+\Omega/\omega g)^2} - \frac{1}{(1-\Omega/\omega g)^2}\right] - \sin\alpha\left[\frac{\sin(1+\Omega/\omega g)\phi_0}{(1+\Omega/\omega g)^2}\right.$$

$$\left.\left. + \frac{\sin(1-\Omega/\omega g)\phi_0}{(1-\Omega/\omega g)^2} - \frac{\phi_0}{(1+\Omega/\omega g)} - \frac{\phi_0}{(1-\Omega/\omega g)}\right]\right\}$$

Equation 5 may be written in the form

$$\phi = \phi_0 + \frac{u'a}{g}\sin(\omega t_1 - \psi') \tag{6}$$

which is identical with the form of Equation 1 of the previously developed analysis. (See page I-3 of Bimonthly Report No. 2) In this equation the parameters a and ψ' are defined by the equations

$$2a\cos\psi' = \frac{\phi_0}{(1+\Omega/\omega g)} + \frac{\phi_0}{(1-\Omega/\omega g)} - \frac{\sin(1+\Omega/\omega g)\phi_0}{(1+\Omega/\omega g)^2} - \frac{\sin(1-\Omega/\omega g)\phi_0}{(1-\Omega/\omega g)^2} \tag{7}$$

$$2a\sin\psi' = \frac{1}{(1+\Omega/\omega g)^2} + \frac{1}{(1-\Omega/\omega g)^2} - \frac{\cos(1+\Omega/\omega g)\phi_0}{(1+\Omega/\omega g)^2} - \frac{\cos(1-\Omega/\omega g)\phi_0}{(1-\Omega/\omega g)^2} \tag{8}$$

The important point to recognize here is that all of the results obtained for the constant amplitude case can be applied to this cosinusoidal case because the form of the transit time equations is identical for the two cases. Therefore we may immediately write expressions for the various currents:

$$I_{on} = (-1)^n 2 I_0 J_n\left(n\frac{u'a}{g}\right) \tag{9}$$

$$I_{1,1} = -k I_0 J_1\left(\frac{\omega+\omega_m}{\omega}\frac{u'a}{g}\right) \tag{10}$$

$$I_{-1,1} = -k I_0 J_1\left(\frac{\omega-\omega_m}{\omega}\frac{u'a}{g}\right) \tag{11}$$

where the current at the entrance plane ($z = 0$) is given by

$$I = I_0\left[1 + k\cos(\omega_m t_1 - \chi)\right] \tag{12}$$

The modification of the expression for the conversion gain is easily determined. If P is the power output of the BWO and R is the circuit impedance for the backward wave, then

$$P = E_0^2/(2\beta^2 R)$$

Because $v_0 \doteq v_\phi$,

$$u' = \frac{E_0 l}{2V_0 \omega l / v_0 g} \cong \frac{\sqrt{RP/2}}{V_0 g} \tag{13}$$

With $\Phi_o = g\phi_o = -\pi$, as required for efficient BWO operation, the amplitude of the i.f. current may be written as

$$I_{if} = -kI_o J_1\left[\frac{\omega_{if}}{\omega}\frac{\sqrt{KP/2}\,a}{V_o(\pi/\phi_o)^2}\right] \tag{14}$$

If the argument of the Bessel function is sufficiently small,

$$I_{if} \doteq -\frac{kI_o}{2}\frac{\omega_{if}}{\omega}\frac{\sqrt{KP/2}}{\pi^2 V_o}\left(\frac{\omega l}{v_o}\right)^2 a \tag{15}$$

We assume that the backward wave amplifier is linear and introduce a transconductance coefficient, χ, defined by

$$\chi = kI_o/V_{in}$$

where V_{in} is the amplitude of the input signal to the BWA. The output voltage at the i.f. frequency is $I_{if}R_L$ where R_L is the impedance of the collector at resonance and is assumed to be a pure resistance; so

$$I_{if}R_L = V_{o,if} = \frac{-\chi R_L}{4\eta}\omega_{if}\omega\frac{\sqrt{KP/2}}{\pi^2 V_o^2} l^2 a\, V_{in} \tag{16}$$

The conversion gain, defined by

$$G = 20\log_{10}\left|\frac{V_{o,if}}{V_{in}}\right|$$

is given by

$$G = 20\log_{10}\left\{\frac{\chi R_L a}{4\pi^2}\right\} + 20\log_{10}\left\{\frac{\omega_{if}\omega l^2}{\eta V_o}\right\} + 10\log_{10}\left\{\frac{KP}{2V_o^2}\right\} \tag{17}$$

The value of the ratio $\Omega/\omega g$ which appears in Equations 7 and 8 may be readily determined for the special case of $\Phi_o = -\pi$. For this case

$$g\omega l/v_o = g\phi_o = \Phi_o = -\pi$$

and

$$\Omega = \pi v_o/(2l)$$

Therefore $\Omega/\omega g = -\frac{1}{2}$. For the same situation we find that $a \doteq 3.35$.

APPENDIX II

BWC BALLISTIC ANALYSIS WITH SPACE CHARGE

The approximate analysis of the backward wave converter has been extended to include the effects of space-charge and of the cosinusoidal envelope of the electric field in the backward wave oscillator section of the device. This analysis combines the simple ballistic analysis presented earlier with the space-charge analysis developed by the workers at STL (1,2).

We begin by assuming an infinite electron beam and space-charge neutralization of the d.c. space-charge. Under these assumptions Maxwell's equations and the equation of motion may be written in the following form:

$$\epsilon \frac{\partial E}{\partial t} + i - i_0 = 0 \tag{1}$$

$$\epsilon \frac{\partial E}{\partial z} = \rho - \rho_0 \tag{2}$$

$$\frac{dv}{dt} = \eta (E + E_a) \tag{3}$$

where

i - current density
i_0 - d.c. current density
v - velocity
ρ - charge density
ρ_0 - d.c. charge density
ϵ - permittivity
E - electric field strength due to space-charge
E_a - applied electric field
t - time
η - specific charge of an electron

These equations have been given in an earlier report (2), and are included here only for completeness.

We assume that the applied electric field is given by the real part of

$$E_a(z,t) = E_0 \cos[\pi z/(2\ell)]\, \epsilon^{j(\omega t - \beta z)} \qquad (0 \le z \le \ell) \tag{4}$$

With $z = v_0(t - t_1)$, $\Omega = \frac{\pi v_0}{2\ell}$, $g = 1 - v_0/v_0$, and $\omega_p = \sqrt{\frac{\eta \rho_0}{\epsilon}}$, we may write

$$E_a(z,t) = \frac{E_0}{4}\left\{\epsilon^{j\Omega(t-t_1)} + \text{c.c.}\right\}\left\{\epsilon^{j[\omega_p t + (1-g)\omega t_1]} + \text{c.c.}\right\} \tag{5}$$

From Eqs. 1,2,3, and 5, it follows that the differential equation for the electron velocity is

$$\frac{d^2v}{dt^2} + \omega_p^2 v = \omega_p^2 v_0 + \frac{\eta E_0}{4}\left\{ \varepsilon^{j(\Omega+\omega_g)(t-t_1)} \varepsilon^{j\omega t_1} + \varepsilon^{j(\Omega-\omega_g)(t-t_1)} \varepsilon^{-j\omega t_1} + c.c. \right\} \tag{6}$$

where c.c. denotes the complex conjugate. Carrying out the differentiation we obtain

$$\frac{d^2v}{dt^2} + \omega_p^2 v = \omega_p^2 v_0 + \frac{\eta E_0}{2} Re\left\{ j(\Omega+\omega_g)\varepsilon^{j(\Omega+\omega_g)(t-t_1)} \varepsilon^{j\omega t_1} + j(\Omega-\omega_g)\varepsilon^{j(\Omega-\omega_g)(t-t_1)} \varepsilon^{-j\omega t_1} \right\} \tag{7}$$

From this point on we shall work with the complex equation and take only the real part of the result. We assume a solution to Eq. 7 of the following form:

$$v = v_0 + A\varepsilon^{j\omega_p(t-t_1)} + B\varepsilon^{-j\omega_p(t-t_1)} + C\varepsilon^{j(\Omega+\omega_g)(t-t_1)} \varepsilon^{j\omega t_1} + D\varepsilon^{j(\Omega-\omega_g)(t-t_1)} \varepsilon^{-j\omega t_1} \tag{8}$$

where A, B, C, and D are constants which may be determined from the initial conditions and the differential equation. The initial conditions are

$$v = v_0 \tag{9}$$

and

$$dv/dt = \eta E_\omega \tag{10}$$

at the time of entry, $t = t_1$. From the differential equation we obtain by direct substitution

$$C = j\frac{\eta E_0}{2}\frac{\Omega+\omega_g}{\omega_p^2 - (\Omega+\omega_g)^2} \tag{11}$$

and

$$D = j\frac{\eta E_0}{2}\frac{\Omega-\omega_g}{\omega_p^2 - (\Omega-\omega_g)^2} \tag{12}$$

From the initial conditions we find

$$A = -j\frac{\eta E_0}{4}\left\{ \frac{\Omega+\omega_g+\omega_p}{\omega_p^2-(\Omega+\omega_g)^2}\varepsilon^{j\omega t_1} + \frac{\Omega-\omega_g+\omega_p}{\omega_p^2-(\Omega-\omega_g)^2}\varepsilon^{-j\omega t_1} \right\} \tag{13}$$

and

$$B = -j\frac{\eta E_0}{4}\left\{ \frac{\Omega+\omega_g-\omega_p}{\omega_p^2-(\Omega+\omega_g)^2}\varepsilon^{j\omega t_1} + \frac{\Omega-\omega_g-\omega_p}{\omega_p^2-(\Omega-\omega_g)^2}\varepsilon^{-j\omega t_1} \right\} \tag{14}$$

Substitution for A, B, C, and D in Eq. ( ) and integration leads to

$$z = v_0(t-t_1) - \frac{\eta E_0}{4j\omega_p}\left\{\frac{j(\Omega+\omega_g+\omega_p)}{\omega_p^2-(\Omega+\omega_g)^2}\varepsilon^{j\omega t_1} + \frac{j(\Omega-\omega_g+\omega_p)}{\omega_p^2-(\Omega-\omega_g)^2}\varepsilon^{-j\omega t_1}\right\} \quad (15)$$

$$\times\left\{\varepsilon^{j\omega_p(t-t_1)} - 1\right\} + \frac{\eta E_0}{4j\omega_p}\left\{\frac{j(\Omega+\omega_g-\omega_p)}{\omega_p^2-(\Omega+\omega_g)^2}\varepsilon^{j\omega t_1}\right.$$

$$\left. + \frac{j(\Omega-\omega_g-\omega_p)}{\omega_p^2-(\Omega-\omega_g)^2}\varepsilon^{-j\omega t_1}\right\}\left\{\varepsilon^{-j\omega_p(t-t_1)} - 1\right\}$$

$$+ \frac{\eta E_0}{2}\left\{\varepsilon^{j\omega t_1}\frac{\left[\varepsilon^{j(\Omega+\omega_g)(t-t_1)}-1\right]}{\omega_p^2-(\Omega+\omega_g)^2} + \varepsilon^{-j\omega t_1}\frac{\left[\varepsilon^{j(\Omega-\omega_g)(t-t_1)}-1\right]}{\omega_p^2-(\Omega-\omega_g)^2}\right\} \quad (15)$$

After taking the real part and combining terms, we obtain

$$z = v_0(t-t_1) - \frac{\eta E_0}{2\omega_p}\cos(\omega t_1)\left\{\frac{\omega_p}{\omega_p^2-(\Omega+\omega_g)^2}\cos[\omega_p(t-t_1)] + \right.$$

$$\frac{\omega_p}{\omega_p^2-(\Omega-\omega_g)^2}\cos[\omega_p(t-t_1)] - \frac{\omega_p}{\omega_p^2-(\Omega+\omega_g)^2}\cos[(\Omega+\omega_g)(t-t_1)] \quad (16)$$

$$\left. - \frac{\omega_p}{\omega_p^2-(\Omega-\omega_g)^2}\cos[(\Omega-\omega_g)(t-t_1)]\right\} + \frac{\eta E_0}{2\omega_p}\sin(\omega t_1)\left\{\frac{\Omega+\omega_g}{\omega_p^2-(\Omega+\omega_g)^2}\sin[\omega_p(t-t_1)]\right.$$

$$- \frac{(\Omega-\omega_g)}{\omega_p^2-(\Omega-\omega_g)^2}\sin[\omega_p(t-t_1)] + \frac{\omega_p}{\omega_p^2-(\Omega-\omega_g)^2}\sin[(\Omega-\omega_g)(t-t_1)] \quad (16)$$

$$\left. - \frac{\omega_p}{\omega_p^2-(\Omega+\omega_g)^2}\sin[(\Omega+\omega_g)(t-t_1)]\right\}$$

The transit angle is $\phi = \omega(t_2-t_1)$, where t_2 is the time at which the electron arrives at $z = \ell$. If we make the approximation that $\phi \approx \phi_0 = \omega\ell/v_0$ in the terms in the braces, we find

$$\phi = \phi_0 + \frac{\eta\omega E_0}{2v_0(\omega_g)^2}\left\{\cos(\omega t_1)\left[\frac{\cos\left(\frac{\omega_p}{\omega_g}\phi_0\right)}{\left(\frac{\omega_p}{\omega_g}\right)^2-\left(\frac{\Omega}{\omega_g}+1\right)^2} + \frac{\cos\left(\frac{\omega_p}{\omega_g}\phi_0\right)}{\left(\frac{\omega_p}{\omega_g}\right)^2-\left(1-\frac{\Omega}{\omega_g}\right)^2}\right.\right. \quad (17)$$

$$\left. - \frac{\cos\left[\left(1+\frac{\Omega}{\omega_g}\right)\phi_0\right]}{\left(\frac{\omega_p}{\omega_g}\right)^2-\left(1+\frac{\Omega}{\omega_g}\right)^2} - \frac{\cos\left[\left(1-\frac{\Omega}{\omega_g}\right)\phi_0\right]}{\left(\frac{\omega_p}{\omega_g}\right)^2-\left(1-\frac{\Omega}{\omega_g}\right)^2}\right]$$

$$+ \sin(\omega t_1)\left[\frac{\sin\left[\left(1+\frac{\Omega}{\omega_g}\right)\phi_0\right]}{\left(\frac{\omega_p}{\omega_g}\right)^2-\left(1+\frac{\Omega}{\omega_g}\right)^2} - \frac{\sin\left[\left(1-\frac{\Omega}{\omega_g}\right)\phi_0\right]}{\left(\frac{\omega_p}{\omega_g}\right)^2-\left(1-\frac{\Omega}{\omega_g}\right)^2}\right. \quad (17)$$

$$\left.\left. - \frac{\frac{\omega_p}{\omega_g}\left(1+\frac{\Omega}{\omega_g}\right)\sin\left(\frac{\omega_p}{\omega_g}\phi_0\right)}{\left(\frac{\omega_p}{\omega_g}\right)^2-\left(1+\frac{\Omega}{\omega_g}\right)^2} - \frac{\frac{\omega_p}{\omega_g}\left(1-\frac{\Omega}{\omega_g}\right)\sin\left(\frac{\omega_p}{\omega_g}\phi_0\right)}{\left(\frac{\omega_p}{\omega_g}\right)^2-\left(1-\frac{\Omega}{\omega_g}\right)^2}\right]\right\}$$

We may write Eq. 17 in the form

$$\phi = \phi_0 + \frac{\mu'}{\alpha} a \sin(\omega t_1 - \psi') \tag{18}$$

where

$$\mu' \triangleq \epsilon_0 c \left[2 V_0 \left(\frac{a_1 \ell}{v_0}\right) q\right]^{-1}$$

as before, and

$$2a\cos\psi' = \frac{\sin\left[\left(1+\frac{\Omega}{\omega_g}\right)\phi_0\right]}{\left(\frac{\omega_e}{\omega_g}\right)^2 - \left(1+\frac{\Omega}{\omega_g}\right)^2} + \frac{\sin\left[\left(1-\frac{\Omega}{\omega_g}\right)\phi_0\right]}{\left(\frac{\omega_e}{\omega_g}\right)^2 - \left(1-\frac{\Omega}{\omega_g}\right)^2}$$
$$- \frac{\left(\frac{\omega_g}{\omega_e}\right)\left(1+\frac{\Omega}{\omega_g}\right)\sin\left(\frac{\omega_e}{\omega_g}\phi_0\right)}{\left(\frac{\omega_e}{\omega_g}\right)^2 - \left(1+\frac{\Omega}{\omega_g}\right)^2} - \frac{\left(\frac{\omega_g}{\omega_e}\right)\left(1-\frac{\Omega}{\omega_g}\right)\sin\left(\frac{\omega_e}{\omega_g}\phi_0\right)}{\left(\frac{\omega_e}{\omega_g}\right)^2 - \left(1-\frac{\Omega}{\omega_g}\right)^2} \tag{19}$$

and

$$2a\sin\psi' = \frac{\cos\left[\left(1+\frac{\Omega}{\omega_g}\right)\phi_0\right]}{\left(\frac{\omega_e}{\omega_g}\right)^2 - \left(1+\frac{\Omega}{\omega_g}\right)^2} + \frac{\cos\left[\left(1-\frac{\Omega}{\omega_g}\right)\phi_0\right.}{\left(\frac{\omega_e}{\omega_g}\right)^2 - \left(1-\frac{\Omega}{\omega_g}\right)^2}$$
$$- \frac{\cos\left(\frac{\omega_e}{\omega_g}\phi_0\right)}{\left(\frac{\omega_e}{\omega_g}\right)^2 - \left(1+\frac{\Omega}{\omega_g}\right)^2} - \frac{\cos\left(\frac{\omega_e}{\omega_g}\phi_0\right)}{\left(\frac{\omega_e}{\omega_g}\right)^2 - \left(1-\frac{\Omega}{\omega_g}\right)^2} \tag{20}$$

Because the form of [illegible] the same as the form of the corresponding equation for the constant amplitude case, the results obtained for that case may be immediately modified to apply to this case as well. The procedure is the same as that given [illegible] and will not be discussed any further here. Eq. 17 of that note remains valid for the conversion provided by Eqs. 19 and 20 of this note [illegible].

BIBLIOGRAPHY

1. Millimeter-Wave Converter Studies, Bimonthly Report No.2, Contract NASw-490, ITT Components Division, July 15-Sept. 14, 1962, Appendix 1.

2. Ibid., Appendix 2.

Murray D. Sirkis

Murray D. Sirkis

December 10, 1962

APPENDIX III

Variation of circuit wave amplitude and gain of the BWA calculated from 3 wave theory

The normalised amplitude of the circuit wave is given by Johnson [7] in the following form :-

$$f_c(z) = \sum_{i,j,k} \frac{\delta_i^2 + d_2 C}{(\delta_i - \delta_j)(\delta_i - \delta_k)} e^{j\delta_i C_e z} \qquad (A.1)$$

where δ_i can be determined from the characteristic equation

$$a_0 + a_1 \delta + a_2 \delta^2 + \delta^3 = 0 \qquad (A.2)$$

where

$$a_0 = d_1 d_2 = \gamma_3 \qquad a_1 = d_2 C_e^2 \qquad a_2 = j(d_1 + \gamma_3)$$

b,d - Pierce's parameters

This result is compared with that of 3-wave theory for $d = 0$ and $QC_e = 0$ in Fig

At the design frequency $f_c(z) = 1$, that is the condition of oscillation. At a different frequency the same device can be used as an amplifier, the gain is then given by the expression

$$\left[\quad \right]^2 \qquad (A.3)$$

going to infinity

$$= \frac{}{} \qquad (A.4)$$

where K is independent of frequency. K can be calculated by assuming that at a slightly different frequency all the coefficients in Eqn (2) will be slightly different resulting in slightly different roots. Substituting these perturbed roots into Eqn (A.1) we get :-

$$K = \sum_{i,j,k} \frac{\delta_i^2 + 4QC}{(\delta_i - \delta_j)(\delta_i - \delta_k)} \left\{ \frac{2\delta_i v_i + 8QC}{\delta_i^2 + 4QC} - \frac{v_i - v_j}{\delta_i - \delta_j} \right.$$

$$\left. - \frac{v_i - v_k}{\delta_i - \delta_k} + \beta_e CL \ (v_i - \delta_i) \right\} \ e^{\beta_e C \delta_i L} \qquad (A.5)$$

where

$$v_i = - \frac{\varepsilon_2 \delta_i^2 + \varepsilon_1 \delta_i + \varepsilon_o}{3\delta_i^2 + 2a_2 \delta_i + a_1} \qquad (A.6)$$

$$\varepsilon_o = \varepsilon_1 a_2 + \varepsilon_2 a_1, \qquad \varepsilon_1 = 8QC,$$

$$\varepsilon_2 = j \left[\frac{1 + \alpha_1}{C} + b + jd \right]$$

$\alpha_1 = \frac{v_o}{v_g}$, v_g - group velocity.

If QC is sufficiently large the asymptotic solution of Eqn (A.2)

$$\delta_1 = -j(4QC)^{\frac{1}{2}} + \frac{j}{2(QC)^{1/4}}$$

$$\delta_2 = j(4QC)^{\frac{1}{2}} \qquad \text{(A.7)}$$

$$\delta_3 = -j(4QC)^{\frac{1}{2}} - \frac{j}{2(QC)^{1/4}}$$

Substituting Eqn (A.7) into Eqn (A.5) using the fact that QC is large and employing the asymptotic conditions of oscillation

$$\frac{\beta_e CL}{2(QC)^{1/4}} = \frac{\pi}{2} \qquad \text{and} \qquad b = (4QC)^{\frac{1}{2}} \qquad \text{(A.8)}$$

we get for the case of zero loss

$$K = \left[\frac{9\pi^2}{16} + \left(\frac{1 + \alpha_1}{C} \right)^2 \sqrt{QC} \right]^{\frac{1}{2}} \qquad \text{(A.9)}$$

which agrees with the expression given by 2-wave theory (see in Appendix 3.2).

APPENDIX IV

Variation of circuit wave and slow space charge wave, and gain of the BWA calculated from 2-wave theory

Assuming a lossy circuit and taking account of the interaction of the circuit wave and of the slow space charge wave, the coupled wave equations [8] result in the following formulae for the amplitudes

$$\left| A_s \right| = B_s \, e^{-\frac{\alpha}{2}(L - z)} \sin \sqrt{1 - y^2} \; d_{cs} \; z \tag{A.10}$$

$$\left| A_c \right| = B_s \, e^{-\frac{\alpha}{2}(L - z)} \left\{ y \sin \sqrt{1 - y^2} \; d_{cs} z + \right.$$

$$\left. + \sqrt{1 - y^2} \cos \sqrt{1 - y^2} \; d_{cs} \, z \right\} \tag{A.11}$$

where

$B_s \, e^{-\frac{\alpha}{2} L}$ - amplitude of the circuit wave at $z = 0$.

$d_{cs} = \beta_e C/2(QC)^{1/4}$ - coupling coefficient between circuit wave and slow space charge wave.

$y = \frac{\alpha}{2d_{cs}}$

α - attenuation coefficient of the circuit wave.

The oscillation condition is that at $z = L$ the expression in the curly brackets of Eqn (A.11) has to be equal zero. This gives a relationship between αL and $d_{cs} L$ which is plotted in Fig 24.

The gain in first approximation can be obtained similarly to that in Appendix III. If $\omega_1 \neq \omega_2$ $A_c(L) \neq 0$ from which the gain can be calculated. Following the same procedure we get :-

$$K = (1-y^2)^{-\frac{1}{2}} \left\{ \frac{1}{4} \; \sin \; \frac{1}{4} \left(\frac{\omega_1 - \omega_2}{\omega_1 + \omega_2} \right)^2 \; \left[\; \right] \right\}^{\frac{1}{2}}$$

which reduces to Eqn (A.10) if $\omega_1 = \omega_2$.

For calculating the i-f current we need A_{sn} (given now by A.10 if $\beta_e L$ is chosen in such a way that the oscillation condition is satisfied at ω_1

Assuming again that the spatial variation is the same at ω_a as at ω_b we can write for the one circuit case

$$\left| A_{sb} \right| = B_{cb}\, g\, e^{-\frac{\alpha}{2}(L-z)} \sin \sqrt{1-y^2}\, d_{cs} z \qquad (A.13)$$

where B_{cb} - amplitude of input signal.

Substituting (A.10) and (A.13) into Eqn (5) using the derived formulae for g (fast wave is neglected in this 2-wave approximation) and integrating we get for the i-f current

$$i_{if} = \frac{B_{sa}\, B_{cb}}{V_o} F(\alpha L,\ \alpha_1,\ h) \qquad (A.14)$$

where

$$F(\alpha L,\ \alpha_1,\ h) = \frac{1}{2} e^{-\alpha L} \sqrt{1-y^2} \left\{ \frac{1}{y} \left(e^{\alpha L} - 1\right) - y \left[\left(4y^2 - 3\right) e^{\alpha L} - 1 \right] \right\} \left\{ \frac{9}{4} h \left(d_{cs} + y\right)^2 + \left(1 + \alpha_1\right)^2 1 + \frac{\alpha L}{2} \right)^2 \right\}^{-\frac{1}{2}}$$

(A.15)

In the two-circuit case $\left| A_{sb} \right|$ is simply assumed to be constant (the gain is now independent of the parameters of the oscillator circuit) which gives for the i-f current at the collector :-

$$i_{if} = \frac{\omega_{if}}{\omega_a} \frac{4N}{V_o} g\, B_{cb} \left(B_{sa}\, e^{-\frac{\alpha}{2}L} \right) \left[\sqrt{1 - y^2} + 2y e^{\frac{\alpha}{2}L} \sin \sqrt{1 - y^2} d_{cs} l \right]$$

(A.16)

References

1 WEBSTER, D.L. 1939, J. Appl. Phys. 10, 501

2 HAHN, W.C. 1939, Gen. Elect. Rev. 42, 258

3 RAMO, S. 1939, Proc. IRE, 27, 757

4 PASCHKE, 1957, RCA Rev., 18, 221.

5 SOLYMAR, L. 1961, TEC, 10, 165.

6 DE GRASSE, R.W. 1958, Rep. No. 386-2, El. Dev. Lab. Stanford University

7 JOHNSON, H.R. 1955 Proc. IRE 43, 684

8 GOULD, R.W. 1955, Trans. IRE, ED-2, 37.

Appendix V

Backward-Wave Converter Bibliography

1. H.R. Johnson, "Backward Wave Oscillators," Proc. IRE, Vol. 43, pp. 684-697; June 1955.

2. Pierce, J.R., Traveling-Wave Tubes. D. Van Nostrant Co., New York, N. Y. - 1950.

3. R. Kompfner and N.T. Williams, "Backward Wave Tubes," Proc. IRE, Wol. 41, pp. 1602-1611; November 1953.

4. H. Heffner, "Analysis of the Backward-Wave Traveling-Wave Tube," Elec. Res. Lab. Rept. No. 48, Stanford Univ., Stanford, Calif., June 1952.

5. L.R. Walker, "Starting Currents in the Backward-Wave Oscillator," Jour. Appl. Phys. Vol. 24, pp. 854-859; July 1953.

6. M. Muller, "Traveling-Wave Tube Amplifiers and Backward-Wave Oscillators," Proc. IRE, Vol. 42, pp. 1651-1658; November 1954.

7. D.A. Watkins, and A.E. Siegman, "Helix Impedance Measurements using an Electron Beam," Jour. Appl. Phys., Vol. 24, pp. 917-922; July 1953.

8. J.W. Sullivan, "A Wide-Band Voltage-Tunable Oscillator," Proc. IRE, Vol. 42, pp. 1658-1665; November 1954.

9. D.A. Watkins and E.A. Ash, "The Helix as a Backward-Wave Circuit Structure," Jour. Appl. Phys., Vol. 25, pp. 782-790; June 1954.

10. S. Ramo, "Space Charge and Field Waves in an Electron Beam," Phys. Rev., Vol. 56, pp. 276-283; August 1, 1939.

11. D.A. Watkins and N. Rynn, "Effect of Velocity Distribution on Traveling-Wave Tube Gain," Jour. Appl. Phys., Vol. 25, pp. 1375-1379; November 1954.

12. J. Putz., "Folded Line Traveling-Wave Amplifier," IRE Conference on Electron Devices, Ottawa, Ont., Can.; June 1952.

13. R. Kompfner, Bell Labs. Record, Vol. 31, 281, (1953).

14. G.A. Gray, "Investigation of Mixing in Traveling-Wave Tube Amplifiers," Ser. No. 60, Issue No. 151, Elec. Res. Lab., University of Calif., Berkeley, Calif; November 11, 1955.

15. J.L. Putz, "Nonlinear Phenomena in Traveling-Wave Amplifiers, "Tech. Rep. No. 37 (N6 onr 251), Elec. Res. Lab., Stanford University, Stanford, Calif.; October 15, 1951.

16. Mr. R. Currie and J.R. Whinnery, "The Cascade Backward-Wave Amplifier: A High-Gain Voltage-Tuned Filter for Microwaves," Proc. IRE, Vol. 43, pp. 1617-1632; November 1955.

17. Brillouin, L., Wave Propagation on Periodic Structures. McGraw-Hill Book Company, Inc., ch V; 1948.

18. S. Sensiper, "Electromagnetic Wave Propagation on Helical Conductors," Sc. D. Dissertation, MIT, ch. II; 1951.

19. D.A. Watkins, "Traveling-Wave Tube Noise Figure," Proc. IRE, Vol. 40, pp. 65-70; January 1952.

20. C.F. Quate, "Power Series Solution of Traveling-Wave Tube Equation," Bell Tel. Lab. Tech. Memo. 53-1, pp. 500-36; October 1953.

21. W.A. Harman, "Backward-Wave Interaction in Helix-Type Tubes," Stanford Elec. Research. Lab. Report No. 13; April 1954.

22. H. Heffner, "Backward-Wave Tubes," Electronics, Vol. 26, pp. 135-137; October 1953.

23. Mr. R. Currie, "The Electronic Impedance Characteristics of Waves on Helix," Tech. Rep. No. 60, E.R.L., University of California; April 1, 1954.

24. P.K. Tien, "Traveling-Wave Tube Helix Impedance," Proc. IRE, Vol 41, pp. 1617-1623; November 1953.

25. J.R. Pierce and W.E. Danielson, "Minimum Noise Figure of Traveling-Wave Tubes with Uniform Helices," Jour. Appl. Physics, Vol. 25, pp. 1163-1165; September 1954.

26. R. Peter and S. Bloom, "A Minimum Noise Figure for the Traveling-Wave Tube," RCA Rev., Vol. 15, pp. 252-267; June 1954.

27. J.R. Pierce, "A Theorem Concerning Noise in Electron Streams," Jour. Appl. Physics, Vol. 25, p 931; August 1954.

28. T.E. Everhart, "Concerning the Noise Figure of a Backward-Wave Amplifier," Hughes Aircraft Co. Rep. 40-31-00-3; October 1954.

29. S. Ramo, "The Electronic Wave Theory of Velocity Modulation Tubes," Proc. IRE, Vol. 27, pp. 757-763; December 1939.

30. R.W. DeGrasse, "Frequency Mixing in Microwave Beam-Type Devices," Tech. Report No. 386-2, Stanford Electronic Laboratory, July 28, 1958.

46. V.N. Shevchik, "A Simplified Theory of Backward-Wave Oscillators," Radio Eng. & Electronics, Vol. 3, No. 6, pp. 181-187; June 1956.

47. P. Butcher, "The Coupling Impedance of Tape Structures," JIEE, Vol. 1043 pp. 177-187; March 1957.

48. E.A. Ash and A.C. Studd, "A Ladder Structure for Millimeter Waves," Tech. Memo No. 305, Standard Telecommunications Laboratories, Ltd., London Road, Harlow, Essex; February 1961.

49. A. Karp, "Traveling Wave Tube Experiments at Millimeter Wavelengths with a New Easily Built Space Harmonic Circuit," Proc. IRE, Vol. 43, pp. 41-46; January, 1955.

50. R.M. White, C.K. Birdsall and R.W. Grow, "Multiple Ladder Circuits for Millimeter Wavelength Traveling Wave Tubes," Proc. Symposium on MM Waves, Brooklyn, N.Y., (Polytechnic Press), pp. 367-402; 1959.

51. J. Walling, "Interdigital and Other Slow-Wave Structures," Journal of Electronics, Vol. 3, pp. 239-258; 1957.

52. R.C. Fletcher, "A Broad Band Interdigital Circuit for Use in Traveling Wave Type Amplifiers," Proc. IRE, Vol. 39, pp. 951-958; August 1952.

53. E.A. Ash, "A New Type of Slow Wave Structure for Millimeter Wavelengths," JIEE, Vol. 1058, Supp. II: May 1958.

54. C.K. Birdsall and T. Everhart, "Modified Contrawound Helix Circuits for High Power TWT's," Trans. IRE, Vol. ED-3, No. 4, pp. 190-204; October 1956.

55. J.R. Pierce, "Propagation in Linear Arrays of Parallel Wires," Trans. IRE, Vol. ED-2, No. 1, pp. 13-24.

56. A.H. Beck, A.B. Cutting, G. King, and A.D. Brisbane, "The Deviated Nickel (B.N.) Cathode Parts I & II," V.I.T.R. 551, Standard Telephones and Cables Ltd., Valve Division, Brixham Road, Paignton, Devon, England.

57. D.L. Webster, "The Theory of Klystron Oscillation," J.A.P., Vol. 10, pp. 864-872; [illegible] 1939.

58. L. Solymar, [illegible] Klystron Frequency Stabilization," Electronic T[illegible] 264; September [illegible].

59. N. Chodorow, [illegible] J. Applied [illegible] Jan. 1[illegible]

60. [illegible] Hughes Research [illegible] May, 1956.

61. R. W. Gould, "A Coupled Mode Description of the Backward Wave Oscillator and the Kompfner Dip Condition," Trans. IRE, ED-2, 37, October 1955.

62. G. M. Branch, T. G. Mikran, "Plasma Frequency Reduction Factors in Electron Beams," Trans. IRE, ED-2, 3, April 1955.

63. D. A. Dunn, W. A. Harmen, L. M. Field, and G. S. Kino, "Theory of the Transverse Current Traveling Wave Tube," Proc. IRE, 44, 879-887, July 1956.

64. R.W.Grow, D.A. Watkins,"Backward Wave Oscillator Efficiency," Proc. IRE,Vol. 43,p.848,July 1955

65. D.W. Maurer, E.J. Becker, D.E. Koontz,"A New Nickel Matrix Cathode," 1962 Electron Devices Conference, Washington, D. C.,Oct. 1962.

66. L. Solymar,"Exact Solution of the One-Dimensional Bunching Problem," Journal of Electronics and Control, Vol.10,No.3,p.165,March 1961.